Structural Characterization of Cell Wall and Plasma Membrane Proteins of *Arabidopsis thaliana*

DISSERTATION

Zur Erlangung des akademischen Grades eines Doktors der
Naturwissenschaften (Dr. rer. nat.)

Fachbereich Chemie

der Universität Hamburg

vorgelegt von

Haifa El Kilani

aus Sousse, Tunesien

Hamburg, Juni 2016

Die vorliegende Arbeit wurde im Zeitraum von Dezember 2012 bis Mai 2016 in der Arbeitsgruppe von Prof. Ch. Betzel am Institut für Biochemie und Molekularbiologie des Fachbereichs Chemie der Universität Hamburg und in der Arbeitsgruppe von Prof. St. Hoth am Institut für Molekulare Pflanzenphysiologie am Biozentrum Klein Flottbeck durschgeführt.

Gutachter:

Prof. Dr. C. Betzel

Prof. Dr. R. Bredehorst

Tag der Disputation: 22. Juli 2016

To my lovely family

Table of Contents

III

Abbreviations

A. thaliana: Arabidopsis thaliana

AAO3: Abscisic aldehyde oxygenase 3

ABA: Abscisic acid

Ad5: Adenovirus type 5

AHT: Anhydrotetracycline

Amp: Ampicillin

APC: Adenomatous polyposis coli

APS: Ammonium peroxodisulfate

ARM: Armadillo

AtGSLO5: *Arabidopsis thaliana* glucan synthase-like 5

BLAST: Basic local alignment search tool

CalS: Callose synthase

CD: Circular dichroism

CF: Cystic fibrosis

CIAP: Calf intestinal alkaline phosphates

Cm: Chloramphenicol

CV: Column volume

D: Diffusion coefficient

d: Distance

DLS: Dynamic light scattering

Dmax: Maximum distance available in particle

EFR: EF-Tu receptor

EM: Electron microscopy

$\mathbf{F(S)}$: Structure factors

FLS2: Flagellin-sensing 2

f_H: Frictional coefficient for the mass equivalent hard sphere

f_M: Frictional coefficient for the hydrodynamic sphere

GPI: Glycophosphatidylinositol

GSL: Glucan synthase-like

GST: Glutathion-s-transferase

HEPES: 4-(2-hydroxyethyl)-1 piperazineethanesulfonic acid

His: Histidin

I: Intensity

IL: Intracellular loop

IPTG: Isopropyl-β-D-thiogalactopyranosid

k_B: Boltzmann's constant

Kd: Binding affinity

LB: *Luria-Bertani*

LCPL: Left-handed circularly polarised light

M: Molar

MAD: Multi-wavelength anomalous diffraction

MALDI: Matrix assistant laser desorption ionization

MAP: Mitogen-activated protein

Mbp: Mega base pairs

MES: 2-(N-morpholino) ethanesulfonic acid

mg: Milligram

MIR: Multiple isomorphous replacements

ml: Milliliter

mM: Millimolar

MR: Molecular replacement

MS: Mass spectrometry

MST: Microscale thermophoresis

N_A: Avogadros number

NMR: Nuclear magnetic resonance

P(r): Density distribution function & Patterson function

PAMP: Pathogen-associated molecular patterns

PCR: Polymerase chain reaction

PEG: Polyethylenglycol

PMR4: Powdery mildew resistant 4

PR2: Pathogenesis-related protein 2

PRR: Pattern recognition receptors

PT: Transduction pathways

q: Momentum transfer

RCPL: Right-handed circularly polarised light

R_G: Radius of gyration

R_H: Hydrodynamic radius

R_M: Mass equivalent spherical radius

SA: Salicylic acid

SAUL1: Senescence associated ubiquitin ligase1

SAXS: Small angel X-ray scattering

SDS: Sodium dodecyl sulfat

SEC: Size exclusion chromatography

SL: Single layer of solvent

Strep: Streptavidin

T: Temperature

TEM: Transmission electron microscopy

TEMED: Tetramethylethyldiamin

TOF/TOF: 2 coupled time-of-flight mass analyzers

V: Volume

η: Viscosity

λ: Wavelength

ρ: Electron density

α: Phase

$\overline{V}$: Partial specific volume

μl: Microliter

μM: Micromolar

2θ: Scattering angle

1 Introduction

1.1 *Arabidopsis thaliana*

Viridiplantae, also called green plants, are the world´s main molecular oxygen source and the basis of the earth's biosphere. Green plants are multicellular eukaryotes also used as an important source of drugs and medicines (Yue *et al*., 2012). They form an unranked clade that includes the conifers, flowering plants, ferns, gymnosperms, hornworts, clubmosses, mosses, green algae and the liverworts. Plants obtain their energy via photosynthesis from sunlight. Derived from endosymbiosis with cyanobacteria, the presence of chlorophylls a and b in their chloroplasts give plants their green color. Parasitic plants are not able to photosynthesize or produce sufficient amounts of chlorophyll (Field *et al*., 1998).

Due to their unique physiological and organizational properties and the conserved ancestral features between animals and plants, flowering plants such as *Arabidopsis thaliana* are considered to be the best candidates to understand the genetic differences between eukaryotes and plants.

Figure 1: Arabidopsis thaliana: small flowering plant:

Taken from: http://www.pflanzenforschung.de/index.php?cID=7115

Arabidopsis thaliana is a small plant (approximately 30 cm tall, Figure 1), belonging to the family of *Brassicaceae*. It was discovered in 1577 by the German physician Johannes Thal, hence the name is *thaliana*. The genus name derives from the Greek word "*Arabis*" meaning "resembling".

1 Introduction

Over 750 variants of *Arabidopsis thaliana* were founded around the world among different environments from North Africa, Indian subcontinents to East Asia and most European countries (Figure 2; The Arabidopsis Information Resources "TAIR", 2015).

Figure 2: Arabidopsis thaliana distribution around the world:

Arabidopsis thaliana is found in different countries and continents such as North Africa, Indian, East Asia and different European countries. A. thaliana distribution around the word is shown by small green stars.

Figure modified from: http://www.landkartenindex.de/kostenlos/?cat=4

The relatively small nuclear genome (125 Mbp), the rapid lifecycle and the large number of offsprings make *Arabidopsis thaliana* the most important plant model for gene identification and analysis (Arabidopsis Genome Initiative, 2000). *Arabidopsis thaliana* contains 25498 genes, which encode about 11000 protein families and have significant similarities to genes that cause human diseases, such as cancer and cystic fibrosis (CF).

1.2 Membrane proteins and membrane associated proteins

In plant, as well as in animal cells, membrane proteins play a crucial role as membrane receptor proteins and in many other biological processes such as cell differentiation and proliferation, cell to cell communication, signal detection and transmission, regulation of metabolites and ion transport (Almén *et al.,* 2009). Mutations or misfolding of membrane proteins in cells can be associated with a broad range of diseases such as CF, heart disease, obesity, depression and cancer (Terstappen & Reggiani, 2001; Davey, 2004).

Membrane proteins have a vital role for the survival of many different organisms and are very attractive targets in drug discovery. Almost 30 % of proteins in eukaryotic cells are membrane proteins. However, they are also the most challenging targets in structural biology (Wallin & von Heijne, 1998). Nowadays over 116000 biological macromolecular proteins 3D structures have been solved, but less than 3% of the Protein Data Bank entries are membrane proteins.
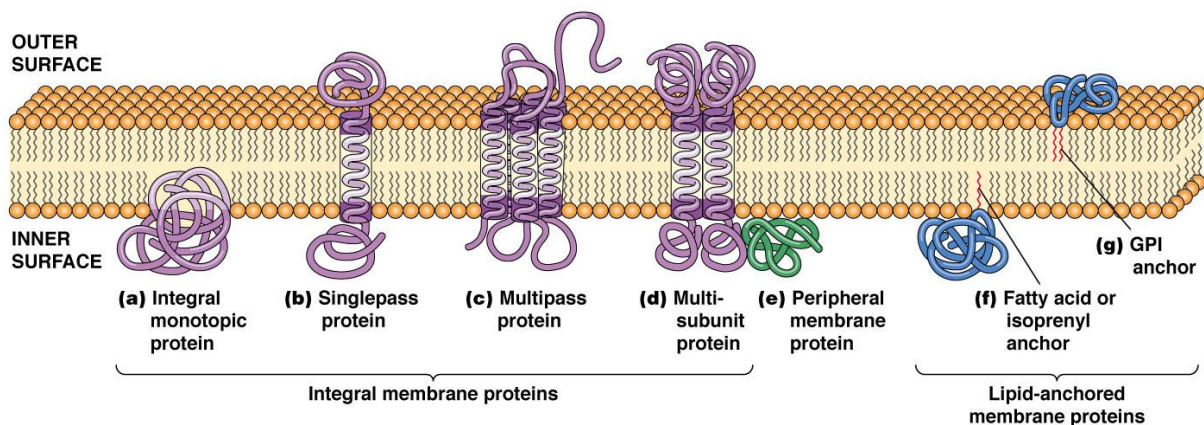
Figure 3: Main classes of membrane proteins
Taken from http://www.mun.ca/biology/desmid/brian/BIOL2060/BIOL2060-07-08/CB07-08.html

There are three main classes of membrane proteins, (1) integral membrane proteins (monotopic or transmembrane), which can only be removed from the cell membrane using detergents, (2) peripheral membrane proteins, temporarily attached to the lipid bilayer or to integral proteins by weak electrostatic forces, and (3) lipid anchored proteins, covalently bound by fatty acid or GPI anchors (Figure 3). To maintain a membrane protein in a folded

and functional state, a solubilization using detergents is usually required, since the disruption of the biological membrane can only be achieved by using specific detergents. Unfortunately, the functional, active form of the majority of these proteins, which is readily maintained in their native membrane environment, can be lost during the solubilization process by detergents, causing aggregations and/or instability (Privé, 2007). Due to their hydrophobic surface, the lack of stability and their relative flexibility, the overexpression, solubilization and purification of these proteins is difficult, making their structural investigation more difficult (Moraes *et al*., 2014; Carpenter *et al*., 2008).

1.3 Biotic and abiotic stress

Many membrane systems in plant cells are responsible for signal processing in response to biotic and abiotic stress. Thus, the characterization of the plasma membrane is of high importance. As sessile organisms, plants are exposed to different environmentally changing conditions. Different biotic and abiotic stresses, such as drought and pathogen infections, affect plant growth. Understanding molecular events regulating plant responses to abiotic and biotic stresses is highly important to improve plant resistance to different stress scenarios and thus the productivity of plants.

Abscisic acid (ABA) is an isoprenoid hormone, which plays a key role in plant development, senescence, and responses to environmental stress and pathogens (Kang, 2002; Seo & Koshiba, 2002). It has also been shown that ABA is involved in modulating callose deposition as a response to plant–pathogen interactions, enhancing plants resistance to pathogen attack (Flors *et al*., 2005). Abscisic aldehyde is produced by the dehydrogenation of xanthoxin via xanthtoxin dehydrogenases. A selective oxidation via abscisic aldehyde oxygenase is the key step in ABA biosynthesis (Cutler & Krochko, 1999). ABA promotes callose deposition through the transcriptional repression of the pathogenesis-related protein 2 (PR2) in *Arabidopsis.*

The plant U-box type E3 ligases, such as the senescence associated ubiquitin ligase1 protein (SAUL1/AtPUB44) negatively regulate ABA biosynthesis by targeting the abscisic aldehyde oxygenase 3 (AAO3) for proteasomal, ubiquitin-dependent degradation (Raab *et al*., 2009). The perception of the different stress signals occurs at two cellular interaction modules of plants cells, cell wall and plasma membrane. Consequently, a signal transduction cascade is activated and the respective stress signal is forwarded to the individual cells.

1.4 Interaction module "cell wall"

1.4.1 (1,3)-β-glucan formation and defense system activation

During a pathogen exposition, the plant detects pathogen-associated molecular patterns (PAMPs) via specialized pattern recognition receptors (PRRs) (Knep per & Day, 2010). Two PRRs were identified in *A. thaliana*, flagellin-sensing 2 (FLS2*) (Gomez-Gomez *et al*., 1999; Gomez-Gomez & Boller, 2000) and EF-Tu receptor (EFR) (Zipfel *et al.,* 2006*;* Lacombe *et al.,* 2010). Both EFR and FLS2 induce the activation of the MAP kinase (mitogen-activated protein kinase) cascade via signal transduction pathways, such as PTI (pattern triggered immunity). Thus, enhance the activation of defense-related transcription genes, oxidative burst and callose deposition (Zhang & Zhou, 2010).
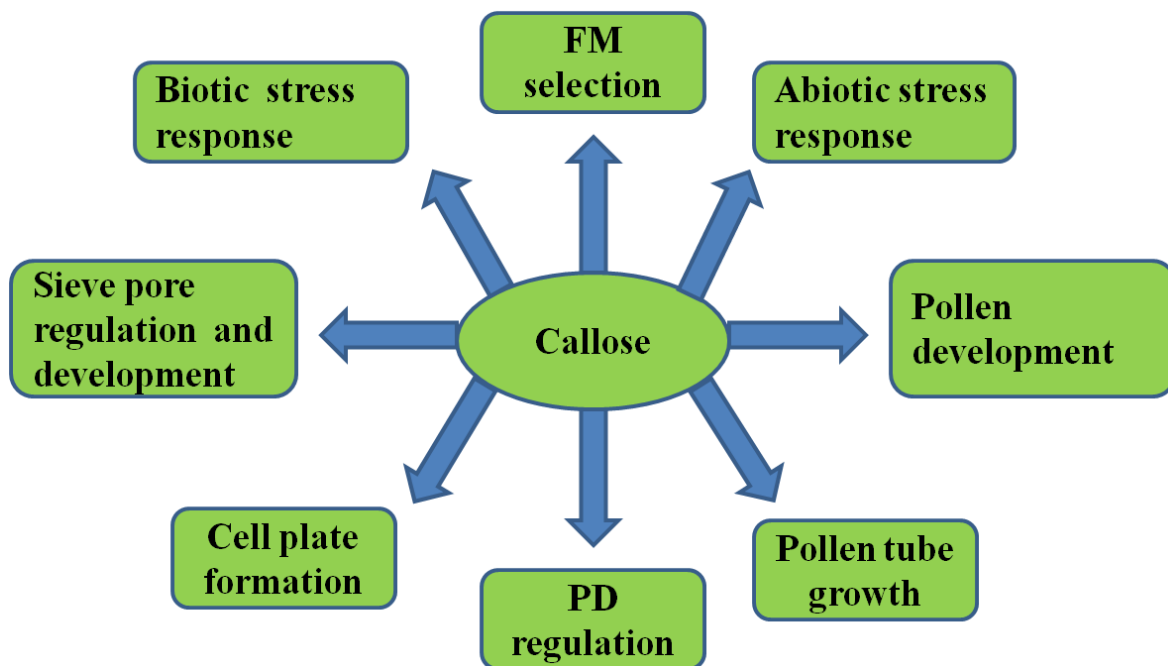
Figure 4: Callose deposition in response to multiple aspects: Plant growth and development, biotic and abiotic stress, functional megaspore (FM) selection, plasmodesmata (PD) regulation, cell plate formation and Sieve pore regulation and development (Stone & Clarke, 1992).

The (1,3)-*β*-glucan callose is one of the main cell wall structural components in fungi, yeasts, bacteria as well as in a wide diversity of higher plants such as *A. thaliana* (Pitson, 1993; Stone & Clark, 1992). *β*-glucans are deposited between the cell wall and the plasma membrane of plants as response to a variety of abiotic and biotic stress factors. Callose, which is a polysaccharide composed of (1,3)-*β*-glucan branched to (1,6)-*β*-side-chains, is also involved in different aspect of plant development and growth (Figure 4). *β*-glucan deposition is followed by cellulose (1,4)-*β*-glucan deposition (Stone & Clarke, 1992). (1,3)-*β*-glucanases are responsible for callose degradation.

1.4.2 (1,3)-β-glucan callose synthase:

Callose is synthesized from UDP-glucose by (1,3)-*β*-glucan synthase (GS) also called callose synthase (CalS) complex. Callose synthases are membrane-bound enzymes of about 200 kDa encoded by different glucan synthase-like (GSL) genes (Cui *et al*., 2001; Doblin *et al*., 2001; Hong *et al*., 2001; Østergaard *et al*., 2002).

There are twelve different *A. thaliana* GSL genes, encoding one putative callose synthase each, AtGSL1 to AtGSL12 (Richmond & Somerville, 2000). The GSL family is subdivided into four main families (Figure 5): The first subfamily includes AtGSL1, AtGSL5, AtGSL8 and AtGSL10, the second subfamily includes AtGSL2, AtGSL3, AtGSL6 and AtGSL12, the third subfamily includes AtGSL7 and AtGSL11, and the last subfamily contains AtGSL4 (Chen & Kim, 2009). Previews studies indicate that GSLs from different subfamilies exhibit redundant functions during pollen fertilization or development (Stone & Clarke, 1992; McCormick, 1993). Moreover, single GSL can have also diverse roles. For example, GSL5 synthesize callose in leaf tissue in response to wounding or plant-pathogen interaction. Thiele (Thiele *et al*, 2009) demonstrated that, GSL8 play a crucial role in plant cytokinesis by deposing callose at cell plate (Chen & Kim, 2009). Rather their own catalytic activity, GSLs proteins, such as GSL8 and GSL10, might interact with receptor-like kinases (RLKs) to perform indirect regulatory functions (Töller *et al*., 2008). Dong reported that AtGSL6 may interact with lectin-containing receptor-like kinase 1 (LecRLK1) through its amino terminus (Dong, 2005).

All GSL proteins from *A. thaliana* are located at the plasma membrane and consist of N-terminal and C-terminal multiply predicted transmembrane domains and a central cytosolic loop (Figure 6) carries the catalytic domain which is responsible for the formation of (1,3)-ß-glucan. The intracellular loop (IL) is divided into two subdomains: the glycosyltransferase

domain and the UDP-glucose binding domain (Chen & Kim, 2009), characterized by a conserved QXXRW motif and a triplet of aspartic acid (Verma & Hong, 2001; Thiele *et al.*, 2009; Dong *et al.*, 2005).
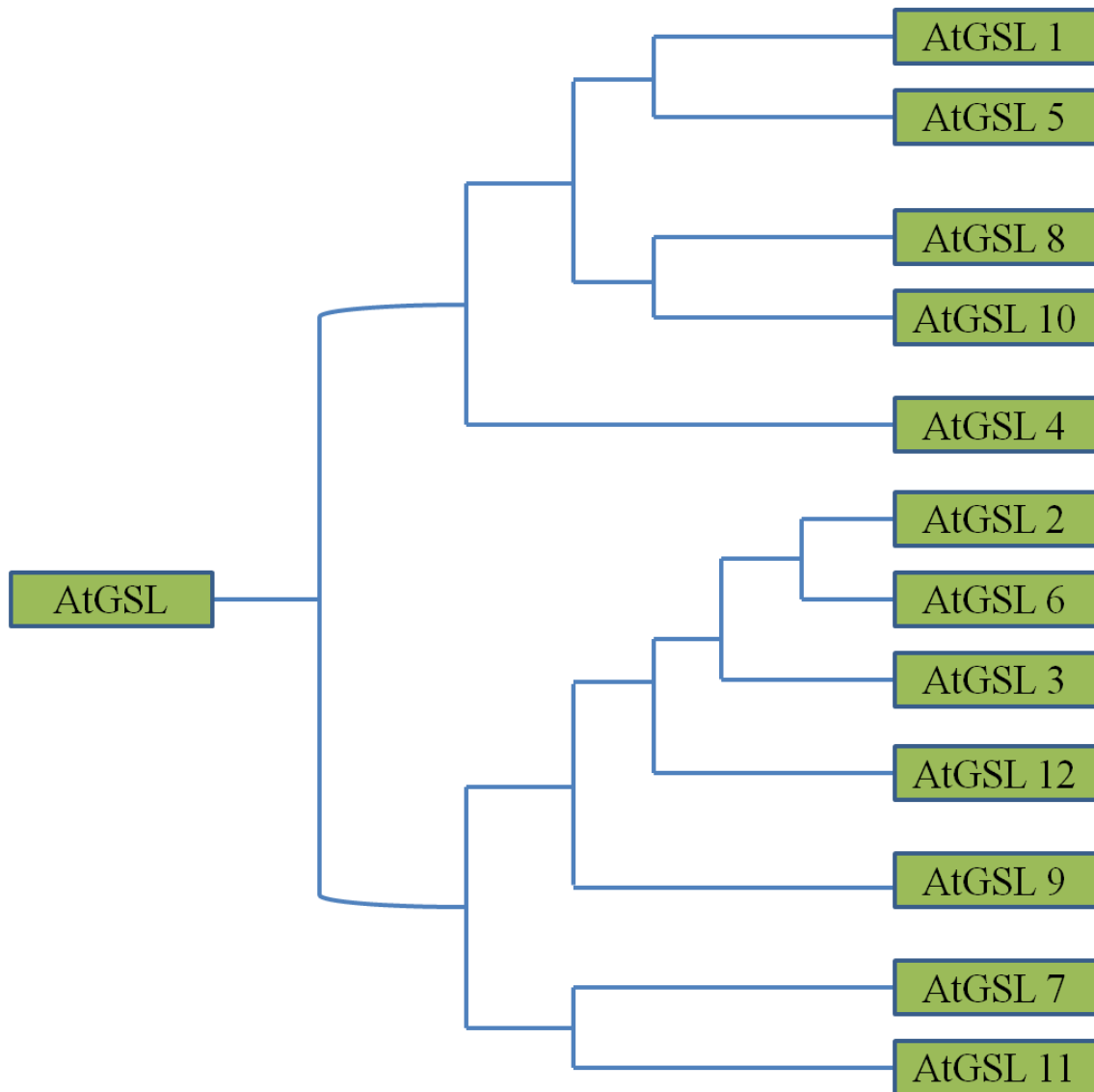
Figure 5: Glucan synthase-like (GSL) genes: *Phylogenetic analysis of Arabidopsis thaliana: Four main subfamilies: AtGSL1, AtGSL5, AtGSL8 and AtGSL10; AtGSL2, AtGSL3, AtGSL6 and AtGSL12; AtGSL7 and AtGSL11; AtGSL4 (Chen & Kim, 2009).*

Exoplasm

Cytoplasm
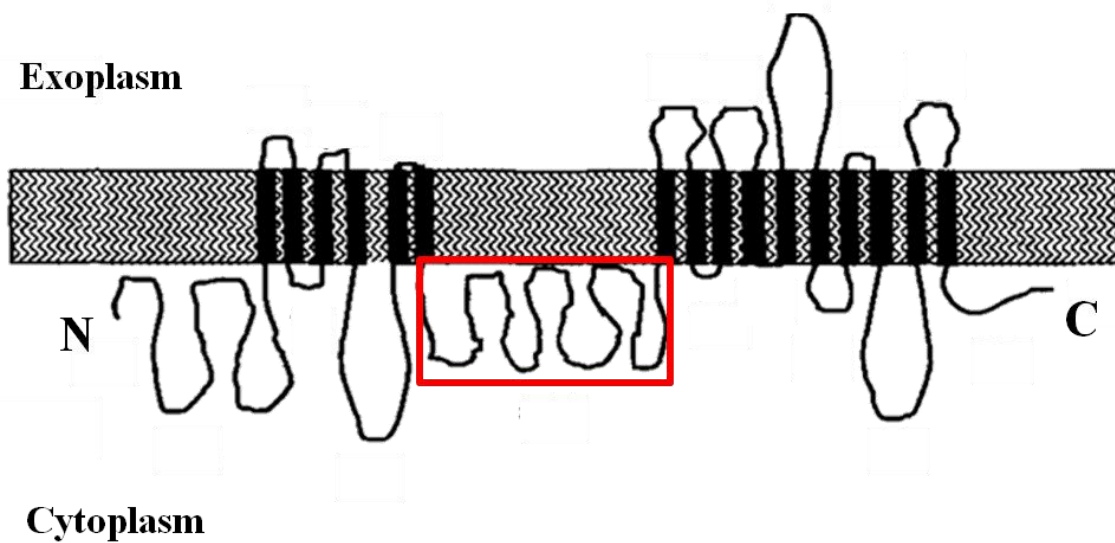
Figure 6: General predicted structure of a (1,3)-ß-glucan synthase: *Organization of AtGSL proteins in the plasma membrane. The red rectangle represents the predicted well conserved intracellular loop. Figure adapted from Kurtz and Douglas, 1997.*

1.4.3 *Arabidopsis thaliana* glucan synthase-like 5: AtGSLO5

The *Arabidopsis thaliana* GSL5, also known as AtGSLO5, has a predicted size of 207 kDa, 16 transmembrane domains and three major domains: N-terminal domains with six transmembrane regions (about 67 kDa), the intracellular loop domain (about 75 kDa) and the C-terminal domain with ten transmembrane regions (about 65 kDa) (Østergaard *et al*., 2002). N- and C-terminal domains might be involved in channel formation and membrane anchorage at the plasma membrane, to facilitate delivery of (1,3)-*β*-glucan to the cell wall, whereas the central cytosolic loop (AtGSLO5-IL) was considered to be the putatively conserved catalytic domain (Østergaard *et al*., 2002).

GSL5, also called callose synthase 12 or PMR4 (powdery mildew resistant 4), plays an essential role in pollens and plants fertility and development. Only some chromosome mutations in GSL5 can induce pollen and plants infertility (Enns *et al*., 2005; Shi *et al*., 2015). The GSL5 from *Arabidopsis* is also required for papillary and wound callose formation. It however also stops the effective growth of *Peronospora parasitica* and of several virulent powdery mildew species (Jacobs *et al*., 2003). Pathogen-induced callose synthase PMR4-overexpressing shows more resistance to pathogens (Ellinger *et al*., 2013; Eggert *et al*., 2014). As a response to a plant-pathogen interaction GSL5 deposes a (1,3)-ß-

glucan callose forming a three-dimensional network with the (1,4)-ß-glucan cellulose elucidated in figure 7 (Eggert *et al.*, 2014). Blocking only the salicylic acid (SA, a PR2 antagonist) defense signaling pathway, by a double-mutant, was sufficient to restore the PMR 4 pathogens susceptibility, suggesting that GSL5 negatively regulates SA production, which may negatively influence the callose production (Nishimura *et al.*, 2003; Wawrzynska *et al.*, 2010).
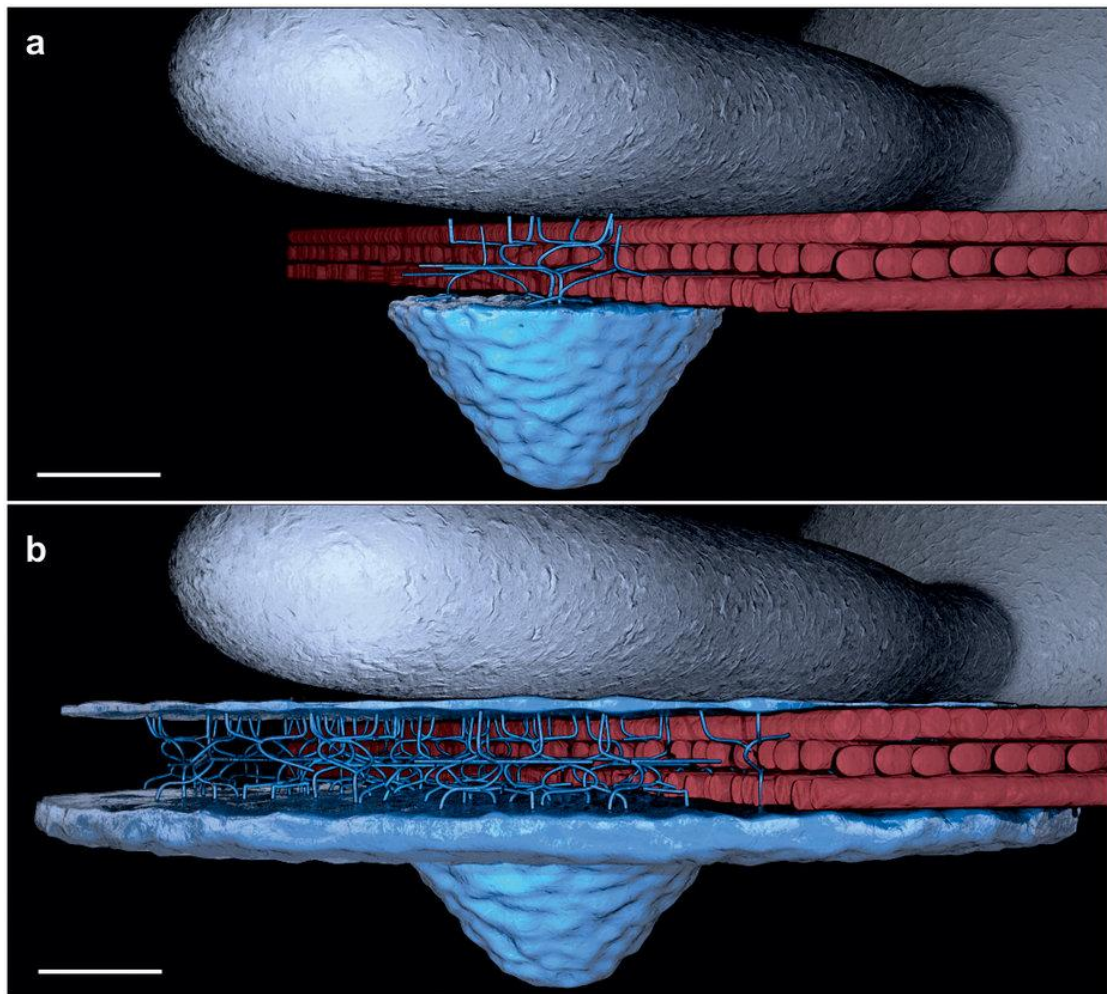
Figure 7: Plant- pathogens interaction response: 3D model of callose/cellulose polymer.
(a): wild-type GSL5 A. thaliana, (b) PMR4 pathogen-induced callose synthase overexpression. Red: (1,4)-β-glucan cellulose, blue: (1,3)-β-glucan callose, and grey: Powdery Mildew fungal structures. The overexpressed-PMR4 of A. thaliana depose a (1,3)-β-glucan callose forming a three-dimensional network with the (1,4)-ß-glucan cellulose, as a response to a plant-pathogen interaction. Scale bars = 2 μm. Taken from: Eggert et al., 2014.

1.5 Interaction module "plasma membrane"

1.5.1 E3 ubiquitin ligases

Two major pathways mediating protein degradation in eukaryotic cells: The lysozomal proteolysis and the ubiquitin-proteosome pathway (Cooper, 2000).

The small regulatory protein ubiquitin has been found in all mammalian and plant eukaryotic cells, suggesting the importance of this protein, for example to counteract several diseases, such as Liddle's syndrome and cystic fibrosis. In many cases, the regulation of signaling pathways is mediated by a post-translational modification pathway, called ubiquitination, enabling disposing of damaged or misfolded proteins (Stieren *et al*, 2011*;* Hofmann, 2009). The attachment of ubiquitin molecules, such as the ubiquitin-26S, to a protein results to proteasomal degradation (Mudgil *et al.,* 2004).
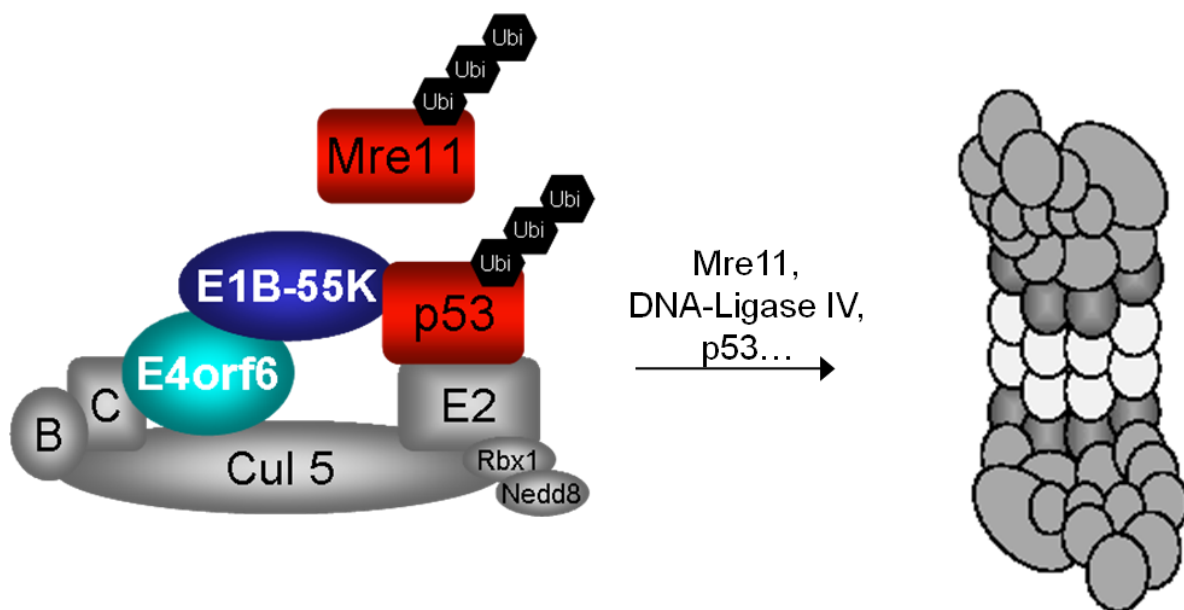
Figure 8: E3 ubiquitin ligase and 23S proteasome:

The E1B-55K and E4orf6-dependent ligase ubiquitinates various cellular proteins, and thus induces their proteasomal degradation by the 23S proteasome. These targets include proteins of the cellular DNA damage response (Mre11, DNA-Ligase IV) and the tumor suppressor protein p53.

1 Introduction

The human adenovirus type 5 (Ad5) E1B-55K and E4orf6 proteins promote viral replication by regulating a selective export of the viral late mRNAs. Additionally, both proteins assemble a virus-dependent E3 ubiquitin ligase. This complex ubiquitinates specific cellular proteins and thus labels them for proteasomal degradation (Figure 8, Schmid *et al.*, 2011).
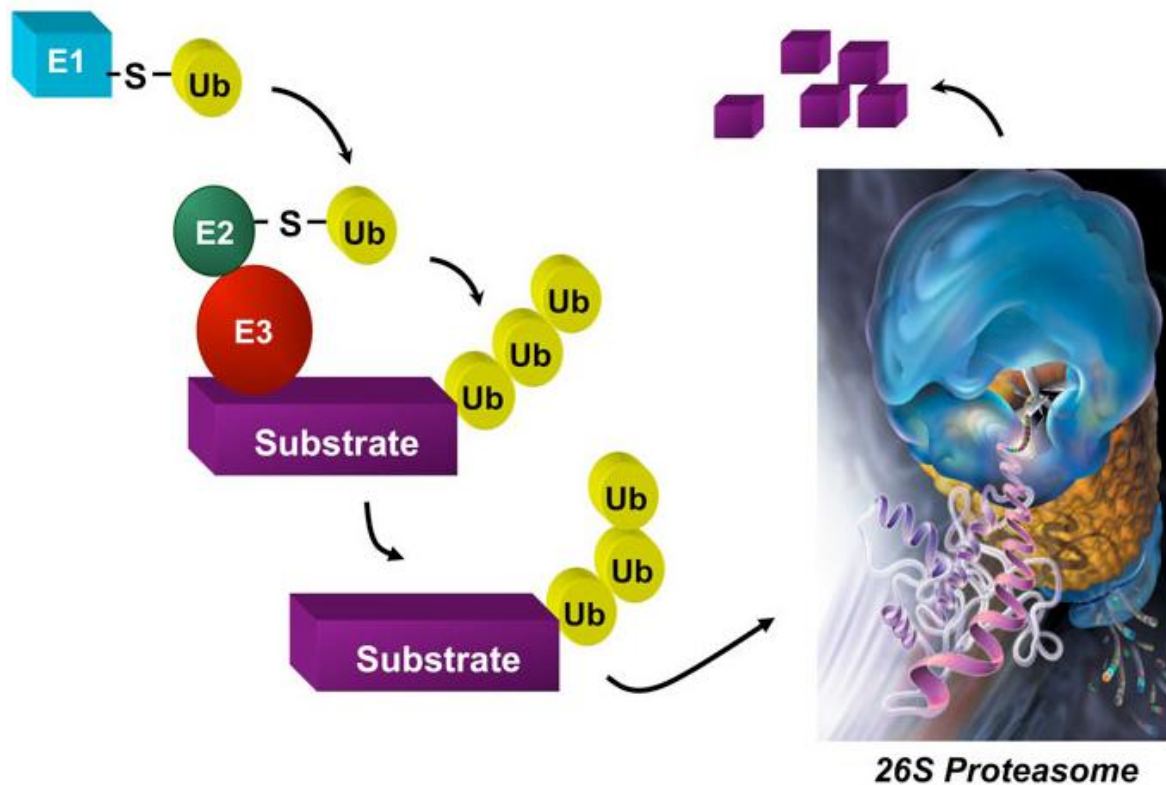
Figure 9: The ubiquitin-proteasome system:

The activating enzyme E1 transfers the ubiquitin to the conjugating enzyme E2. Finally, the recognition and the binding to the target protein is facilitated by the E3 ubiquitin protein ligase, which is responsible for substrate specificity (Pickart, 2001), inducing their degradation by the proteasome. For polyubiquitination the transfer process is repeating multiple times. Figure taken from: http://elledgelab.med.harvard.edu/?page_id=312

Three enzymes are involved in protein ubiquitination: Ubiquitin is first activated by an E1 ubiquitin-activating enzyme. The transfer of the ubiquitin to the E2 protein is energy-dependent, requiring ATP and catalyzed by E2 ubiquitin-conjugating enzymes (van Wijk & Timmers, 2010). Finally, an E3 ubiquitin protein ligase attaches ubiquitin molecules to lysine

residues and labels the target substrate for proteosomal degradation (Figure 9; Pickart, 2001). While E2 proteins are characterized by highly conserved catalytic domains, only a few conserved motifs in E3 ligases have been suggested, indicating the specificity of this process. E3 ligases of the plant *A. thaliana* are divided into four types based on their different functions and protein domains: HECT, RING, cullin-RING and U-box ligases (Drechsel *et al.*, 2011).

1.5.2 Senescence associated ubiquitin ligase 1: SAUL1

The senescence associated ubiquitin ligase1 (SAUL1/AtPUB44) of *A. thaliana* belongs to the plant U-Box type E3 ligases. The plant U-box (PUB) protein family is characterized by a highly conserved U-box, which is essential for the activity of these ligases, and multiple tandem armadillo (ARM) repeats forming interfaces for protein–protein interaction. SAUL1 (senescence associated ubiquitin ligase1, ~ 88.8 kDa) is a plasma membrane-associated protein that serves as a suppressor of premature senescence and cell death under unfavorable environmental conditions, such as low light or salt stress (Raab *et al*, 2009; Drechsel *et al.*, 2011).
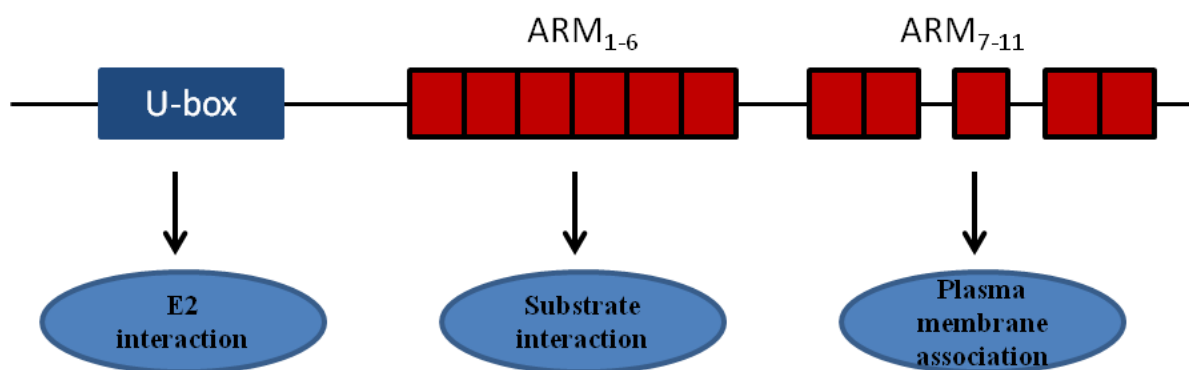
Figure 10: SAUL1 consists of three domains: U-box, ARM 1-6 and ARM 7-11.

U-box is responsible for the interaction with E2, ARM 1-6 repeats were hypothesized to be responsible for protein-protein interaction and ARM 7-11 repeats were hypothesized to be responsible for plasma membrane association. Figure adapted from Drechsel et al., 2011.
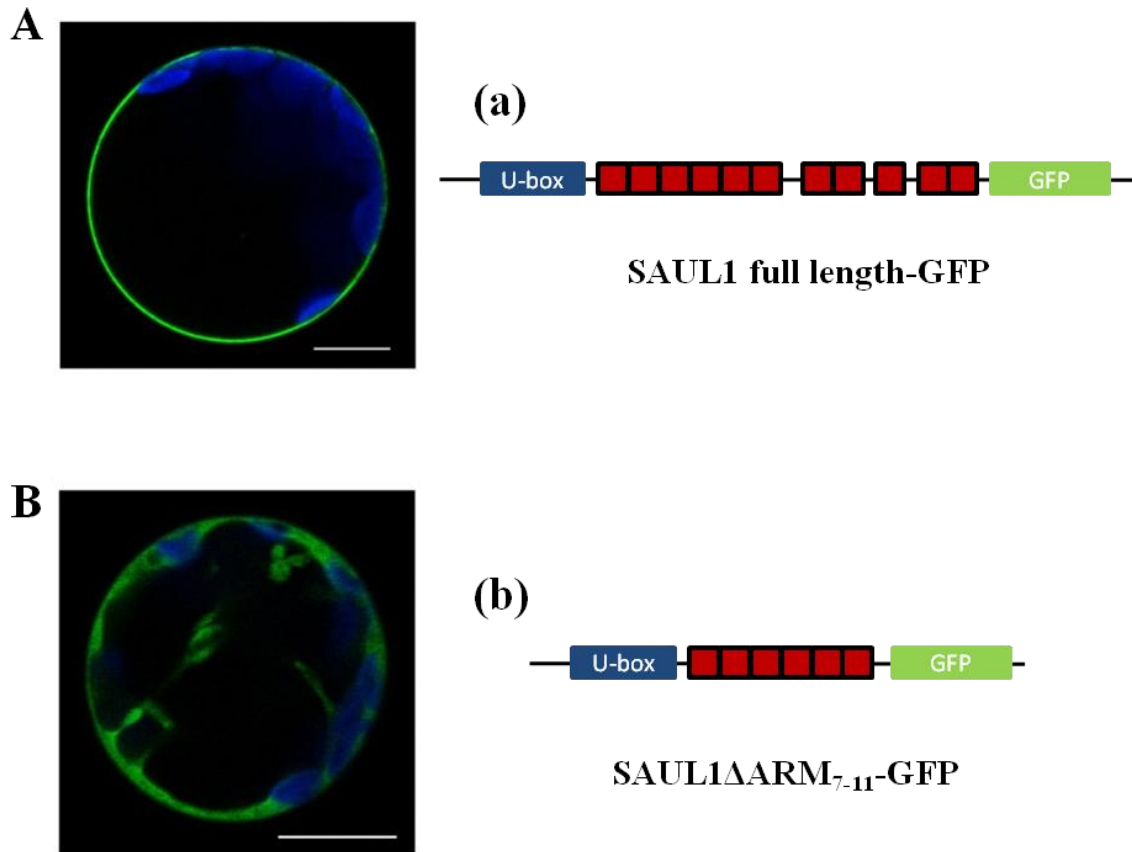
Figure 11: Confocal laser scanning microscopy of GFP-SAUL1 (A) and GFP-SAUL1ΔARM7-11 (B) fusion proteins:

(A) and (B): Fluorescence signals of Arabidopsis protoplast. (a): Schematic illustration of GFP-SAUL1 protein. (b): Schematic illustration of SAUL1ΔARM7–11–GFP protein. Fluorescence of GFP–SAUL1 and SAUL1ΔARM7–11–GFP, are shown in green. Autofluorescence of chlorophyll is shown in blue. GFP-SAUL1 and SAUL1DARM7–11–GFP was expressed in Arabidopsis protoplasts. Green fluorescence of GFP–SAUL1 was detected at the plasma membrane of transformed protoplasts (A). After deletion of ARM 7-11 repeat GFP signals were detected in the cytoplasm confirming the loss of plasma membrane association of SAUL1(B). Figure adapted from Drechsel et al., 2011.

SAUL1 consists of three putative domains: an N-terminal U-box (Figure 10), which most likely mediates the interaction with the corresponding ubiquitin-conjugating enzyme E2, followed by two series of connected armadillo repeats (ARM), among which the C-terminal

part (ARM 7-11) is essential for the association of SAUL1 to the plasma membrane (Figure 11), whereas the first ARM-domain (ARM 1-6) is hypothesized to interact with target proteins (Drechsel *et al*., 2011). ARM repeats are a repeated, long tandem sequence motif characterized by the triangular arrangement of three right-handed helices consisting of about 40 amino acids (Huber *et al*., 1997). They were found in the tumor suppressor protein APC (the adenomatous polyposis coli), the junctional plaque protein (plakoglobin) and the armadillo mammalian homolog beta-catenin. Armadillo, also called beta-catenin-like repeats, were initially detected in the armadillo locus, which is a DNA region coding for several segment polarity genes, required for *Drosophila* embryogenesis (Perrimon & Mahowald, 1987, Wieschaus & Riggleman, 1987). They possess a concave with a peptide-binding groove and an extended hydrophobic cores indispensable for thermodynamic stability (Amador *et al*., 2001; Azevedo *et al*., 2001; Stone *et al*., 2003).

The strongly conserved U-box motif was first described for the UFD2 protein of yeast (Koegl *et al*., 1999) and is crucial for the ubiquitin ligase activity. It consists of about 70 amino acids, resembling modified RING-domains lacking essential metal binding residues (Aravind and Koonin, 2000).

2 Goals of the thesis

Various stress signals are often detected at the plasma membrane of plant cells. Consequently, a signal transduction cascade is activated and the respective stress signal is forwarded to the individual cells. The regulation of signaling pathways is in many cases mediated by protein ubiquitination, via the attachment of ubiquitin molecules to a protein, resulting in a proteasomal degradation (Mudgil *et al.,* 2004), or via cell wall calloses and cellulose, deposition in response to plant-pathogens interactions (Stone and Clarke, 1992).

Selected structures of the components of the interaction modules "plasma membrane of the cell" and "plant cell wall" need to be elucidated at a high resolution to understand the function and to identify and characterize selected interaction modules responsible for plant stress response. My research focuses on the structure analysis of the transmembrane enzyme callose synthase 12 of *Arabidopsis thaliana*, and of the plasma membrane-associated ubiquitin ligase SAUL1 (senescence associated ubiquitin ligase1) of *Arabidopsis thaliana*, which serves as a suppressor of stress-induced premature senescence and cell death in plants.

The aim of the research was to overexpress, purify and analyze the 3D structures of the putative cytosolic domain of the cell wall-related (1,3)-β-glucan synthase, such as the *Arabidopsis thaliana* glucan synthase-like 5 (AtGSLO5-IL), the membrane associated E3 ubiquitin ligase SAUL1, as well as selected ARM repeats of SAUL1. Complementary molecular biological, biochemical, structural biology and biophysical methods, particular small-angle X-ray scattering (SAXS) were applied.

3 Materials and Methods

3.1 Materials

Table 3.1.1: Equipments

Materials	Producers
Acrylamide gel chamber	SE275 (Hoefer, USA)
Agarose gel chamber	SE260 Mighty Small II Deluxe Mini electrophoresis unit (Hoefer, USA)
Amicon Ultra-15 membran	PLTK Ultracel-PL, 30 kDa UFC903024 (Merck Millipore, Germany)
Balance	TE3102S (Sartorius AG, Germany), LP224S-0CE (Sartorius AG, Germany)
CCD cameras	2K wide angle CCD camera, Veleta (Olympus Soft Imaging Solutions, Germany), Tietz F114 Fast Scan (TVIPS, Germany)
CD spectrometer	J-815 (Jasco, Germany)
Centrifuge	Centrifuge 5804R/5810R/5415R/5424 (Eppendorf, Germany), Centrifuge Minispin® Plus (Eppendorf, Germany), Optima TL ultracentrifuge (Beckman Coulter, USA)
Crystal imaging system	CrystalScore (Diversified Scientific Inc., USA), microscope SZX12 with camera DP10 (both Olympus, Japan)
Crystal plate incubator	RUMED 3001 (Rubarth, Germany) incubators
DLS SpectroSIZE 300	Xtal Concepts, Germany
Electronmicroscopes	FEI Tecnai G20 (FEI company, Netherlands), Philips CM100 microscope (TSS, USA)
Electrophoresis power supply	EV 231 (Peqlab, Germany), Power PAC 200 (Bio-Rad, Germany)
Freezer (-20 °C)	Liebherr premium (Liebherr, Germany)
Gelfiltration column	HiLoad 16/600 Superdex 200 prep grade (GE

	Healthcare, UK)
Hot-plate magnetic stirrer	VMS-A (VWR, USA), MR 3001 (Heidolph, Germnay)
Incubator	37-30 °C Incubator Kelvitron® T (Thermo scientific, USA), 4 °C Incubator (Rubarth, Germany), 20 °C Incubator (Rubarth, Germany)
Mass spectrometer	Ultraflex III (Bruker Daltonik, Germany
Microbalance	Sartorius CP224S-OCE (Sartorius, Germany)
Micropipette	Micropipette Research (Eppendorf, Germany)
Microwave	Microwave MR-6450 (Hitachi, Japan)
Octet HTX system	Forte` Bio, (Pall Corp, Germany)
PCR machines	UNO II (Biometra, Germany)
pH meter	SevenEASY (Mettler Toledo, USA)
Pipetting robot	Honeybee 961 (Zinsser Analytic Gmbh, Germany), Oryx 4 (Douglas, UK)
SDS-PAGE power supply	EV734 (Consort, Belgium)
shaker	IRC-1-U (Adolf Kühner AG, Switzerland), Innova® 43/43R (New Brunswick Scientific, USA), Innova® 4330 (New Brunswick Scientific, USA), GFL 3017 (GFL, Germany)
SONICC	(Benchtop, Formulatrix.Inc, USA)
Sonifier	250/450 (Branson Sonifier Emerson Electric Co, USA)
Spectra/Porous 2 dialysis membrane	MWCO: 12,000-14,000 (Spectrum, Germany)
Spectrophotometer	GeneQuant 1300 (GE Healthcare, UK), Nanodrop 2000c (Thermo Scientific, Peqlab, Germany), GENios microplate reader (Tecan, Schweiz)
TEM grid	400 mesh and 300 mesh (Electron Microscopy Sciences, USA)
Thermocycler	Mastercycler® gradient, Mastercycler® personal (Eppendorf, Germany)
Thermomixer	Thermomixer comfort (Eppendorf, Germany)

Table 3.1.2: Chemicals used

Chemicals	Supplier
Ampicillin	Carl Roth
Anhydrotetracycline (AHT)	IBA
BenchMark prestained protein ladder	Invitrogen
Chloramphenicol	Carl Roth
Gluthatione Sepharose 4B media	GE Healthcare
Isopropyl-β-D-thiogalactopyranosid (IPTG)	Carl Roth
MES (2-(N-morpholino) ethanesulfonic acid)	Applichem
Native Marker Liquid Mix for BN/CN	SERVA
Ni-NTA resin	QIAGEN
PageRuler Plus prestained protein ladder, 10 to 250kDa	Thermo Scientific
Plasmid: pASK-IBA43plus	IBA
Plasmid: pGEX-6p-1	Addgene
PreScission TM-protease	GE Healthcare
Protease Inhibitor Cocktail Tablets: cOmplete™, EDTA-free	Sigma
Sodiumdodecylsulfat (SDS)	Carl Roth
peqGOLD gel extraction kit	PEQLAB Biotechnology

Table 3.1.3: SDS buffers used

Buffer	Composition
2 x sample buffer	50 mM Tris, pH 6.8, 2 % SDS (w/v), 10 %

	glycine (w/v), 0.05 % β-mercaptoethanol (v/v) and 0.02 % bromophenol blue (w/v)
APS	10 % in distilled water
Distaining solution	20% (v/v) acetic acid
Running buffer	25 mM Tris-HCl, 192 M glycine and 0.1 % SDS in distilled water
SDS buffer	10 % (w/v) in distilled water
Separating	1.5 M Tris-HCl, pH 8.9
Stacking	0.5 M Tris-HCl, pH 6.9
Staining solution	0.25% (w/v) Coomassie Brilliant Blue G-250, 25% (v/v) 2-propanol and 10% (v/v) acetic acid

Table 3.1.4: Agarose gel electrophoresis buffers used

Buffer	Composition
1% Agarose	1 g in 100 ml in distilled water
1X Electrode buffer	25 mM Tris-HCl, 192 mM Glycin pH 8.3 and 0.1 % (w/v) SDS
50X TAE	500 mM Tris-Base, 5.7 % (w/v) acetic acid and 50 mM EDTA- Sodium formate
Ethidium bromide	10 mg/ml in distilled water
Loading dye	0.05 % Bromophenol Blue, 0.25 % Xylene Cyanol, 1 mM EDTA, 50 % glycerol

Table 3.1.5: Western blot buffers used

Buffer	Composition
AP	100 mM Tris pH 9.5 4 mM MgCl2
Blocking	3% BSA in TBS
PBS	150 mM NaCl, 2.7 mM KCl, 10 mM Na2HPO4, and 2 mM KH2PO4, pH 7.0
TBS	50 mM Tris pH 7.5, 150 mM NaCl

TBS-T	50 mM Tris pH 7.5, 150 mM NaCl and 0.1 % Tween-20 (v/v)
Transfer	192 mM Glycin, 25 mM Tris and 20% Isopropanol (v/v)

3.1.6 Plasmid and bacterial strains used

Host strain: BL21 (DE3); pGRO7 Cm^r

Plate: LB (Amp; 100 μg/ml); LB (Amp; 100 μg/ml, Cm; 34 μg/ml)

Plasmid: pGEX-6p-1 Amp^r; pASK-IBA43plus Amp^r

3.1.7 Protein sequences

SAUL1 full length sequence:

Translated sequence from pGEX-6p-1: SAUL1 full length (GST-tag; PreScission protease recognition site LEVLFQGP, linker: LGS, residues 1-801);

The arrow indicates the PreScission protease cleavage site

MSPILGYWKIKGLVQPTRLLLEYLEEKYEEHLYERDEGDKWRNKKFELGLEFPNLPYYIDGD
VKLTQSMAIIRYIADKHNMLGGCPKERAEISMLEGAVLDIRYGVSRIAYSKDFETLKVDFLS
KLPEMLKMFEDRLCHKTYLNGDHVTHPDFMLYDALDVVLYMDPMCLDAFPKLVCFKKRIEAI
PQIDKYLKSSKYIAWPLQGWQATFGGGDHPPKSDLEVLFQGPLGSMVGSSDGDQSDDSSHFE
RGVDHIYEAFICPLTKEVMHDPVTLENGRTFEREAIEKWFKECRDSGRPPSCPLTSQELTST
DVSASIALRNTIEEWRSRNDAAKLDIARQSLFLGNAETDILQALMHVRQICRTIRSNRHGVR
NSQLIHMIIDMLKSTSHRVRYKALQTLQVVVEGDDESKAIVAEGDTVRTLVKFLSHEPSKGR
EAAVSLLFELSKSEALCEKIGSIHGALILLVGLTSSNSENVSIVEKADRTLENMERSEEIVR
QMASYGRLQPLLGKLLEGSPETKLSMASFLGELPLNNDVKVLVAQTVGSSLVDLMRSGDMPQ
REAALKALNKISSFEGSAKVLISKGILPPLIKDLFYVGPNNLPIRLKEVSATILANIVNIGY
DFDKATLVSENRVENLLHLISNTGPAIQCKLLEVLVGLTSCPKTVPKVVYAIKTSGAIISLV
QFIEVRENDDLRLASIKLLHNLSPFMSEELAKALCGTAGQLGSLVAIISEKTPITEEQAAAA
GLLAELPDRDLGLTQEMLEVGAFEKIISKVFGIRQGDIKGMRFVNPFLEGLVRILARITFVF
NKEARAINFCREHDVASLFLHLLQSNGQDNIQMVSAMALENLSLESIKLTRMPDPPPVNYCG
SIFSCVRKPHVVNGLCKIHQGICSLRETFCLVEGGAVEKLVALLDHENVKVVEAALAALSSL
LEDGLDVEKGVKILDEADGIRHILNVLRENRTERLTRRAVWMVERILRIEDIAREVAEEQSL
SAALVDAFQNADFRTRQIAENALKHIDKIPNFSSIFPNIA

3 Materials and Methods

ARM 7-11ΔC sequence:

Translated sequence from pGEX-6p-1: ARM 7-11ΔC (GST-tag; PreScission protease recognition site LEVLFQGP, linker: LGS, residues 1-413);

The arrow indicates the PreScission Protease cleavage site

MSPILGYWKIKGLVQPTRLLLEYLEEKYEEHLYERDEGDKWRNKKFELGLEFPNLPYYIDGD
VKLTQSMAIIRYIADKHNMLGGCPKERAEISMLEGAVLDIRYGVSRIAYSKDFETLKVDFLS
KLPEMLKMFEDRLCHKTYLNGDHVTHPDFMLYDALDVVLYMDPMCLDAFPKLVCFKKRIEAI
PQIDKYLKSSKYIAWPLQGWQATFGGGDHPPKSDLEVLFQGPLGSANIVNIGYDFDKATLVS
ENRVENLLHLISNTGPAIQCKLLEVLVGLTSCPKTVPKVVYAIKTSGAIISLVQFIEVREND
DLRLASIKLLHNLSPFMSEELAKALCGTAGQLGSLVAIISEKTPITEEQAAAAGLLAELPDR
DLGLTQEMLEVGAFEKIISKVFGIRQGDIKGMRFVNPFLEGLVRILARITFVFNKEARAINF
CREHDVASLFLHLLQSNGQDNIQMVSAMALENLSLESIKLTRMPDPPPVNYCGSIFSCVRKP
HVVNGLCKIHQGICSLRETFCLVEGGAVEKLVALLDHENVKVVEAALAALSSLLEDGLDVEK
GVKILDEADGIRHILNVLRENRTERLTRRAVWMVERILRIEDIAREVAEEQSLSAALVDAFQ
NADFRTRQIAENALKHIDKIPNFS

AtGSLO5-IL sequence:

Translated sequence of AtGSLO5-IL cloned to pASK-IBA43plus (His-tag, Linker 1: GAGDRGPEFELGTRGSC, residues 1-639, linker 2: HAHGLSA; Strep-tag);

MASRGSHHHHHHGAGDRGPEFELGTRGSCAVVGLFDHLGEIRDMGQLRLRFQFFASAIQFNL
MPEEQLLNARGFGNKFKDGIHRLKLRYGFGRPFKKLESNQVEANKFALIWNEIILAFREEDI
VSDREVELLELPKNSWDVTVIRWPCFLLCNELLLALSQARELIDAPDKWLWHKICKNEYRRC
AVVEAYDSIKHLLLSIIKVDTEEHSIITVFFQIINQSIQSEQFTKTFRVDLLPKIYETLQKL
VGLVNDEETDSGRVVNVLQSLYEIATRQFFIEKKTTEQLSNEGLTPRDPASKLLFQNAIRLP
DASNEDFYRQVRRLHTILTSRDSMHSVPVNLEARRRIAFFSNSLFMNMPHAPQVEKMMAFSV
LTPYYSEEVVYSKEQLRNETEDGISTLYYLQTIYADEWKNFKERMHREGIKTDSELWTTKLR
DLRLWASYRGQTLARTVRGMMYYYRALKMLAFLDSASEMDIREGAQELGSVRNLQGELGGQS
DGFVSENDRSSLSRASSSVSTLYKGHEYGTALMKFTYVVACQIYGSQKAKKEPQAEEILYLM
KQNEALRIAYVDEVPAGRGETDYYSVLVKYDHQLEKEVEIFRVKLPGPVKLGEGKPENQNHA
MIFTRGDAVQTIDMNQDSYFEEALKMRNLLQEYNHYHGIRKPTILGVRHAHGLSAWSHPQFE
K

3.2 Methods

3.2.1 Bioinformatics tools and softwares used for sequence and structural analysis

Phyre2: A homology modeling server used to calculate homology models (Kelley *et al*., 2015).

IntFOLD: Web server for protein modelling, prediction and analysis (McGuffin *et al*., 2015).

ProtParam: A tool which allows computation of various physical and chemical parameters of proteins such as molecular weight, amino acid composition, atomic composition, estimated half-life, molar extinction coefficient, aliphatic index, instability index, and grand average of hydropathicity from the given protein sequence (Gasteiger *et al*., 2005).

Clustal Omega: A multiple sequence alignment program used to generate alignments between three or more protein or nucleotide sequences (Goujon *et al*., 2010; McWilliam *et al.*, 2013; Sievers *et al.*, 2011).

BLAST (basic local alignment search tool): An algorithm used for comparing biological sequence information in proteins and nucleic acids (Altschul *et al.,* 1990).

DAMMIN: An algorithm used for *ab initio* shape determination by simulated annealing using a single phase dummy atom model (Svergun, 1999).

DAMMIF: An algorithm which speeds up model reconstruction by a factor of 25-40 in comparison with DAMMIN (Franke & Svergun, 2009).

CRYSOL: An algorithm used for evaluation of the solution scattering from macromolecules with known atomic structure and fitting to experimental data (Svergun *et al*., 1995).

CORAL: An algorithm used for rigid body modelling of multidomain protein complexes against multiple data sets (Konarev & Svergun, 2012).

SASREF: An algorithm used for modelling of multisubunit complexes with known atomic structure against solution scattering data (Petoukhov & Svergun, 2005).

3.2.1 Cloning

A plasmid of the cloned pASK-IBA43plus-AtGSLO5-IL was provided by Prof. Dr. Christian A. Voigt, Department of Molecular Phytopathology and Genetics of the Biocenter Klein Flottbeck, University of Hamburg.

SAUL1 full length and ARM 7-11ΔC was pre-cloned in a pGEX-6p-1 Amp^r plasmid by myself and Catharina Brieske in the Laboratory of Prof. Dr. Stefan Hoth, Molecular Plant Physiology, Biocenter Klein Flottbeck, University of Hamburg.

3.2.1.1 Polymerase chain reaction (PCR)

PCR is a widely applied technique to amplify a single copy or a few copies of a segment of DNA. PCR was performed for DNA fragment amplification using *Dream Taq*-polymerase I (Invitrogen, USA). The reaction was carried out by applying a thermocycler (Eppendorf, Germany) and the samples were applied according to the standard protocols. For the reaction, primers (Metabion, Germany) were diluted to a final concentration of 100 pM and 1 µl of each forward and reverse was used. The first step in the amplification reaction was denaturation for 10 min at 94 °C followed by 30 cycles of denaturation for 45 sec at 94 °C, annealing for 1 min at 56 °C (based on the oligonucleotide annealing temperature, determined by the supplier) and followed by elongation for 30 s at 72 °C (this step could be modified based on the number of base pairs to be amplified. When the reaction was carried out overnight, samples were stored at 4 °C within the PCR device. The PCR products were applied onto a 1 % agarose gel. The components listed below were typically mixed in a 0.5 ml reaction tube for PCR and placed in a thermocycler.

Table 3.2.1.1 Components for PCR reaction

Components	Amount
DNA template	1 µl
Green buffer	5 µl
dNTPs, (2 mM)	5 µl
Forward primer	1 µl
Revers primer	1 µl
***Dream-Taq* polymerase**	1 µl

DMSO	1 μl
dH2O	add to 50 μl

3.2.1.2 DNA purification

The purification of the nucleic acid after PCR was performed using the PCR clean–up kit (NucleoSpin Extract II Kit, Macherey-Nagel). All steps were performed according to the manufacturer's specifications. Instead of elution buffer, 50 μl dH2O was used to elute the DNA.

3.2.1.3 Digestion of the DNA fragments

Restriction enzyme digestion was used to either prepare DNA fragments for ligation into a plasmid or to examine the success of the ligation. In the cloning procedure, all fragments were ligated into the selected vectors. PCR products and vectors were digested according to the manufacturer's protocols. After digestion, the vectors were dephosphorylated by the addition of 1 μl calf intestinal alkaline phosphatase (CIAP) followed by incubation at 37 ℃ for 1 h, while the digested PCR products were stored on ice. The PCR products and vectors were purified separately (see DNA purification) and eluted in 50 μl ddH2O for the PCR products and 30 μl dH2O for the vectors. To verify the success of cloning, 0.5 μg of plasmid isolated after transformation of *E. coli* were digested with relevant restriction endonucleases and visualized on an agarose gel.

3.2.1.4 Agarose gel electrophoresis

Agarose electrophoresis is a technique used to separate DNA fragments based on their size. Negatively charged DNA is attracted by the anode and moves through an agarose gel depending on agarose concentration, size and conformation of the fragment and applied power. The DNA samples were applied to a 1 % agarose gel and analyzed electrophoretically. The gel was prepared by dissolving 1 % (w/v) agarose in 1× TAE buffer supplemented with ethidium bromide solution (Sigma, USA) to visualize DNA fragments with UV-light. Samples were mixed with 6 × DNA loading dye and applied to the gel. A suitable size marker was used to estimate the length of the DNA fragments. The electrophoresis run was performed at a constant voltage of 100 V. The DNA fragments from PCR and restriction

digestion were exposed to UV light for detection, cut with a scalpel from the gel and purified using the peqGOLD gel extraction kit (PEQLAB Biotechnology GmbH).

3.2.1.5 Ligation

Plasmid vectors and DNA fragments were ligated using a molar ratio of 1:5 with the addition of 1 µl of T4 ligase and 2 µl of 10 x ligation buffers in a total volume of 20 µl. The reaction mixtures were incubated overnight at 18 °C. Afterwards, the ligation mixtures were directly incubated at 65 °C for 15 min to stop the reaction of the T4 ligase. The reaction mixtures were used for a transformation of XL10-Gold or DH5α *E .coli* cells. The cells were plated out onto agar plates containing 100 mg/ml ampicillin and incubated overnight at 37 °C.

3.2.1.6 Preparation of chemically competent cells

A single *E. coli* colony or a glycerol stock (200 µl) was used to inoculate 100 ml *Luria Bertani* (LB)-medium and incubated at 37 °C overnight. The overnight culture was diluted 1:50 in LB-medium (10 ml of overnight culture were added to 500 ml LB-medium) and grown at 37 °C to an optical density of 0.6-0.8 at 600 nm (OD600). Reaching this OD600, the solution was cooled on ice for 10 min and centrifuged at 4 °C and 4000 rpm for 10 min. The supernatant was discarded and cells were re-suspended in a sterile solution containing 0.1 M $CaCl_2$ and incubated for 15 min on ice. This suspension was again centrifuged at 4 °C and 4000 rpm for 10 min and the supernatant was discarded. The cells were re-suspended in 5 ml cold 0.1 M $CaCl_2$/10 % glycerol containing buffer. Aliquots of 200 µl were flash-frozen in liquid nitrogen and stored at -80 °C.

3.2.1.7 DNA-Sequencing

To investigate the success of cloning, plasmid DNA was sequenced by SeqLab by extended hotshot sequencing. Samples were prepared by mixing 6 µl of DNA with 1 µl of sequencing forward or reverse primer.

3.2.2 Transformation

One hundred microliters of competent cells of BL21 (DE3) or pGRO7, thawed on ice, were incubated with 1 µl (20 ng) of plasmid DNA for 20 min on ice. The heat shock was performed for 45 s at 42 °C. Thereafter, 0.5 ml LB (medium without antibiotics) was added. The mixture

was then incubated for 1 h at 37 °C and 250 rpm. Afterwards, 100 µl of the transformation mixture was inoculated on an agar plate with antibiotics for selection. The agar plate was finally incubated at 37 °C for overnight. 2 × 1 L and 1 × 50 ml of LB medium were prepared and autoclaved.

3.2.3 Recombinant protein expression

3.2.3.1 Recombinant expression of the AtGSLO5-IL

An N-terminal Strep-tag and C-terminal His-tag fusion with AtGSLO5-IL (total size 79 kDa) was generated to enable subsequent purification from *Escherichia coli* after heterologous expression. For the pre-culture 100 ml of LB medium were prepared and autoclaved. 2-3 single colonies were inoculated to 100 ml of LB medium (Amp; 100 µg/ml, Cm; 34 µg/ml) and incubated for overnight at 37 °C with shaking at 180 rpm. 1:50 of the overnight culture in LB medium was transferred to 1 L of LB containing the same concentration of antibiotics (Amp 100 µg/ml, Cm 34 µg/ml) in a 5L flask. The flask was then incubated in a shaker-incubator at 37 °C and 160 rpm, until the OD at 600 nm reached 0.4. A pre-induction with 0.5 mg/ml L- Arabinose (200 mg/ml) was performed. The flask was then incubated in the shaker for further 30 min. Thereafter, the temperature was reduced to 30 °C and 2 mg/ml (1:10000) of AHT (Anhydrotetracycline) was added. The culture was incubated for further 6h with shaking at 160 rpm. In order to harvest the cells, the culture was centrifuged for 30 min at 4° C and 5000 x g. The supernatant was discarded and the cell pellet was resuspended gently in 30 ml buffer, 20 mM Tris-HCl, pH 7.3, and 50 mM NaCl, and centrifuged again for 10 min (using 50 ml centrifugation tubes; 17000 x g at 4 °C). The supernatant was discarded and the weight of cell pellet was measured (usually 3 gram wet cell pellet was harvested from 1 L culture). The pellet was then stored at -20 °C.

3.2.3.2 Recombinant expression of SAUL1 and ARM 7-11∆C

An N-terminal GST-tag fusion with SAUL1 (total size 115 kDa) and ARM 7-11∆C (total size 73 kDa) was generated to enable subsequent purification from *Escherichia coli* after heterologous expression. For the pre-culture, 100 ml of LB medium were prepared and autoclaved. 2-3 single colonies were inoculated to 100 ml of LB medium (Amp; 100 µg/ml) and incubated for overnight at 37 °C with shaking at 180 rpm. One to fifty of the overnight culture in LB medium was transferred to 1 L of LB containing the same concentration of

antibiotics (Amp; 100 µg/ml) in a 5 L flask. The flask was then incubated in a shaker-incubator at 37 °C and 160 rpm, until the OD at 600 nm reached 0.5. The temperature in the shaker-incubator was reduced to 18 °C and 1 µM of IPTG (isopropyl-ß,D-thiogalactopyranoside) was added. The culture was incubated for overnight with shaking at 160 rpm. In order to harvest the cells, the culture was centrifuged for 30 min at 4 °C and 4000 x g. The supernatant was discarded and the cell pellet was resuspended gently in 30 ml PBS buffer, and centrifuged again for 10 min (using 50 ml centrifugation tubes; 17000 x g at 4 °C). The supernatant was discarded and the weight of cell pellet was measured (usually 6 gram wet cell pellet was harvested from 1 L culture). The pellet was then stored at -20 °C.

3.2.3 Purification

3.2.3.1 Purification of His-tagged protein: AtGSLO5-IL

After the expression step of the protein, a cell pellet of approximately 3 grams could be harvested. The thawed cell pellet was suspended in 40 ml of PBS buffer and the cells were disrupted by sonication for 15 min (30 s pulse on; 30 s pulse off; amplitude 30). The cell lysate was centrifuged at 17000 x g for 1 h at 4 °C and the supernatant was filtrated using a 0.45 µm cut-off filter device. The filtered supernatant was then applied onto a Ni-NTA resin. The cell lysate was incubated at 4 °C for 30 min into the pre-equilibrated Ni-NTA resin matrix with 2 CVs lysis buffer (20 mM Tris pH 7, 200 mM NaCl and 5 mM Imidazole). The column was then washed with 50 ml of lysis buffer and the His-tagged protein was eluted with a linear gradient of 0 to 100 % elution buffer. The His-tagged protein started eluting at 100 mM Imidazole. 20 µl of the fractions were applied to 10 % SDS-PAGE analysis to trace the purified protein. The fractions containing the His-tagged protein were pooled for a gel filtration chromatography. The column was washed, regenerated and stored at 4 °C for subsequent use. The pooled fraction from Ni^{2+}-affinity chromatography was concentrated using AmiconUltra ultrafiltration device and followed by purified with pre-equilibrated HiLoad 16/60 Superdex 200 prep grade gel filtration column with 20 mM Tris-HCl, pH 7.3, and 50 mM NaCl buffer.

3.2.3.2 Purification of GST-tagged proteins: SAUL1 and ARM 7-11ΔC

After the expression step of the protein, a cell pellet of approximately 6 grams could be harvested. The cell pellet was re-suspended in 40 ml of lyses buffer and the *E. coli* cells were disrupted by sonication for 10 min (30 sec pulse on; 30 sec pulse off; amplitude 30). The cell lysate was centrifuged at 17000 x g for 1 h at 4 °C and the supernatant was filtrated using a membrane with a 0.45 µm cut-off. The cell lysate was then applied onto a pre-washed and pre-equilibrated Gluthatione sepharose 4B media (GE Healthcare) respectively with MilliQ-water and PBS buffer (5-fold bed volume of the column). The matrix was then washed for ten column volumes using wash buffer (50 mM Tris pH 9 and 250 mM NaCl). The GST-tagged proteins were eluted using a linear gradient from 5 to 30 mM L-Gluthatione reduced (GSH). The GST-SAUL1 and GST-ARM 7-11ΔC fusion proteins were eluted at about 10 mM GSH. The column was washed and regenerated with 10 CVs of water and 1 CV 6 M Guanidine hydrochloride. For subsequent use the GST matrix was stored at 4 °C in a 50 % suspension with 20 % ethanol. The cleaved protein sample was collected for a further purification step. The chromatography affinity purification was followed by an overnight PreScission protease cleavage for the bound GST-tag in the cold room (40 U of PreScission protease for 10 mg protein; estimated from the SDS-PAGE). An SDS-PAGE analysis was done to confirm that all GST-tagged protein had been cleaved. The pooled fractions were concentrated using AmiconUltra ultrafiltration device followed by purification with pre-equilibrated HiLoad 16/60 Superdex 200 prep grade gel filtration column. A chromatogram at 280 and 220 nm was recorded and analyzed. Proteins purity was analyzed by SDS-PAGE.

3.2.3.3 Size exclusion chromatography (SEC)

The pooled fractions after affinity chromatography were concentrated to less than 5 ml using an AmiconUltra MWCO: 30 kDa device. The concentrated protein solution was applied onto a HiLoad 16/600 Superdex 200 prep grade column pre-equilibrated with elution buffer at 1.0 ml/min flow rate and collected in 2 ml fractions. SDS-PAGE analysis was performed with 20 µl of the fractions. Fractions containing the purified protein were pooled and concentrated for DLS studies. The calculation of the molar extinction coefficient at 280 nm depends on the number of the aromatic amino acid residues, tyrosin and tryptophan, in the sequence and the number of disulfide bonds. The molar extinction coefficient was determined with the analysis program "ProtParam" (http://au.expasy.org/tools/protparam.html). According to the Beer-

3 Materials and Methods

Lambert law, the concentration of the solution was calculated by measuring the absorbance at 280 nm:

$$E(280 \, nm) = \varepsilon \times c \times d \rightarrow c = \frac{E \times dilution \, factor}{\varepsilon \times d}$$

Where E is the absorption at 280 nm, d is the cuvette width (cm) and ε is the molar extinction coefficient ($L \cdot mol \cdot cm^{-1}$). The relative molecular weight of the eluted proteins was interpolated from a linear calibration plot of elution volume versus log molecular weight. A calibration curve was prepared using the standards Ribonuclease A (13.7 kDa), Carbonic Anhydrase (29 kDa), Ovalbumin (44 kDa), Conalbumin (75 kDa), Aldolase (158 kDa), Ferritin (440 kDa) and Thyroglobulin (669 kDa). This calibration was used to estimate protein sizes in this work.

3.2.3.4 SDS-polyacrylamide gel electrophoresis (PAGE)

Electrophoresis is a tool used in biochemistry, molecular biology, and biotechnology to separate biological macromolecules as proteins or nucleic acids, according to their electrophoretic mobility. The mobility depends on the charge and molecular weight of the molecule. SDS-PAGE is a simple method used to determine size and purity of the protein sample under denaturing conditions. The separation of macromolecules is driven by an electric field, whereby it is called electrophoresis. It is considered as a very popular method to separate proteins by electrophoresis applying varying polyacrylamide concentration as a support medium and sodium dodecyl sulfate (SDS) as a denaturing agent. SDS is an anionic detergent that binds with peptide chains and maintains a net negative charge within a wide pH range. The negative charges on SDS damage most of the quaternary structure of proteins, and are passively attracted toward an anode (positively-charged electrode) under the effect of the electric field. Polyacrylamide gels act as molecular sieves and restrain larger molecules from migrating as fast as smaller particles. Protein samples were mixed with $6 \times$ concentrated sample buffer and incubated at 96 °C for 10 min for denaturation. The gel was vertically placed in a gel chamber (Hoefer Inc, USA) and connected to an EV 231 power supply (Peqlab, Germany) to adjust the electric field. Electrophoresis was terminated as soon as bromophenol blue reached the low end of the gel. The gel was stained for at least 2 hours in coomassie staining solution and subsequently destained in 20 % (v/v) acetic acid until a sufficient contrast was visualized.

3.2.3.5 Native gel electrophoresis

In the native gel electrophoresis the protein keeps its folding state and charge, therefore, the proteins are not separated according to their molecular mass, but by charge and hydrodynamic radius. There are three native PAGE methods, referred to as native clear, blue native and native quantitative preparative continuous-PAGE (QPNC-PAGE). Pre-cast polyacrylamide gels (4-16 % gradient gels) for blue or clear native PAGE were obtained from SERVA (Germany) and used according to the instructions in the manual applying a mighty small II PAGE chamber (Hoefer, USA). The protein samples were diluted with sample buffer (2 x without SDS) at a volume ratio of 1:1 and applied to the native gel. Since in the electrophoresis much heat is generated, the electrophoresis was carried out on ice to avoid possible denaturation of the native proteins. The electrophoresis was started with a constant voltage of 50 V until the proteins had migrated through the gel. For the migration of proteins through the separation gel, a voltage of 150 to 200 V was chosen. Furthermore, a standard protein marker to approximate the molecular weight, sample buffer as well as anode and cathode buffer was purchased from SERVA (Germany).

3.2.3.6 Western blot

The Western blot was used for the immunological detection of the expressed proteins. Proteins were separated in a 10 % separation gel and blotted according to standard methods (Renart *et al.*, 1979). After successful blotting, the nitrocellulose membrane was blocked with blocking buffer (0.5 % (w/v) BSA in TBS) overnight at 4 °C to prevent nonspecific antibody binding, then washed twice with TBS (750 mM NaCl, 1 M Tris-HCl, pH 7.5). The membrane was incubated with mouse anti-tetra-histidine IgG1 (QIAGEN) in blocking buffer for 2 h at room temperature. After washing with TBST [5 × TBS buffer, 0.05 % (v/v) Tween 20] and TBS, the membrane was incubated with the secondary anti-mouse antibody linked with APC for 45 min. The membrane was washed again with TBS and TBST and transferred to reaction buffer supplemented with 50 g l-1 NBT (dissolved in 70 % DMF) and 20 g l-1 BCIP. After washing the blot color was developed. At a sufficient level of staining, the membrane was rinsed with deionized water to stop the reaction.

3.2.4 Circular dichroism

The difference in light absorbance between left and right-circularly polarised light (CPL) is called circular dichroism (CD, Applied Photophysics, 2015).

$$CD = \Delta A(\lambda)_{LCPL} - \Delta A(\lambda)_{RCPL}$$

With,

λ: Wavelength

LCPL: Left-handed circularly polarised light

RCPL: Right-handed circularly polarised light
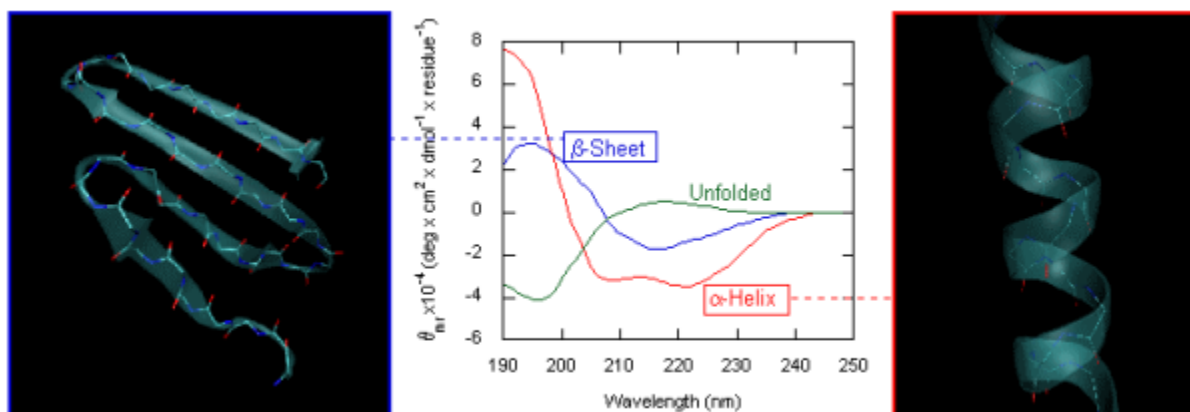
Figure 12: CD spectra of protein secondary structure: *Right: a spectral curve of typical α-helical protein shows two minima at 220 and 208 nm and a maximum at 192 nm (red spectrum). Left is a β-sheet conformation showing a minimum at 215 nm and a maximum at 195 nm (blue spectrum). The green spectrum is a typical unfolded protein conformation (Yang et al., 1986). Figure taken from: https://www.photophysics.com/resources/tutorials/circular-dichroism-cd-spectroscopy (Applied Photophysics, 2015).*

Circular dichroism (CD) is a dichroism requiring circularly polarized light. It is a widely used technique to study macromolecules conformation and protein folding in solution. CD spectrums allow determining important characteristics about the protein's secondary structure (Figure 12) and the approximate percentage of the backbone conformation content in α-helice, β-sheet, or turn structures.

In this work, circular dichroism (CD) spectroscopy of the purified AtGSL05-IL, SAUL1 and ARRM 7-11ΔC were performed using a J-815 CD spectrometer (Jasco, Germany) at wavelengths of 240 to 190 nm to verify the folding quality and for determining the secondary structure composition. To eliminate any optically active materials that may affect the

measurement, protein solutions was dissolved in a 1:1 ratio with water resulting in a final protein concentration of 0.5 mg/ml. The CD spectrometer equipped with a peltier element was calibrated according to the supplier's instructions. The peltier element allows precise investigations concerning the thermal stability of a certain protein fold. The ellipticity of the sample was typically measured in a 1mm quartz cuvette with a wavelength interval ranging from 240-190 nm. The baseline recorded for the corresponding buffer was subtracted. The elasticity θ is defined as the difference in absorbance of clockwise and counter clockwise circular polarized light.

3.2.5 Mass spectrometry

Mass spectrometry (MS) is an analytical technique used for mass-to-charge ratio (m/z) determination of ions. In this work protein bands were excised from the SDS gel and proteins were cleaved into peptides using trypsin. Excised bands of interest, were washed with 50 mM NH_4HCO_3 for 5 min and destained using 100 μl 50 % Acetonitril (ACN) and 50 % 50 mM NH_4HCO_3 at room temperature (RT) until the color became clear (about 30-60 min). After vortexing, the waste was discarded and the gel pieces were incubated in 100 μl 100 % ACN at RT for about 10 min. ACN was then removed and the sample was left to dry in a fume hood. Gel pieces were afterwards incubated for 20 min in a 20 μl trypsin solution (0.01 μg/μl in 50 mM NH_4HCO_3). Finally, 20-50 μl of 50 mM NH_4HCO_3 was added to the solution.

After tryptic digestion the sample was subsequently spotted onto a MALDI-TOF (matrix assisted laser desorption ionization) anchor chip target with α-Cyano-4-hydroxycinnamic acid as matrix as a dried droplet. Finally, the target was introduced into the ionization chamber of the mass spectrometer. Intensities versus mass-to-charge ratios are recorded and graphically displayed as a mass spectrum using FlexAnalysis as software (Bruker Daltonics). Samples were measured by a MALDI-TOF/TOF-MS (2 coupled time-of-flight mass analyzers) using an Ultraflex III mass spectrometer (Bruker Daltonik, Germany). Mass spectra were acquired in reflector mode and externally calibrated using a peptide standard calibration. For protein identification from mass spectra the program mMass (Strohalm *et al*., 2008; Strohalm *et al*., 2010; Niedermeyer & Strohalm, 2012) was used for analysis. Peptide mass fingerprint was performed with following settings: server: Matrix Science (MASCOT), database: NCBI, taxonomy: *Viridiplantae* (green plants), allowed miscleavages: 1, variable modifications: oxidation at methionines, peptide tolerance: 0.3 Dalton, mass type: monoisotopic.

Found proteins were regarded as identified when at least five peptides match to the protein and sequence coverage of 25 % was reached. Furthermore, the internal scoring of the MASCOT server had to be at least 78 to define a protein score as significant.

Tryptic digestion and identification of the proteins via database search using Mascot software, was performed by Anna Ostendorp, Steffen Pahlow and Prof. Dr. Julia Kehr, Department of Molecular Plant Genetic in the Biocenter Klein Flottbeck, University of Hamburg.

3.2.6 Enzymatic activity assay

To exanimate whether the buffer, including pH and salt concentration, has an influence on the enzymatic activity of the AtGSLO5-IL, enzyme linked-immunosorbent assay (ELISA) analysis, after cell lysis and purification of the AtGSLO5-IL, in the presence of UDP-glucose as substrate, was performed using six different buffer solutions (A: pH 8 + 150 mM NaCl; B: pH 8 + 30 mM NaCl; C: pH 7.3 + 3 mM NaCl; D: pH 8 + 150 mM NaCl; E: pH 8.8 + 30 mM NaCl; F: pH 7.3 + 3 mM CaCl$_2$). An anti-(1,3)-β-glucan antibody (Biosupplies, Australia) was used for specific detection of the (1,3)-β-glucan. For the (1,3)-β-glucan synthesis, 20 µl of the purified AtGSLO5-IL protein solution was incubated with 80 µl activity buffer (0.02 % (w/v) digitonin, 2 mM CaCl$_2$, 4 mM Cellobiose, 1.2 mM UDP-Glucose in 50 mM Tris buffer with different pH and NaCl values) in 96-well Corning Costar plates (Corning, USA) at 25 °C and 300 rpm for 60 min. Fractions from empty vector as well as PMR4-IL samples were treated at 95 °C for 20 min and used as controls. To stop the reaction 10 µl 1 M NaOH was added. The synthesized (1,3)-β-glucan was then solubilized for 60 min at 80 °C.

3.2.7 Thermal stability assay

Thermal denaturation assay of SAUL1 protein sample using Proteostat dye (EnzoLife Sciences) and SYPRO Orange dye (Invitrogen) was performed with the help of Sandra Kozak and Dr. Stephane Boivin, EMBL Hamburg. A protein sample at a concentration of 3.5 mg/ml was incubated with a 2 µl Proteostat solution dye or Sypro-Orange solution (10 x) dye in a total volume of 25 µl. The protein solution was then mixed with different concentrations of bivalent metal ions (Ca^{2+}, Zn^{2+}, Cu^{2+}, Fe^{2+}, Mn^{2+}, Ni^{2+}, Co^{2+}, Mg^{2+}). The protein was gradually heated using temperature gradient from 5-95 °C using 1 °C per minute, with a 5 minutes equilibration time at the initial step, in order to slowly unfold the protein, exposing

hydrophobic patches. The protein melting point (Tm) was determined. A sample buffer was used for control. The experiment has been carried out using BioRad MyIQ RT-PCR system.

3.2.8 Dynamic light scattering

Dynamic light scattering (DLS) is an established method used to estimate the size distribution of molecules and nanoparticles by measuring their hydrodynamic radius, dispersity and aggregation state (Berne & Pecora, 1990; Stepanek, 1993). Light from a laser is focused to reach the particles in a microcuvette (Figure 13). The detection of the intensity of the scattered light from the particle distribution allows calculation of the autocorrelation function of the light (Patty & Frisken, 2006). Measuring of the time dependent fluctuations of the scattered light intensity allows the determination of the translational diffusion coefficient, and therefore the hydrodynamic radius (R_H).
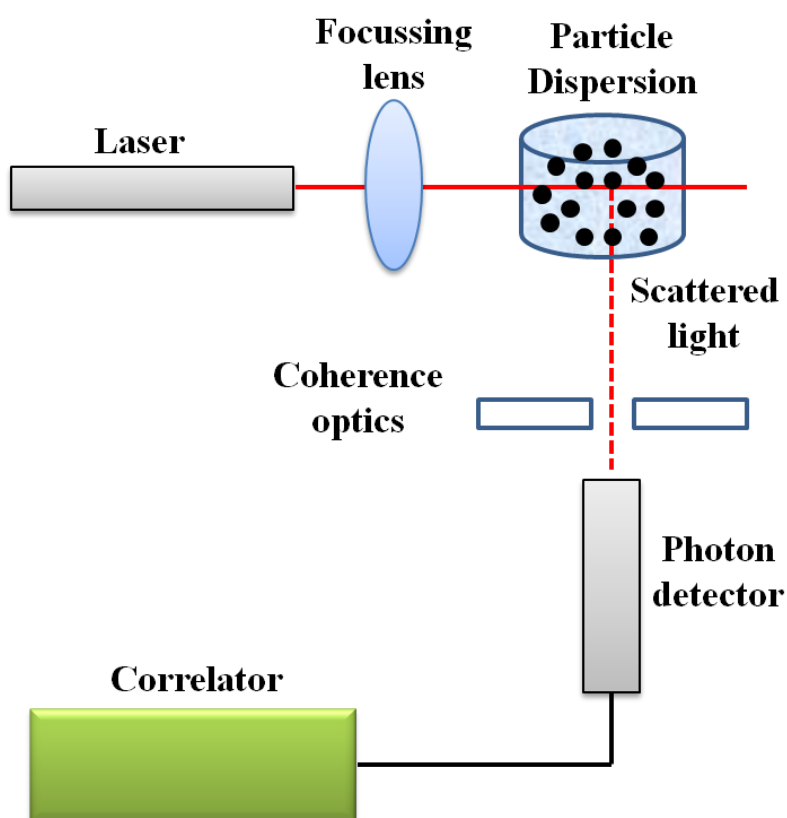
Figure 13: Scheme of a dynamic light scattering instrument:
The fluctuation in the intensity of light scattered by the particles is measured at an angle of 90° over time.

The rate of the fluctuation in the light intensity, resulting from the Brownian motion of the particles, depends on the diffusion coefficient (velocity) and the size of the molecule or particle. The hydrodynamic radius of particles is calculated using the Stokes-Einstein equation (Patty & Frisken, 2006):

$$R_H = \frac{k_B T}{6\pi\eta_s D}$$

R_H is the hydrodynamic radius, η is the solvent viscosity, k_B is the Boltzmann's constant, D is the diffusion coefficient and T is the absolute temperature.

In this work, 20 µl of protein sample was pipetted into to a quartz cuvette for the DLS measurement using a DLS SpectroSIZE 300 instrument (Xtal Concepts, Germany).

3.2.9 Macromolecular crystallography

Macromolecular crystallography is the most widely used technique for the determination of the 3D-structure of biological macromolecules. In brief, crystals of the macromolecule of interest are grown and analyzed using X-rays. From the diffraction pattern and after having solved the crystallographic phase problem, the 3D structure of the macromolecule can be modeled in the calculated electron density map.

3.3.9.1 Crystallization experiments

Several steps are indispensable for growing protein crystals: First, a highly pure and structurally homogeneous protein stock solution in an appropriate solute is required. Second, with the aid of a salt or organic small molecules and a crystallization device/technique, the protein solution is brought to supersaturation (labile zone of the phase diagram; Figure 14) to induce nucleation, which is the main step in crystal growth (Drenth, 1999). After getting a few nuclei, the supersaturation is best reduced to achieve optimal crystal growth in the metastable zone of the phase diagram without formation of additional nuclei. Many crystallization techniques are available such as batch, liquid-liquid diffusion, dialysis, and vapor diffusion crystallization. With the hanging drop method, 1 to 2 µl of protein solution are mixed with 1 to 2 µl of precipitant solution and the mixture is placed on a siliconized glass cover slip. The slips are then placed over the wells of the crystallization trays that contain

each 500 µl of the precipitant solution (Figure 15). The sitting-drop technique is most useful if the solutions have a low surface tension due to the use of detergents (Drenth, 1999). Because of automation, 96-well sitting drop trays have become very popular.
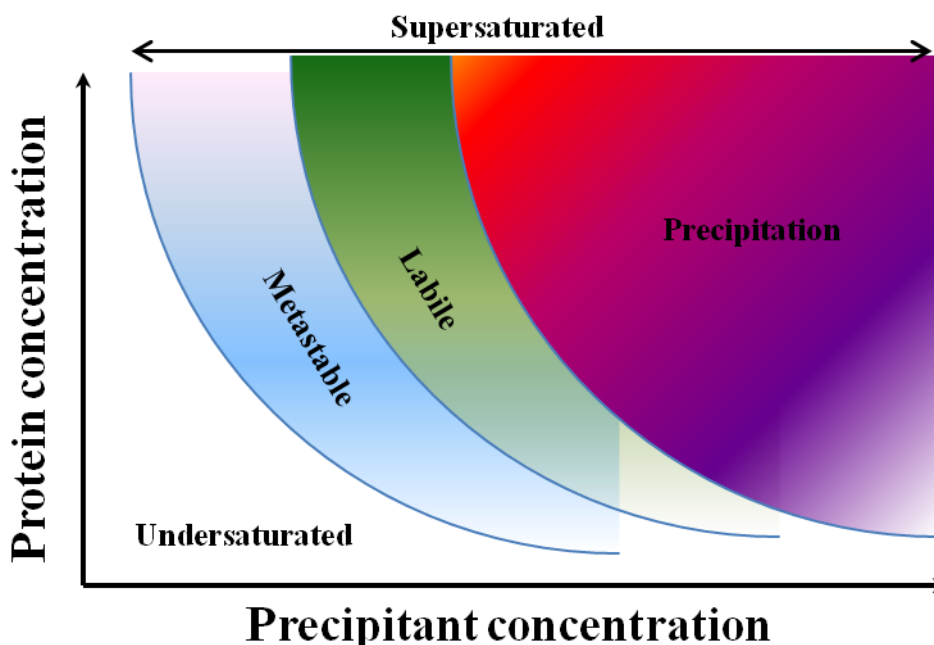
Figure 14: Phase diagram: *In order to achieve protein crystallization we have to either increase the concentration of the protein or diminish repulsive forces or increase attractive forces by adding an organic solvent or varying the pH.*

For the crystallization of the SAUL1 protein more than 200 crystallization conditions were tested, using manual screening techniques, *i.e.* sitting-drop and hanging-drop trays. Protein was purified and the GST-tag was cleaved in order to minimise additional flexible regions within the protein. The purified protein was centrifuged at 25000 x g for 3 h at 4 °C. The monodispersity was verified by DLS. Protein was concentrated using an AmiconUltra (MWCO: 30 kDa) device. A pre-crystallization test (Hampton Research, USA) was performed to obtain the most suitable start concentration for the crystallization experiments. 1 µl of protein solution was mixed with 1 µl of the respective precipitant solution. The reservoir was filled with 500 µl of precipitant solution. Plates were sealed and stored at 4 °C and 20 °C. In addition, lipid cubic phase (LPC) and further conditions using commercial protein screens and kits (Index, PACT, JCSG, Morphous, Compas, Classic, Structure, PGA, MemMeso,

MemGold.) were tested using the Honeybee 961 (Zinsser Analytic GmbH, Germany) and Oryx 4 (Douglas, UK) crystallization robots. 500 nl protein solution was mixed with 500 nl of the respective precipitant solution in one well. The reservoir was filled with 55 μl of precipitant solution. The plates were sealed and stored at 4 °C and 20 °C.
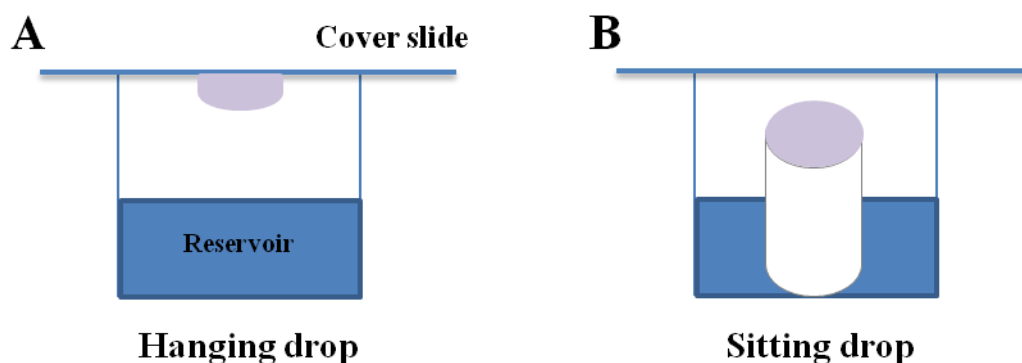
Figure 15: Hanging-drop and Sitting-drop methods:

A drop of protein solution mixed with a drop of precipitant is located above (panel A) or laterally (panel B) in a vessel over a solution having a high concentration of the precipitant. A gradually diffusion (gas phase) of the solvent (water) will take place, which leads to a super saturation in the droplet.

3.2.10 Small angle X-ray scattering

Small angle X-ray scattering (SAXS) is a technique used to investigate three-dimensional shape macromolecule in solution at a resolution of 10 to 20 Å. SAXS is also an important technique for studying structural changes of biological molecules and their behavior, which can be very helpful to understand some diseases such as Alzheimer, Parkinson and various neurodegenerative disorders (Svergun & Koch, 2003). SAXS complements other methods such as nuclear magnetic resonance (NMR) spectroscopy, protein crystallography and electron microscopy. However crystallography and nuclear magnetic resonance have some limitations. In macromolecular crystallography only crystallizable proteins can be investigated, and since we cannot study the behavior of the molecules in solution, the examination of motions is not possible. NMR spectroscopy has size limitations; only low

molecular mass molecules (proteins less than 50 kDa, RNA with less than 50 nucleotides) can be examined (Koch *et al.,* 2003).

After subtracting the scattering of the buffer from the scattering of the sample, a scattering intensity curve I(q) will be obtained (Figure 16, Putnam *et al.,* 2007) where:

$$q = (4\pi sin\theta)/\lambda$$

q: Momentum transfer

2θ: Scattering angle

λ: Wavelength of the incident X-ray beam
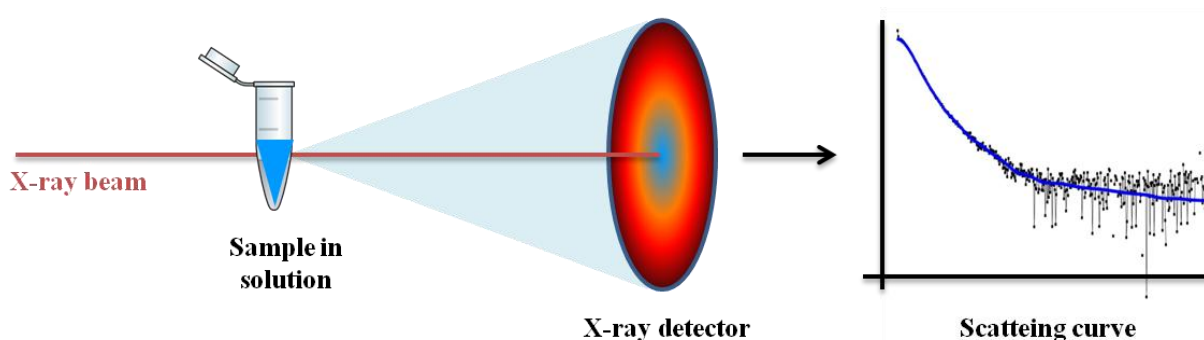
Figure 16: Schematic representation of **small angle X-ray scattering (SAXS):** *The X-ray beam is directed towards the sample in solution. The scattered radiation is captured by the detector and a scattering curve, I(q), is detected.*

Corresponding to the Patterson function in X-ray Crystallography, P(r) is the density distribution function or also called electron distributions of particles, which can be calculated from the electron density or from a Fourier transform of the scattering curve (Putnam *et al.,* 2007):

$$P(r) = \frac{r}{2\pi^2} \int_0^\infty I(q)q\ sin(qr)dq$$

The scattering curve of macromolecules can be derived from the Pair-density distribution function P(r) giving the following equation (Putnam *et al.,* 2007):

3 Materials and Methods

$$I(q) = 4\pi \int_0^{D_{max}} P(r) \frac{\sin q(r)}{q(r)} d(r)$$

Where,

r: Radius

d: Distance

Dmax = Maximum distance available in the scattering particle:

At low resolution, the scattering is calculated using Guinier approximation (Guinier, 1939):

$$I(q) = exp[-(q^2 R_G^2)/3]$$

R_G: Radius of gyration

In this work, data were processed and analyzed with the help of Dr. Alexey Kikhney (EMBL c/o DESY, Hamburg). Synchrotron radiation small angle X-ray scattering data from different solute concentrations of the proteins AtGSLO5-IL, SAUL1, SAUL1-GST complex and ARM 7-11ΔC ranging from 1 to 7 mg/ml in pure water were collected at EMBL beamline P12 at the storage ring PETRA III (DESY, Hamburg, Germany; Blanchet et al., 2015). Data were collected using a 2D photon counting *Pilatus 2M* pixel detector (Dectris) at a sample-detector distance of 3.0 m and a wavelength of $\lambda = 0.124$ nm, the range of momentum transfer $0.04 < s < 4.8$ nm^{-1} was covered ($s = 4\pi \sin\theta/\lambda$, where 2θ is the scattering angle). Data were normalized to the intensity of the transmitted beam and radially averaged. To monitor radiation damage, 20 successive 50 millisecond exposures of protein solutions were compared and only frames before the first signs of damage were averaged. The scattering of the buffer was subtracted and the difference curves were scaled according to the protein concentration. The radius of gyration R_g along with the pair distance distribution function of the particle p(r) and the maximum dimension D_{max} were computed by the automated SAXS data analysis pipeline SASFLOW (Franke *et al.*, 2012). The composite scattering curves were used to generate low resolution *ab initio* shapes of each protein using the program DAMMIF (Franke & Svergun, 2009). This program uses an assembly of densely packed beads to represent the particle shape and employs simulated annealing to construct a compact interconnected model that fits to the experimental data I(s). Ten DAMMIF runs were performed to check solution stability, resulting in well superimposable models. Given the uncertainty in determining the protein concentration, it was difficult to estimate the molecular weight of the solute from the forward scattering. The excluded volume reported by DAMMIF was used to evaluate the

molecular weight assuming that the protein volumes in nm^3 are about two times the MWs in kDa. The excluded volume of the hydrated particle was also computed from the small angle portion of the data (s < 1.1 nm^{-1}) using the Porod equation (Glatter& Kratky, 1982). For globular proteins, Porod (i.e. hydrated) volumes in nm^3 are about 1.6 times the MWs in kDa.

3.2.10.1 Intracellular loop of the glucan synthase-like 5 (AtGSLO5-IL)

Synchrotron radiation small angle X-ray scattering data from 1 mg/ml solute concentration of AtGSLO5-IL in 20 mM Tris with 50 mM NaCl, pH 7.3 were collected at EMBL beamline P12 at the storage ring PETRA III (DESY, Hamburg, Germany; Blanchet *et al.*, 2015). The protein was purified and centrifuged at 25000 x g for 3 h at 4 °C. The monodispersity was verified by DLS. Two different concentrations in the range of 1-2 mg/ml were prepared and the waste from the protein concentrator was used as reference buffer for the measurements. The data were processed and computing with the indirect transform software for small-angle scattering GNOM (Svergun, 1992; Berne & Pecora, 1990; Stepanek, 1993). Rigid body modelling was performed using the program CORAL (Petoukhov *et al*. 2012). Starting from a tentative model, this program uses simulated annealing to search for a non-overlapping interconnected configuration of known domains connected by extended linkers fitting the experimental data. The overall parameters evaluated from SAXS data are summarized in Table 4.1.6. The scattering data and the models are deposited in SASBDB (Valentini *et al*., 2015), code: SASDBN4.

3.2.10.2 Senescence associated ubiquitin ligase1 (SAUL1)

Synchrotron radiation small angle X-ray scattering data from different solute concentrations of the SAUL1, SAUL1-GST complex and ARM 7-11ΔC ranging from 1 to 7 mg/ml in 20 mM Tris with 250 mM NaCl, pH 9 were collected at EMBL beamline P12 at the storage ring PETRA III (DESY, Hamburg, Germany). The purified proteins were centrifuged at 25000 x g for 1 h at 4 °C. The monodispersity was verified by DLS. Proteins were concentrated using an AmiconUltra (MWCO: 30 kDa) device. The waste from the protein concentrator was used as reference buffer for the measurements. The data were processed and calculations were performed using the indirect transform software for small-angle scattering GNOM (Svergun, 1992; Berne & Pecora, 1990; Stepanek, 1993). Ten DAMMIF runs were performed to check solution stability, resulting in well superimposable models.

3.2.11 Electron microscopy

In this work, negative stain electron microscopy was performed at the Max Plank Institute for Molecular Genetics in Berlin, for SAUL1 full length with the help of Jörg Bürger and Dr. Thorsten Mielke. For AtGSLO5-IL, the negative stain electron microscopy was carried out at the Heinrich-Pette-Institut in Hamburg with the help of Carola Schneider and Dr. Rudolph Reimer. Transmission electron microscopy and stochastic optical reconstruction microscopy was performed by Prof. Dr. Christian Voigt, BZF Hamburg.

3.2.11.1 Negative staining electron microscopy (EM)

Electron imaging is considered as powerful tool for visualizing 3D structural details. However, because of the strong interaction of electrons with matter, the electron path of the microscope must be kept under high vacuum to avoid unwanted scattering by gas molecules in the electron path. Consequently, the EM specimen has to be in the solid state for imaging, and special preparation techniques are required to either dehydrate or stabilize hydrated biological samples under vacuum (Jensen, 2010). Negative staining electron microscopy (EM) is a powerful technique that can be used to study 3D structures of purified protein samples, such as using the random conical tilt method (Radermacher *et al*., 1987). Furthermore, this method can have many other applications, such as identifying and analysing two-dimensional (2D) crystals of membrane proteins (Zhao, 2010). Negative stain (EM) is a powerful structural analysis method for protein samples quantitative and qualitative examination. It is a simple sample preparation tool in which protein samples are embedded in a thin layer of a dried heavy metal salt to increase the specimen contrast (Ohi *et al*., 2004).

3.2.11.1.1 Negative staining EM: AtGSLO5-IL

Negative staining electron microscopy (EM) is an established technique, often used, for contrasting a thin specimen with an optically opaque fluid, in diagnostic microscopy. In this method, the background is stained, leaving the actual specimen untouched, and thus being visible (Cheng & Walz, 2009). This requires the collection of several images within one specimen, one untitled and one tilted to 60 °C, both from the same area. 3 µl of the purified AtGSLO5-IL protein was deposited on a glow discharged 400 mesh TEM grid with a formvar carbon film (Electron Microscopy Sciences, Hattfield, PA, USA) and negative stained with 2 % uranylacetate (Merck KGaA, Darmstadt, Germany). The grid was allowed to dry for two

41

minutes, covered for few seconds with a small drop of the 2 % uranylacetate, then rinsed with distilled water to remove the over stain. Transmission electron microscopy was performed on a FEI Tecnai G20 microscope (FEI company, Eindhoven, The Netherlands) equipped with a 2 K wide angle CCD camera (Veleta, Olympus Soft Imaging Solutions, Münster, Germany) using an acceleration voltage of 80 kV."

3.2.11.1.2 Negative staining EM: SAUL1

The negative stain EM enhanced contrast, allows the visualization of relatively small biological samples such as, the determination of three-dimensional (3D) structures of purified proteins or protein complexes (Rabl, 2008). This method can be also used for much broader purposes such as obtaining information about the homogeneity and the heterogeneity of the sample, formation of protein complexes or large assemblies and to evaluate the quality of a protein preparation. 3 µl of the purified SAUL1 full length protein was deposited on a carbon coated grid, discharged by the PELCO easiGlow GlowDischarge system (Ted Pella Inc., USA). The grid was allowed to dry for two minute, covered for 45 seconds with a small drop of 2 % uranyl acetate then rinsed with distilled water to remove the over stain and blotted off with a filter paper. The grid was loaded into the CompuStage of the 100 kV Philips CM100 microscope with a 1kx1k fastscan charge-coupled device (CCD) camera (TVIPS), using 21000 x 29500 x magnification.

4 Results

4.1 Intracellular loop of the *A. thaliana* glucan synthase-like 5 (AtGSLO5-IL)

4.1.1 Cloning and transformation

The gene of the AtGSLO5-IL was cloned into pASK-IBA43plus vector carrying ampicillin resistance, offering an N-terminal Strep-tag and a C-terminal His-tag to enable subsequent purification from *E. coli* after heterologous gene expression. The plasmid of the cloned pASK-IBA43plus-AtGSLO5-IL was kindly provided by Prof. Dr. Christian A. Voigt, Department of Molecular Phytopathology and Genetics of the Biocenter Klein Flottbeck, University of Hamburg. The chloramphenicol resistant transformation of *E coli,* pGRO7 competent cells, with the plasmid was described in more details in the methods section (Chapter 3.2.2).

4.1.2 Purification and mass spectrometry analysis

After recombinant expression (see methods section; Chapter 3.2.3.1), the N-terminal His_6-tagged AtGSLO5-IL protein was purified using Ni^{2+}-affinity chromatography. Analyzing protein fractions by western blot (Figure 17, A) and SDS-PAGE (Figure 17, B), a protein band corresponding to the MW of the AtGSLO5-IL monomer (79 kDa) was detected. To improve the purity and analyze the oligomerization state of the protein, the affinity chromatography step was followed by size exclusion chromatography (SEC) (Figure 18).

The chromatogram showed two peaks. According to the SDS-PAGE analysis and the chromatogram, the AtGSLO5-IL protein was present in the first peak, mainly in the fractions with retention volume 42 ml to 52 ml. In order to avoid any impurity, only fractions with retention volumes 44 ml to 48 ml were pooled. The SEC shows the presence of higher oligomeric states of the protein in solution, corresponding to a calculated molecular weight higher than 600 kDa (Figure 19, C), indicated by a retention volume of about 48 ml. The retention volume was interpolated from a linear calibration plot of the HiLoad 16/60 Superdex 200 prep grade column (see methods section; Chapter 3.2.3.3). Analyzing the SEC protein fractions from the peak at 48 ml retention volume by non reducing SDS-PAGE

showed a predominant protein band corresponding to the MW of the AtGSLO5-IL monomer (79 kDa).
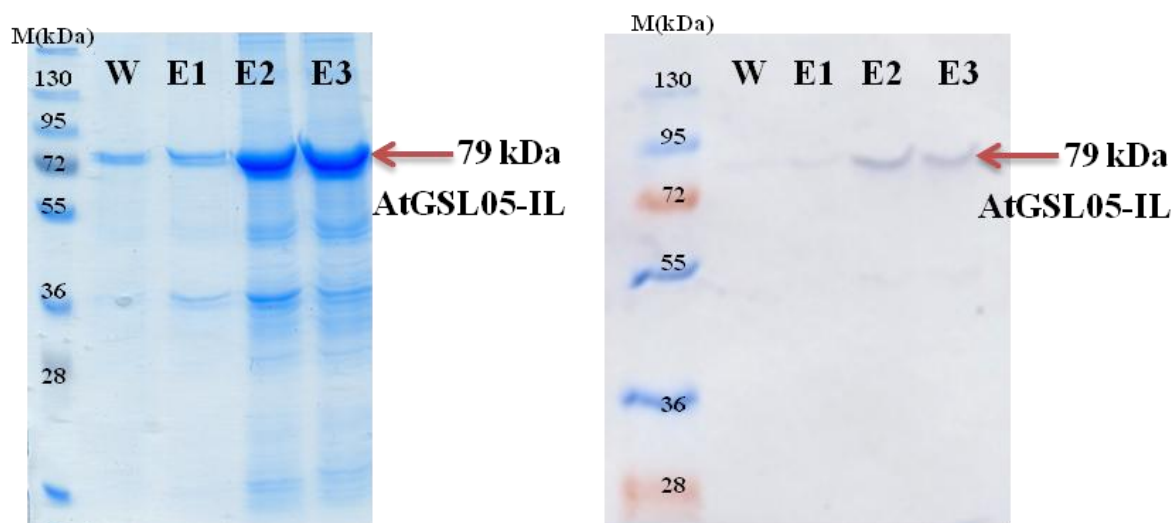
Figure 17: 10 % SDS-PAGE analysis after Nickel-affinity chromatography:

SDS-PAGE and Western blot analysis of the expressed AtGSLO5-IL were performed after Ni^{2+}-affinity chromatography. Western blot was used for the immunological detection using mouse anti-tetra-histidine IgG1 (QIAGEN). 20 μl sample from each of the fractions and 5 μl of the marker (M) were used in the SDS-PAGE (left) and Western blot (right) analysis. W: Wash, E1: 30 mM Imidazole Elution, E2: 150 mM Imidazole Elution, E3: 200 mM Imidazole Elution. Red arrows indicate the AtGSLO5-IL protein bands.

The identification of proteins by mass spectrometry was performed using peptide mass fingerprint (PMF). Therefore, AtGSLO5-IL protein band (Figure 18, B) was excised from the SDS-PAGE gel, and the protein was digested into sequence-specific peptides using trypsin and analyzed by MALDI-TOF mass spectrometry (MALDI-TOF MS) to verify the identity of the single protein band (Figure 19). MS fullscan spectra plot intensities against the mass-to-charge (m/z) ratios of the peptides. Database searches using Mascot software shows that the detected peptides cover 28 % of the full length callose synthase 12/ GSL05 protein sequence from *A. thaliana*.

4 Results

The identified sequences are below and belong to the AtGSLO5-IL protein of *Arabidopsis thaliana* (the detected peptides cover 70 % of the AtGSLO5-IL protein sequence from A. *thaliana*).

Sequence: Callose Synthase 12 full length protein sequence: Protein sequence coverage was 28 % of the full length and 70 % of the AtGSLO5-IL protein sequence. Matched peptides are shown in red

AVVGLFDHLGEIRDMGQLR**LR**FQFFASAIQFNLMPEEQLLNAR**GFGNKFKDGIHRLKLR**YGF GRPFK**KLESNQVEANK**FALIWNEIILAFR**EEDIVSDREVELLELPK**NSWDVTVIR**WPCFLLC NELLLALSQAR**ELIDAPDKWLWHK**ICKNEYRRCAVVEAYDSIK**HLLLSIIKVDTEEHSIITV FFQIINQSIQSEQFTK**TFRVDLLPKIYETLQK**LVGLVNDEETDSGRVVNVLQSLYEIATRQF FIEK**KTTEQLSNEGLTPR**DPASKLLFQNAIRLPDASNEDFYR**QVR**RLHTILTSRDSMHSVPV NLEAR**RR**IAFFSNSLFMNMPHAPQVEKMMAFSVLTPYYSEEVVYSK**EQL**RNETEDGISTLYY LQTIYADEWK**NFKERMHREGIKTDSELWTTKLRDLR**LWASYR**GQTLARTVR**GMMYYYRALKM LAFLDSASEMDIREGAQELGSVRNLQGELGGQSDGFVSENDR**SSLSR**ASSSVSTLYKGHEYG TALMKFTYVVACQIYGSQK**AKK**EPQAEEILYLMKQNEALRIAYVDEVPAGR**GETDYYSVLVK**YDHQLEKEVEIFR**VKLPGPVK**LGEGKPENQNHAMIFTRGDAVQTIDMNQDSYFEEALK**MRNL**LQEYNHYHGIRKPTILGVR**

In summary, SEC revealed the existence of higher oligomeric states of the purified AtGSLO5-IL in solution. The identity of the AtGSLO5-IL protein was also verified with MALDI-TOF MS, applying a single coomassie-stained band excised from the SDS-PAGE gel.
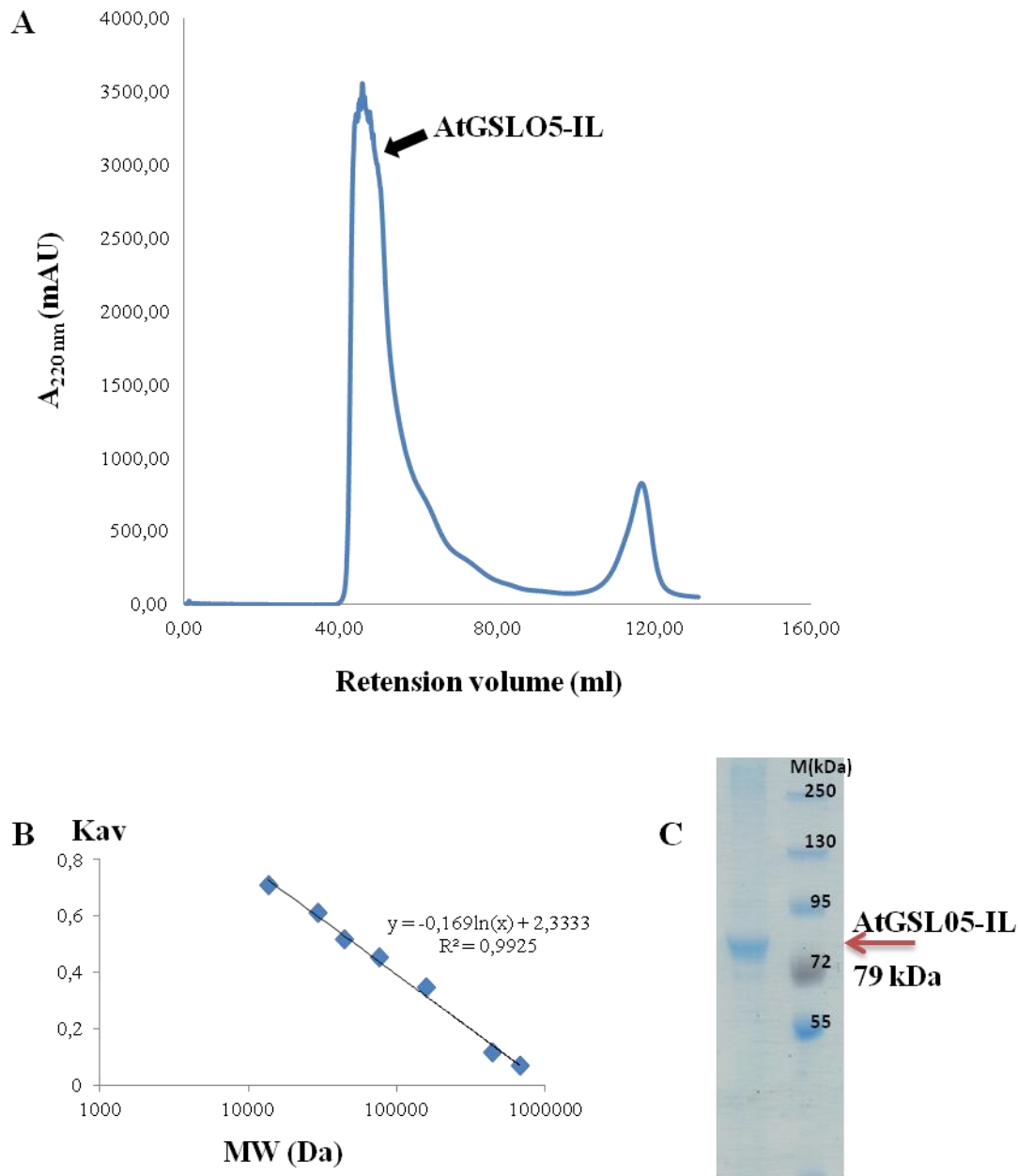
Figure 18: *A: Chromatogram of AtGSLO5-IL after gel filtration. B: HiLoad 16/60 Superdex 200 prep grade matrix calibrations. C: 10 % SDS-PAGE after gel filtration. The protein sample was purified on a HiLoad 16/60 Superdex 200 prep grade gel filtration column. 5 µl of the marker (M) and 20 µl of the His-tagged AtGSLO5-IL protein were used in the SDS-PAGE analysis. Analysis of the purified protein after size exclusion chromatography by non reducing SDS-PAGE (indicated by a red arrow) corresponded to the monomeric MW of the AtGSLO5-IL (79 kDa).*
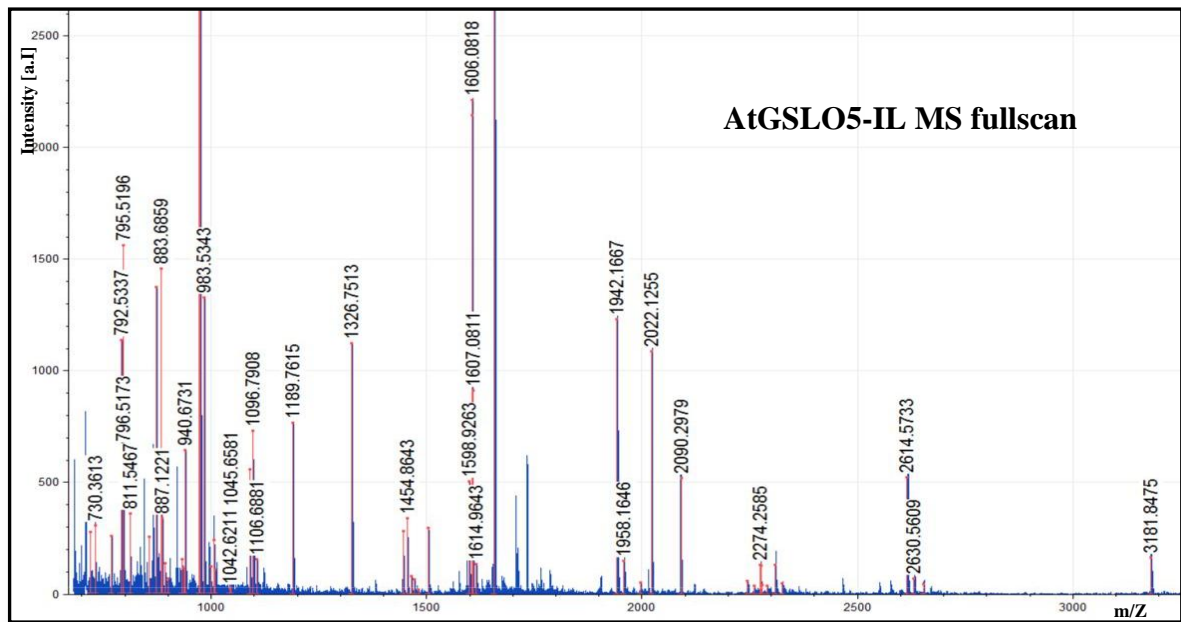
Figure 19: Mass spectrometry spectrum: Spectrum detected with peptide mass fingerprint analysis. Callose Synthase 12/ GSL05 from A. thaliana was clearly identified. Trypsin cuts C-term side of lysine, argenine unless the next residue is a proline. Protein sequence coverage was 28 % of the full length callose synthase 12/ GSL05 and 70 % of the AtGSLO5-IL protein sequence.

4.1.3 Characterization of the β-1,3-glucan synthesis

To investigate the activity of the AtGSLO5-IL protein, transmission electron microscopy analysis was performed after cell lysis and purification of the AtGSLO5-IL to verify in vitro (1,3)-β-glucan synthesis. The transmission electron microscopy (TEM) analysis (Figure 20, a) shows the presence of predominantly nanofibers (Nf) with about 3-5 nm diameter as well as 30-50 nm diameter sized microfibers (Mf) composed of helical twisted nanofibers, indicating the (1,3)-β-glucan biopolymer synthesis by AtGSLO5-IL under membrane-free, in vitro conditions using UDP-glucose as substrate. These biopolymers were not present in assays without UDP-glucose (Figure 20, b1 and b2). The (1,3)-β-glucan biopolymer formation was also associated by the presence of AtGSLO5-IL protein complexes or oligomers (AO5) at the ends of microfibers (Figure 20, a, b1 and b2).
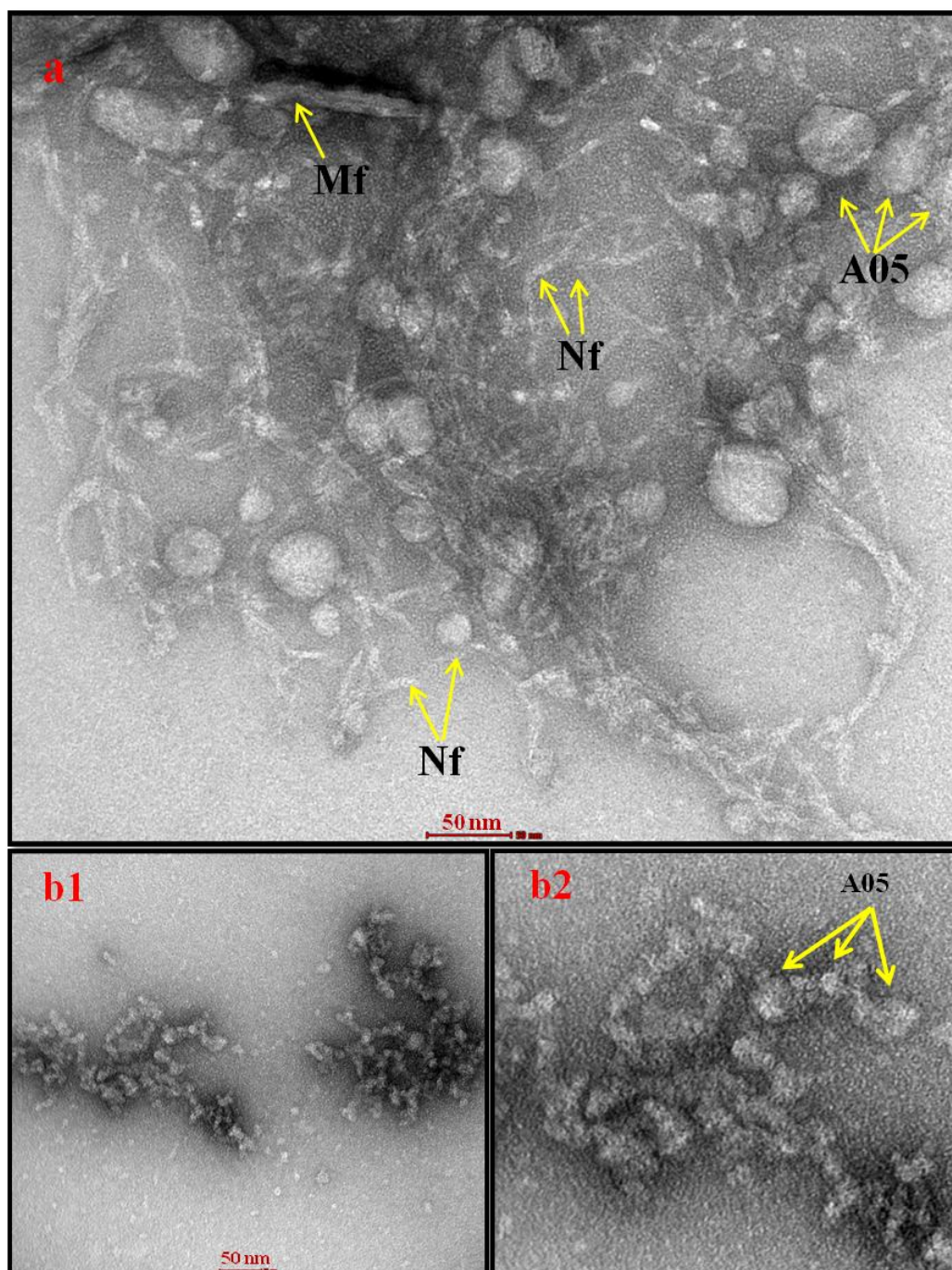
Figure 20: In vitro transmission electron microscopy (TEM) of purified AtGSLO5-IL

In vitro synthesis of (1,3)-β-glucan biopolymer by the purified cytosolic domain of a (1,3)-β-glucan synthase. (a): TEM of assay using UDP-glucose as substrate, (b1) and (b2): TEM of assay without UDP-glucose (negative controle). Mf: Microfibers. Nf: Nanofibers and AO5: AtGSLO5-IL protein complexes (oligomerizations). Presence of 3-5 nm diameter nano-fibers (Nf), 30-50 nm diameter sized microfibers (Mf) and AtGSLO5-IL oligomers (AO5) at the ends of microfibers.

4.1.4 Enzymatic activity assays

To examine whether the pH and salt concentration, have an influence on the enzymatic activity of the AtGSLO5-IL, an enzyme linked-immunosorbent assay (ELISA) test was performed in the presence of UDP-glucose as substrate. Six different pH values with different salt concentrations were tested. The highest (1,3)-β-glucan deposition was observed for 20 mM Tris-HCl, pH 7.3 with 3 mM NaCl (Figure 21). DLS measurements on the cytosolic domain of a (1,3)-β-glucan synthase were also performed without the UDP-glucose substrate (Figure 22).

pH and NaCl values

Legend:
- pH = 7,3; 2 mM CaCl2
- pH = 7,3; 3 mM NaCl
- pH = 8,0; 3 mM NaCl
- pH = 8,0; 30 mM NaCl
- pH = 8,0; 150 mM NaCl
- pH = 8,8; 30 mM NaCl
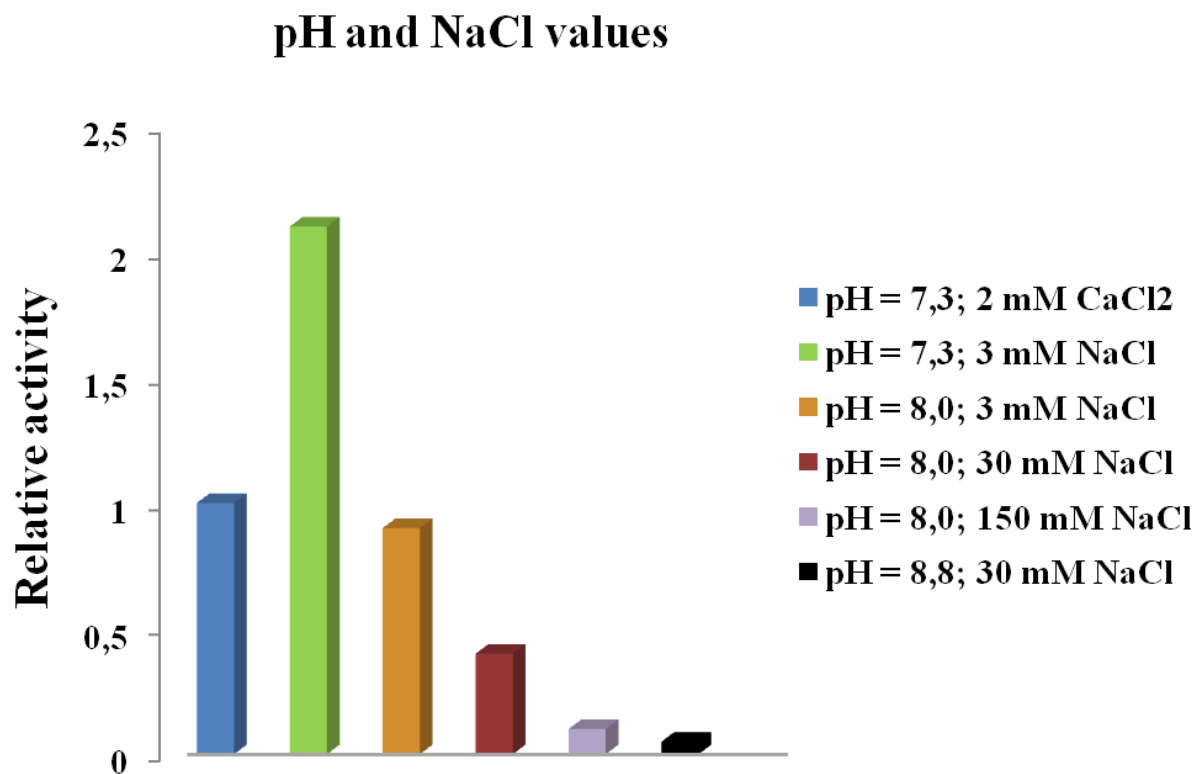
Figure 21: Enzymatic activity test of the cytosolic domain of a (1,3)-β-glucan synthase enzyme linked-immunosorbent assay (ELISA). To test the in vitro (1,3)-β-glucan polymer synthesis by the cytosolic domain of a (1,3)-β-glucan synthase: ELISA was performed for the purified AtGSLO5-IL using different buffers in the presence of UDP-glucose as the substrate. The ELISA was performed by Dr. Björn Sode, reasearch group of Prof. Dr. Christian A. Voigt).
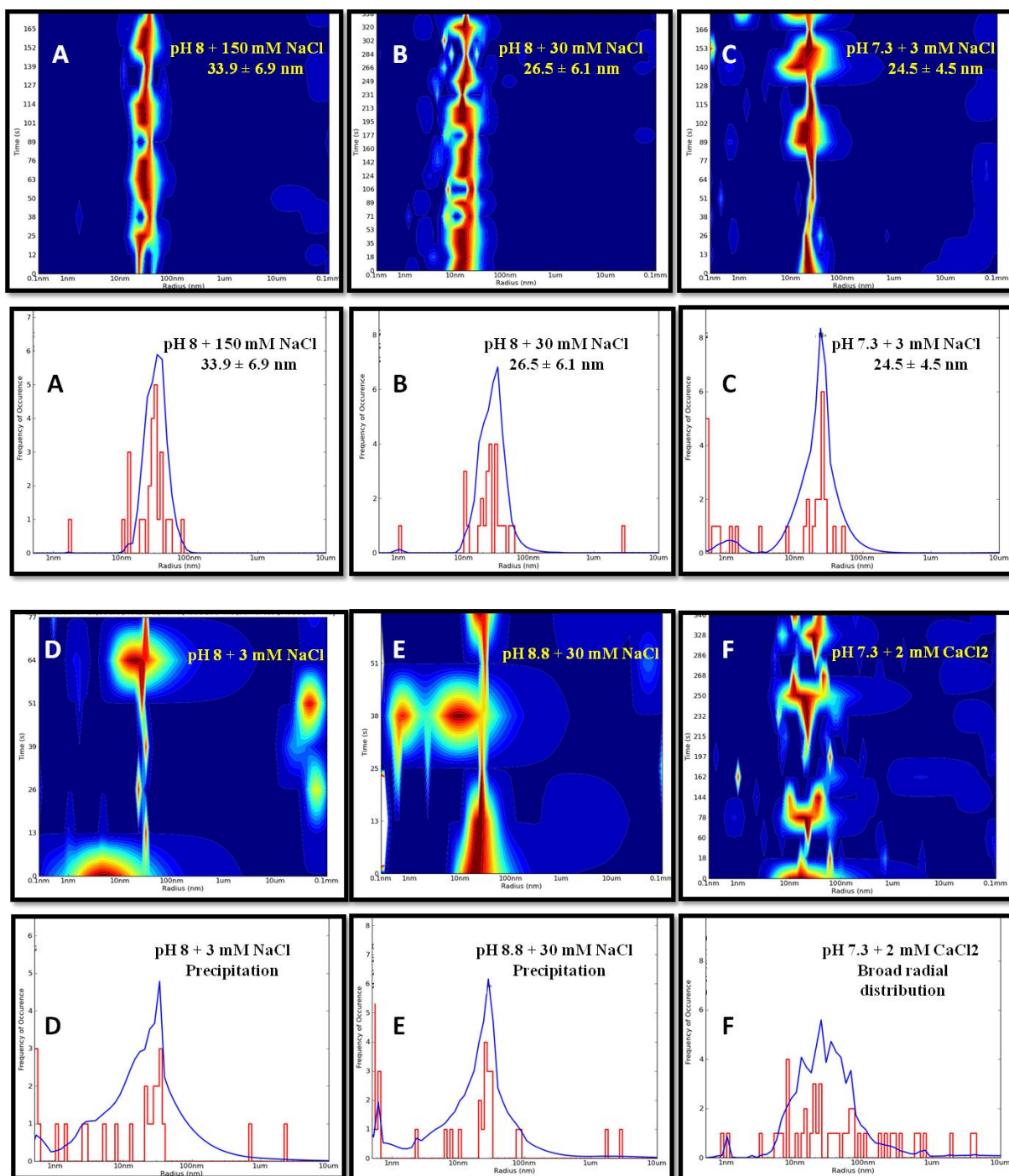
Figure 22: Buffer dependency of the AtGSLO5-IL protein:

Dynamic light scattering (DLS) of AtGSLO5-IL after dialyzing into six different buffers and salt concentrations.

The purified AtGSLO5-IL protein was dialyzed against the same six different buffer solutions used for the enzyme linked-immunosorbent assay. When using buffers D and E, the protein started to significantly precipitate (Figure 22, D and E). With buffer F (Figure 22, panel F), the protein doesn't precipitate but shows a very broad radial distribution indicative of polydispersity of the protein. Buffer A, B and C (Figure 22, A, B and C) revealed radial distributions of 33.9 ± 6.9, 26.5 ± 6.1 and 24.5 ± 4.5 nm respectively.

Concluding, the TEM shows that in vitro (1,3)-β-glucan polymer synthesis by the cytosolic domain of a (1,3)-β-glucan synthase was associated with AtGSLO5-IL oligomerization at the ends of microfibers (Figure 20). The AtGSLO5-IL oligomerization also occurred in the DLS measurements without the UDP-glucose substrate. The lowest radius value (Figure 22, C) and the highest enzymatic activity of the cytosolic domain of a (1,3)-β-glucan synthase (Figure 22) were observed when using buffer C (pH 7.3 + 3 mM NaCl).

4.1.5 Circular dichroism and dynamic light scattering

Circular dichroism (CD) spectroscopy of the purified AtGSL05-IL was performed using a J-815 CD spectrometer (Jasco, Germany) at wavelengths of 240 to 190 nm to verify the folding quality and for determining the secondary structure composition. A protein concentration of 0.5 mg/ml was sufficient to record a CD-spectrum (Figure 23, B) in order to estimate the secondary structure composition and for verifying the folding state of the protein. The secondary structure spectrum for the AtGSLO5-IL revealed one strong positive peak in the vicinity of 196 nm and three minima at 210 nm, 216 nm and 222 nm. Fractions of β-sheet are indicated by the single minimum at 210 nm and the two other minima are characteristic for a largely α-helical structure. The secondary structure, estimated according to Yang *et al.,* 1986 using the JASCO software (Figure 25, D), shows the presence of about 55 % α-helical structure, 8 % of turns, 25 % of β-sheet and approximately 12 % of random coils.

DLS analysis was performed on the protein solution after buffer optimization in order to determine the homogeneity and the oligomerization state of the protein solutions. The radius distribution plot of the protein solution (Figure 23, A) shows a very narrow peak at a hydrodynamic particle radius of 12.0 ± 0.2 nm.

Concluding, the CD-spectrum indicates a well folded AtGSL05-IL protein with more than 50 % α-helical structure. DLS analysis shows a hydrodynamic particle radius of 12 ± 0.2 nm.

As the calculated molecular weight of the protein is approximately 79 kDa, a particle size of around 4 nm is anticipated. However, the particle size in the radius distribution plot indicates that the protein is present in solution as a large oligomer and not as a monomer (Figure 23, A), which was also confirmed by the performed native PAGE (Figure 23, C).

Fractions	Ratio (%)
Helix	55
Beta	25
Turn	8
Random	12
RMS value	4
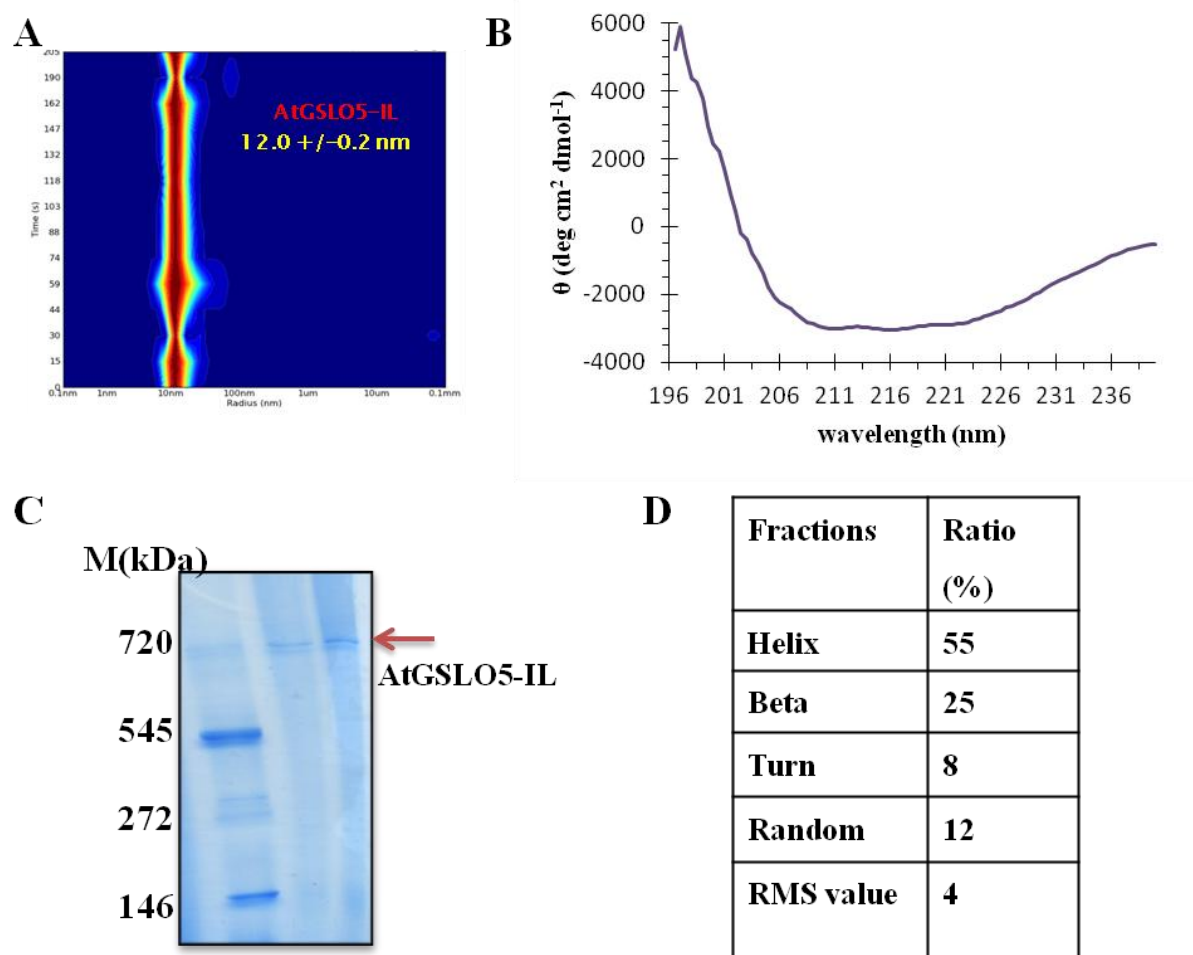
Figure 23: CD spectroscopy and Dynamic light scattering of AtGSLO5-IL:

(A) Radius distribution of the AtGSLO5-IL with N-terminal His-tag and C-terminal Strep-tag fusion after size exclusion chromatography. Fifteen measurements of 15 seconds at an interval of 1 second were collected. (B) CD spectroscopy of purified AtGSLO5-IL indicates protein's secondary structure composition. One positive maximum at about 197 nm and three negative minima were observed at about 210 nm, 216 and 222 nm. (C) Native PAGE: M: Marker (SERVA Electrophoresis). (D) Secondary structure estimation based on Yang et al. (1986) using JASCO software.

4.1.6 Structure investigation applying small angle X-ray scattering (SAXS)

In order to verify the shape and oligomeric state of AtGSLO5-IL in solution SAXS measurements were performed. The processed SAXS pattern from AtGSLO5-IL is displayed in Figure 24. Rigid body modelling was performed using the program CORAL (Petoukhov *et al*., 2012). Starting from a best of tentative model, predicted using the web Server IntFOLD (McGuffin *et al.,* 2015), the CORAL program uses simulated annealing to search for a non-overlapping interconnected configuration of known domains connected by extended linkers fitting the experimental data. The overall parameters evaluated from SAXS data are summarized in Table 4.1.6. The scattering data and the models are deposited in the SASBDB (Valentini *et al*., 2015), code: SASDBN4. The molecular weight (MW) estimated from the Porod volume of the particle in solution is 634 ± 63 kDa, and the MW estimated from the *ab initio* reconstruction is 655 ± 66 kDa, which is compatible with octameric AtGSLO5-IL in solution. The protein is characterized by a radius of gyration (R_g) of 7.8 ± 0.8 nm, the maximum intraparticle distance (D_{max}) is 30 ± 3 nm.

The shape of AtGSLO5-IL in solution was reconstructed *ab initio* using the program DAMMIF: without symmetry restrictions the resulting shape was flat with extended appendages (not shown); the final model was constructed with imposed P8 symmetry (χ^2 = 1.2, Figure 24, A). The extended sprouts on the periphery of the model suggest certain flexibility. To predict disordered sites in the AtGSLO5-IL protein, the server FoldIndex (Prilusky *et al*., 2005) was employed. Based on the amino acid sequence, 28 % of the protein was predicted to be disordered, including the strep-Tag sequence (see below). A tentative model of AtGSLO5-IL was reconstructed using the rigid body modelling program CORAL (Petoukhov *et al*., 2012) resulting in a good fit (χ^2 = 1.0, Figure 24, B). The *ab initio* shape is well compatible with the CORAL model (Figure 24, C1, C2, D1 and D2).

AtGSLO5-IL sequence: Predicted disordered segment are colored in red, the disordered linker is underlined with a thin line and the disordered strep tag is underlined with a thick line

MASRGSHHHHHHGAGDRGPEFELGTRGSCAVVGLFDHLGEIRDMGQLRLRFQFFASAIQFNL
MPEEQLLNARGFGNKFKDGIHRLKLRYGFGRPFKKLESNQVEANKFALIWNEIILAFREEDI
VSDREVELLELPKNSWDVTVIRWPCFLLCNELLLALSQARELIDAPDKWLWHKICKNEYRRC

AVVEAYDSIKHLLLSIIKVDTEEHSIITVFFQIINQSIQSEQFTKTFRVDLLPKIYETLQKL
VGLVNDEETDSGRVVNVLQSLYEI**ATRQFF**IEKKTTEQLSNEGL**TPRDPASKLL**FQNAIRLP
DASNEDFYRQVRRLHTILTSRDSMHSVPVNLEARRRIAFFSNSLFMNMPHAPQVEKMMAFSV
LTPYYSEEVV**YSKEQLRNETEDGISTLYYLQTIYADEWKNFKERMHREGIKTDSELWTTKLR**
DLRLWASYRGQTLARTVRGMMYYYRALKMLAFLDSASEMDIREGAQELGSV**RNLQGELGGQS**
DGFVSENDRSSLSRASSSVSTLYKGHEYGTALMKFTYVVACQIYGSQKAKKEPQAEEILYLM
KQNEA**LRIAYVDEVPA**GRGETDYYSVLVKYDH**QLEKE**VEIFRVKLPGPVKL**GEGKPENQNH**A
MIFTR**GDAVQTIDMNQDSYF**EEALKMRNLLQEYNH**YHGIRKPTILGVR**HAHGLSA**WSHPQFE**
K

Table 4.1.6: SAXS data collection and analysis parameters

Data collection parameters	
Instrument	EMBL beamline P12 (Blanchet *et al.*, 2015)
Wavelength (nm)	0.124
s-range (nm^{-1})	0.03–4.8
Exposure time (s)	0.05×20
Concentration range (mg/ml)	1.0–2.0
Temperature (K)	283
Structural parameters	
R_g (nm) (from Guinier)	7.8 ± 0.8
R_g (nm) (from p(r))	8.0 ± 0.8
D_{max} (nm)	30 ± 3.0
Molecular mass determination	
MW (kDa) from Porod volume	634 ± 63
MW (kDa) from DAMMIF volume	655 ± 66
Calculated MW (kDa) from sequence	79
Software employed	
Primary data reduction and processing	Automated SAXS data analysis pipeline (Franke *et al.*, 2012)
Ab initio **analysis**	DAMMIF (Franke and Svergun 2009)
Rigid body modelling	CORAL (Petoukhov *et al.*, 2012)
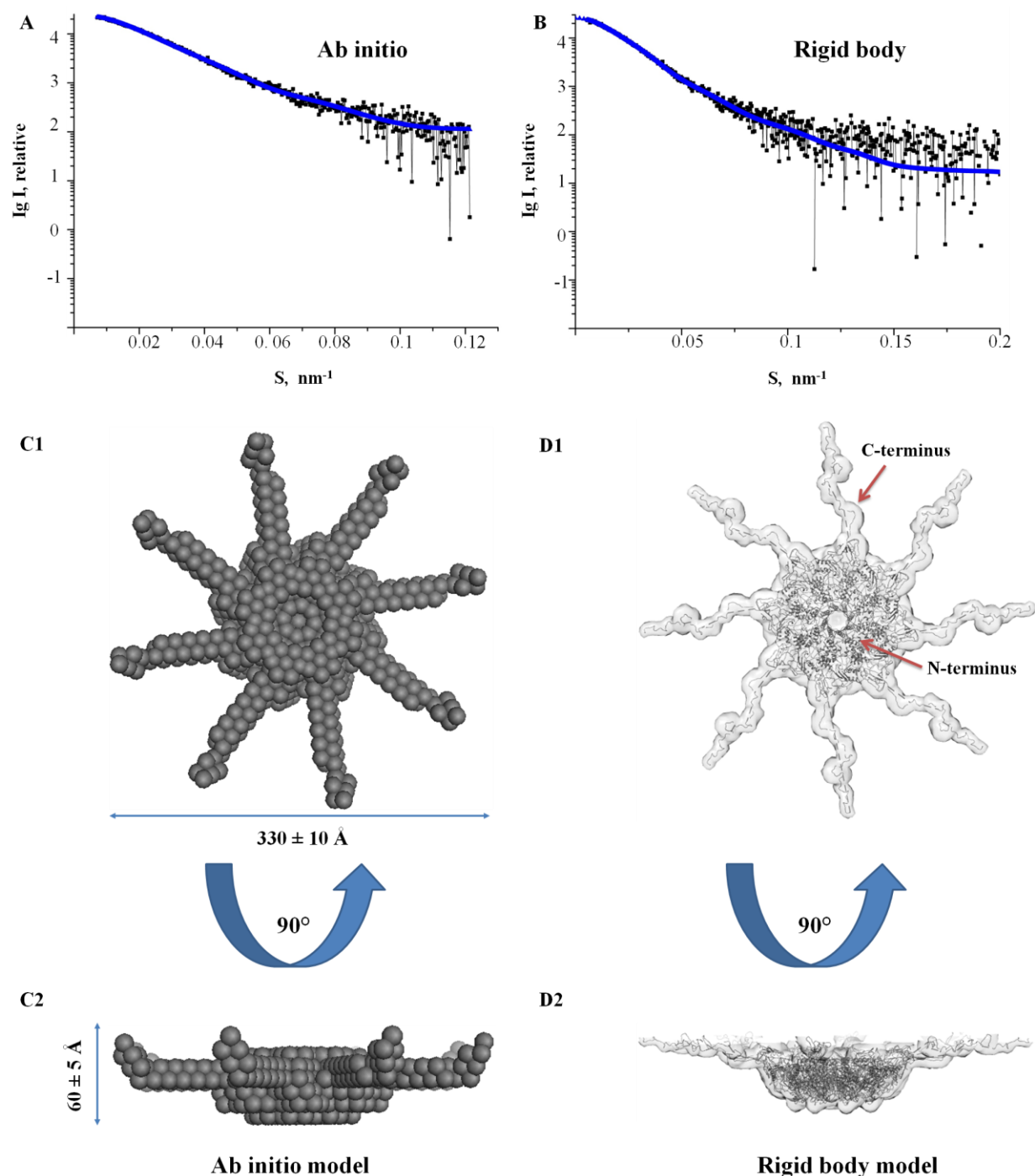
Figure 24: Scattering curves and SAXS ab initio and rigid body modelling of AtGSLO5-IL:
A: *Scattering curve of the DAMMIF ab initio model generated using Origin software, B: Scattering curve of the CORAL rigid body model generated using Origin software. X-ray synchrotron radiation data were collected at the P12 beamline. C1 and C2: Ab initio model performed using DAMMIF. D1 and D2: Multi-domain rigid body model performed using CORAL. Pictures of the Models were generated using CHIMERA (Pettersen et al., 2004) and PyMol (PyMOL Molecular Graphics System, Version 1.3, Schrödinger, LLC.).*

Concluding, the shape and the oligomeric state of AtGSLO5-IL in solution were verified by the SAXS measurements. An *ab initio* model of the AtGGSLO5-IL was constructed with imposed P8 symmetry (χ^2 = 1.2, Figure 24, A) confirming the results obtained by DLS (Figure 23, A) and native page (Figure 23, C) indicating that the protein is present in solution as a large oligomer and not a monomer. The molecular weight (MW) estimated from the Porod volume of the particle in solution (634 ± 63 kDa), and the MW estimated from the *ab initio* reconstruction is 655 ± 66 kDa. The ab initio model shows an oblate form of the protein with extended 8-arm starfish-like sprouts on the periphery. Due to the predictedted intrinsically unfolded regions, an algorithm for modelling of multidomain protein complexes against multiple data sets (Konarev & Svergun, 2012) was needed to build a rigid body model. A tentative model of AtGSLO5-IL was constructed using the program CORAL (Petoukhov *et al*., 2012) resulting in a good fit (χ^2 = 1.0, Figure 24, B). The CORAL model (Figure 24, D1 and D2) was well compatible with the *ab initio* shape (Figure 24, C1 and D2), showing also an oblate form of the protein with extended C-terminal 8-arm starfish-like sprouts on the periphery, including the predicted unfolded C-terminal strep-tag.

4.1.7 Structure investigation applying electron microscopy

As demonstrated in chapters 4.1.3, 4.1.4, 4.1.5 and 4.1.6, the oligomerization state and the shape plays a very major role on the activity of the AtGSLO5-IL protein, further structural investigation was needed. Thus, negative stain electron microscopy was carried out at the HPI Hamburg, to get more information about the shape of the protein (Figure 25, A and B).

The negative stain electron microscopy shows molecules of about 28 - 33 nm diameter (Figure 25, A and B), which corresponds to the particle size calculated from the *ab-initio* SAXS model. *In planta* super-resolution-microscopy (STORM) was also applied (Figure 25, C) by Prof. Dr. Christian A. Voigt, AtGSLO5 full length was coupled to a C-terminal GFP-Tag and injected into the plant leaves of *A. thaliana*. Stochastic optical reconstruction microscopy (STORM) was then performed indicating the AtGSLO5 intrinsic tendency to form octamers.
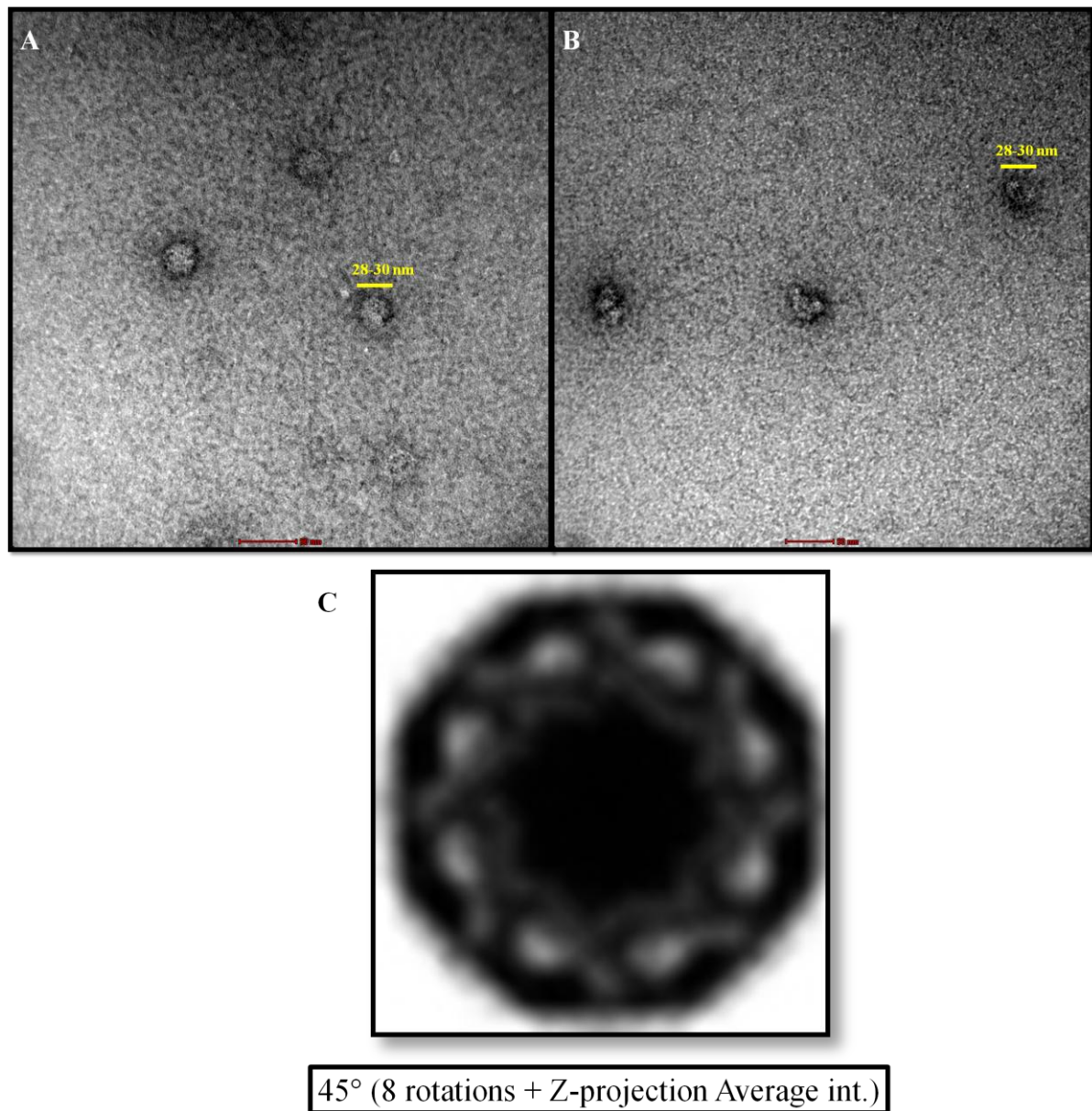
Figure 25: *A and B: Negative stain electron microscopy using uranyl acetate as stain. C: In planta super-resolution-microscopy (STORM): The full length AtGSLO5 was coupled to a C-terminal GFP-Tag.*

4.2 Senescence associated ubiquitin ligase1 (SAUL1) and armadillo (ARM) 7-11 repeats

4.2.1 Cloning and transformation

The genes of the SAUL1 and ARM 7-11ΔC were cloned into a pGEX-6p-1 vector, carrying ampicillin resistance, offering an N-terminal GST-tag to enable subsequent purification from *E. coli* after heterologous gene expression. The cloning was performed with the help of Catharina Brieske in the Lab Prof. Dr. Hoth. The ampicilin resistant transformation of *E coli,* BL21 (DE3) competent cells, with the plasmid was described in more details in the methods section (Chapter 3.2.2).

4.2.2 Purification

After recombinant expression (see methods section; Chapter 3.2.3.2), purification of the N-terminal GST-tagged SAUL1 and ARM 7-11ΔC proteins using GST-affinity chromatography was performed followed by a PreScission Protease cleavage of the GST-Tag.
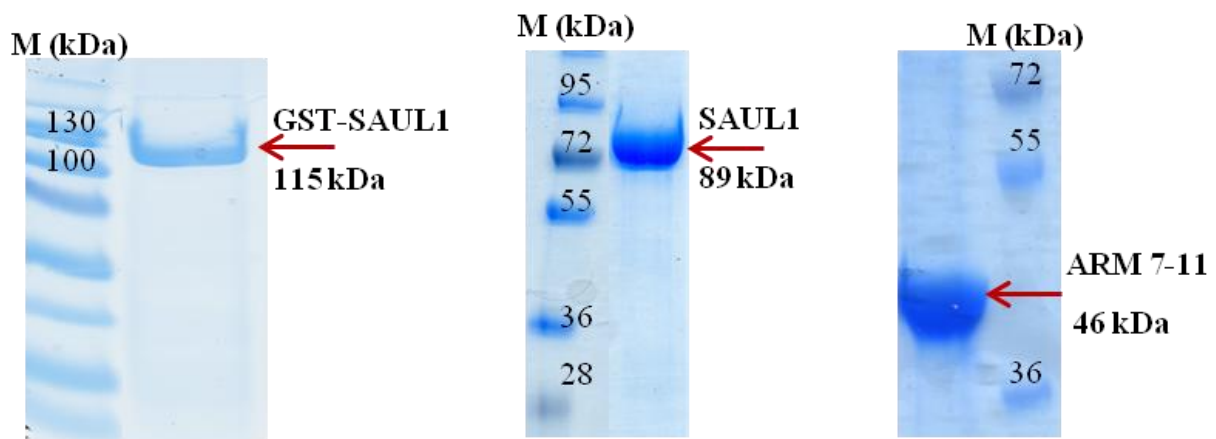
Figure 26: 10 % SDS-PAGE analyses after gel filtration chromatography:

A: GST-SAUL1 fusion protein, B: SAUL1-full length without GST-Tag, C: ARM 7-11ΔC.

20 µl samples from each of the collected fractions and 5µl from the marker (M) were used in the SDS-PAGE analysis. Analyzing of the purified proteins after size exclusion chromatography by non reducing SDS-PAGE (indicated by red arrows) corresponded to the monomeric MW of the GST-SAUL1 (115 kDa), SAUL1 (89 kDa) and ARM 7-11ΔC (45 kDa).
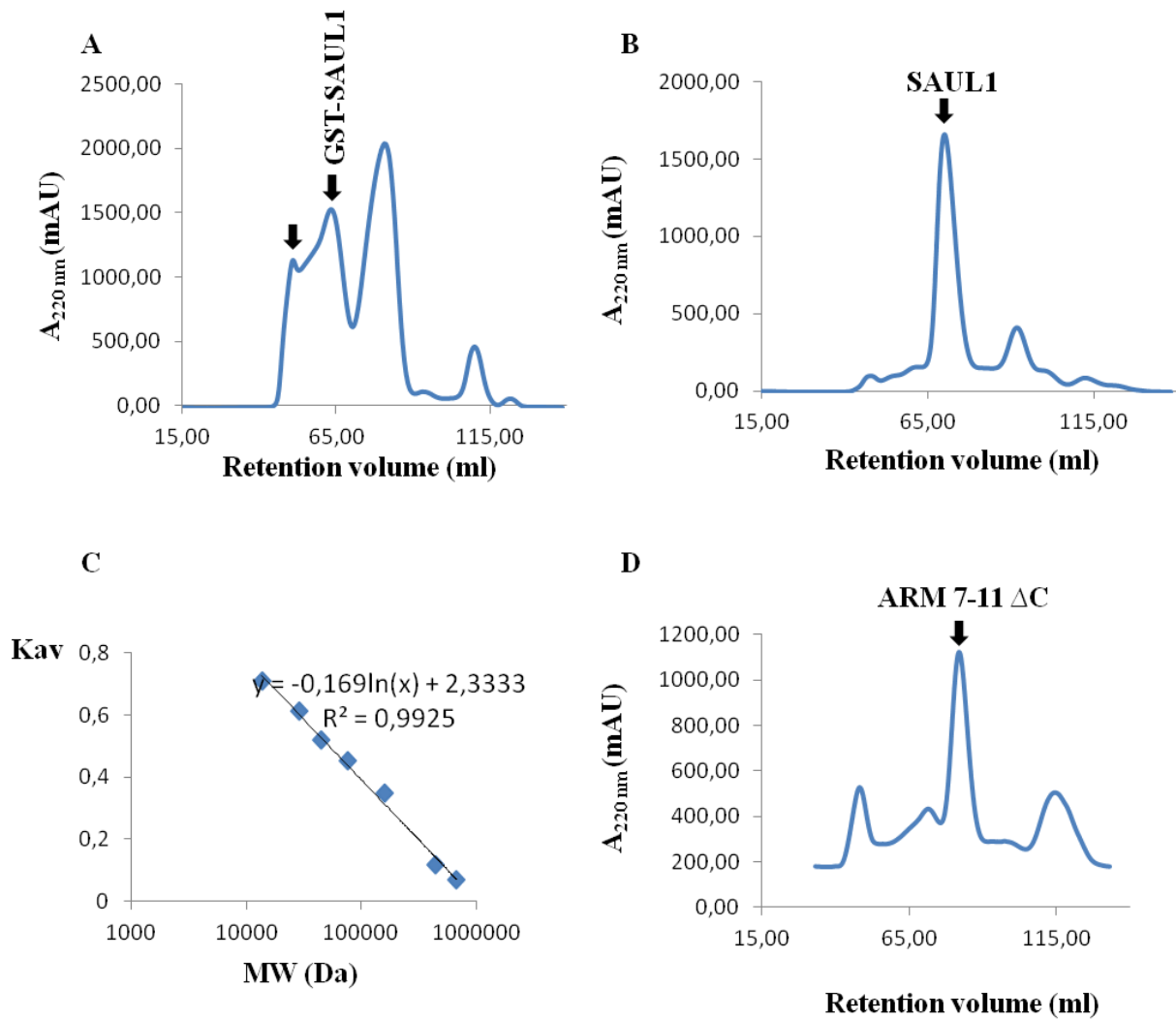
Figure 27: A: Size exclusion chromatogram of the GST- SAUL1, B: Size exclusion chromatogram of SAUL1 protein, C: HiLoad 16/60 Superdex 200 prep grade column calibrations and D: Size exclusion chromatogram of ARM 7-11ΔC protein. Proteins samples were purified by a HiLoad 16/60 Superdex 200 prep grade gel filtration column. The purified GST-SAUL1, SAUL1 and ARM 7-11ΔC proteins peaks are indicated by black arrows.

To improve the purity and analyze the oligomerization state of the proteins, the affinity chromatography step was followed by size exclusion chromatography. Analyzing protein fractions by SDS-PAGE, protein bands corresponding to the MW of the SAUL1-GST (115 kDa) SAUL1 (89 kDa) and ARM 7-11ΔC (45 kDa) monomer were detected (Figure 26, A, B and C respectively).

4 Results

The GST-SAUL1 showed to be found in the first two peaks (Figure 27, A). According to the SDS-PAGE analysis, the GST-SAUL1 fusion protein found to be present mainly in the second peak (the first peak was containing some impurities). The relative molecular weight of the eluted proteins was interpolated from a linear calibration plot of partition coefficient (Kav) versus log molecular weight. The detected retention volumes from chromatograms were about 64 ml (GST-SAUL1), 70 ml (SAUL1) and 81 ml (ARM 7-11ΔC) which, according to the HiLoad 16/60 Superdex 200 prep grade column calibrations, correspond to molecular weights of about 190 kDa (GST-SAUL1), 110 kDa (SAUL1) and 50 kDa (ARM 7-11ΔC). Thus, indicate that after gel filtration chromatography, GST-SAUL1 fusion protein, SAUL1-full length and ARM 7-11ΔC proteins were present as putatively elongated monomers in solution. The identification of proteins by mass spectrometry was performed using peptide mass fingerprint (PMF). Therefore the protein bands of SAUL1 full length and ARM 7-11ΔC were excised from the SDS-PAGE gels and protein was digested into sequence-specific peptides using Trypsin and analyzed by MALDI-TOF mass spectrometry (MALDI-TOF MS). An m/z ratio mass spectrum was graphically displayed and recorded (Figures 28 and 29). MS fullscan spectra show intensities versus the m/z ratio of peptides. Database searches using Mascot software shows that the detected peptides cover 62 % (SAUL1) and 30 % (ARM 7-11ΔC) of the full length SAUL1 protein sequence from *A. thaliana*.

The identified sequences are displayed below and belong to the SAUL1 and ARM 7-11ΔC proteins.

Sequence 1: SAUL1: Protein sequence coverage was about 62 % of the full length protein sequence of SAUL1, matched peptides shown in red

MVGSSDGDQSDDSSHFERGVDHIYEAFICPLTKEVMHDPVTLENGRTFEREAIEKWFKECRD
SGRPPSCPLTSQELTSTDVSASIALRNTIEEWRSRNDAAKLDIARQSLFLGNAETDILQALM
HVRQICRTIRSNRHGVRNSQLIHMIIDMLKSTSHRVRYKALQTLQVVVEGDDESKAIVAEGD
TVRTLVKFLSHEPSKGREAAVSLLFELSKSEALCEKIGSIHGALILLVGLTSSNSENVSIVE
KADRTLENMERSEEIVRQMASYGRLQPLLGKLLEGSPETKLSMASFLGELPLNNDVKVLVAQ
TVGSSLVDLMRSGDMPQREAALKALNKISSFEGSAKVLISKGILPPLIKDLFYVGPNNLPIR
LKEVSATILANIVNIGYDFDKATLVSENRVENLLHLISNTGPAIQCKLLEVLVGLTSCPKTV
PKVVYAIKTSGAIISLVQFIEVRENDDLRLASIKLLHNLSPFMSEELAKALCGTAGQLGSLV
AIISEKTPITEEQAAAAGLLAELPDRDLGLTQEMLEVGAFEKIISKVFGIRQGDIKGMRFVN
PFLEGLVRILARITFVFNKEARAINFCREHDVASLFLHLLQSNGQDNIQMVSAMALENLSLE

SIK**LTRMPDPPPVNYCGSIFSCVRKPHVVNGLCKIHQGICSLR**ETFCLVEGGAVEK**LVALLD
HENVKVVEAALAALSSLLEDGLDVEKGVKILDEADGIRHILNVLRENRTER**LTR**RAVWMVER
ILRIEDIAREVAEEQSLSAALVDAFQNADFRTRQIAENALK**HIDKIPNFSSIFPNIA

Sequence 2: ARM 7-11ΔC: Protein sequence of ARM 7-11ΔC protein is shown in green. Protein sequence coverage was about 30 % of the full length protein sequence of SAUL1 and about 57 % from the ARM 7-11ΔC protein sequence, matched peptides shown in red

ANIVNIGYDFDKATLVSENRVENLLHLISNTGPAIQCKLLEVLVGLTSCPKTVPKVVYAIK**T
SGAIISLVQFIEVREND**DLR**LASIK**LLHNLSPFMSEELAK**ALCGTAGQLGSLVAIISEK**TPI
TEEQAAAAGLLAELPDRDLGLTQEMLEVGAFEKIISKVFGIRQGDIKGMRFVNPFLEGLVR**I
LAR**ITFVFNK**EAR**AINFCR**EHDVASLFLHLLQSNGQDNIQMVSAMALENLSLESIKLTRMPD
PPPVNYCGSIFSCVR**KPHVVNGLCKIHQGICSLR**ETFCLVEGGAVEK**LVALLDHENVKVVEA
ALAALSSLLEDGLDVEKGVKILDEADGIRHILNVLRENRTER**LTR**RAVWMVERILRIEDIAR
EVAEEQSLSAALVDAFQNADFRTRQIAENALK**HIDKIPNFS
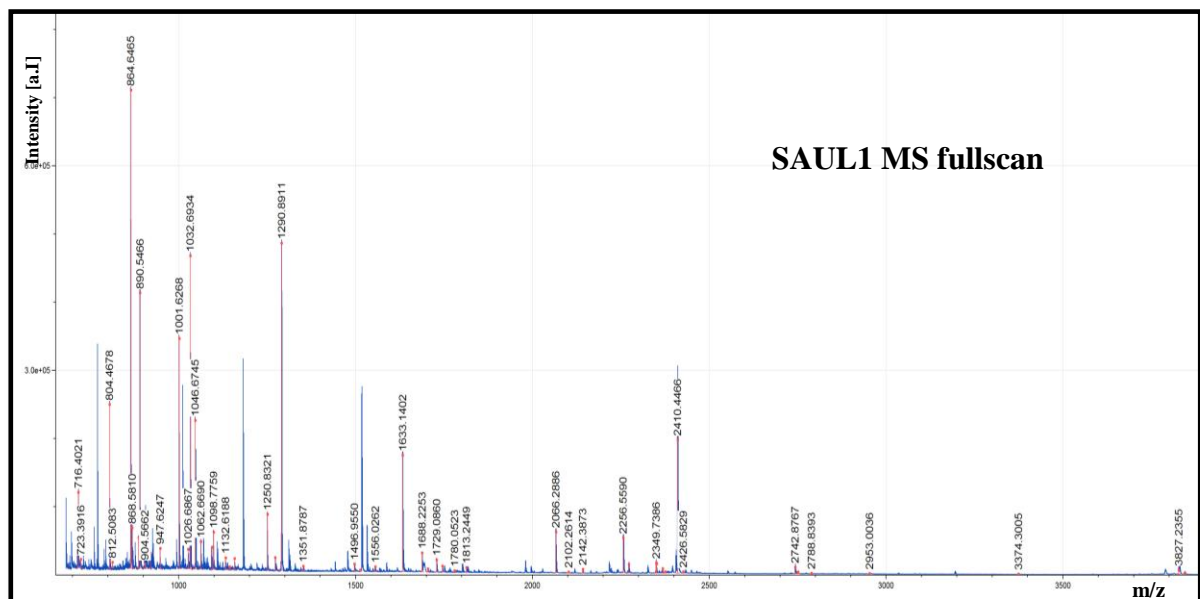

Figure 28: Mass spectrometry spectrum of SAUL1: *Spectrum detected with Peptide Mass Fingerprint analysis. SAUL1 from A. thaliana was clearly identified. Trypsin cuts at the C-terminal side of K and R (Lysine, Argenine) unless the next residue is P (Proline). Detected peptides coverage was 62 % (SAUL1) of the full length SAUL1 protein sequence from Arabidopsis thaliana.*
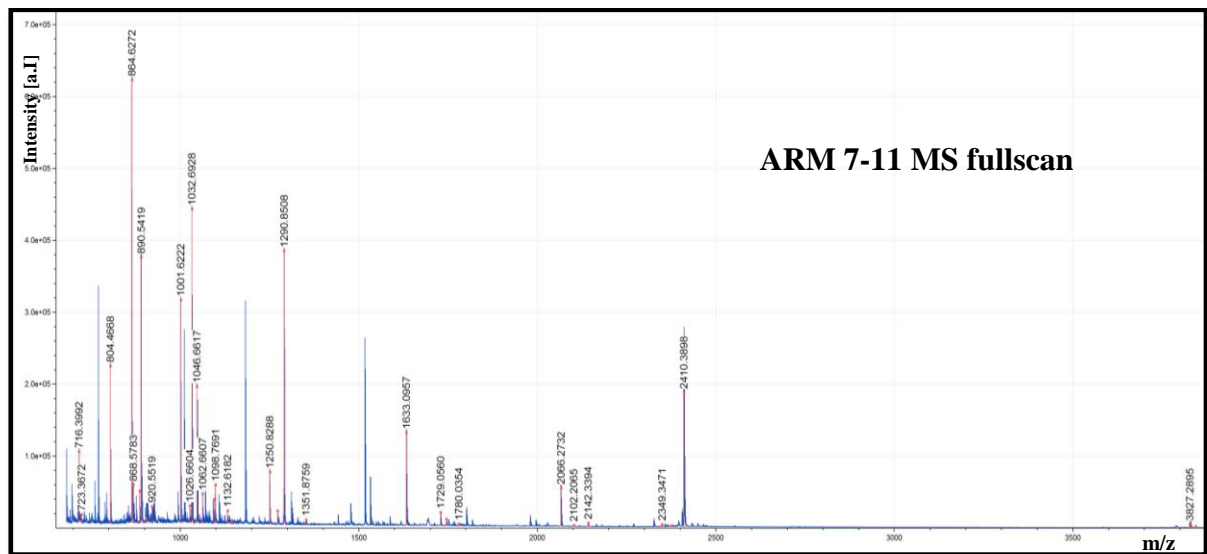
Figure 29: Mass spectrometry spectrum of ARM 7-11ΔC: Spectrum detected with Peptide Mass Fingerprint analysis. ARM 7-11ΔC from A. thaliana was clearly identified. Trypsin cuts at the C-terminal side of K and R (Lysine, Argenine) unless the next residue is P (Proline). Detected peptides coverage was 30 % (ARM 7-11ΔC) of the full length SAUL1 protein sequence from Arabidopsis thaliana.

4.2.3 Circular dichroism of SAUL1 and ARM 7-11ΔC

Circular dichroism (CD) spectroscopy of the purified SAUL1-full length and ARM 7-11ΔC fractions was then performed using J-815 CD spectrometer (Jasco, Germany) at wavelengths of 240 to 190 nm to verify the folding and for determining the secondary structure composition. To eliminate any optically active materials that may affect the measurement, the protein solution was diluted in a 1:1 ratio with water resulting in a final protein concentration of 0.5 mg/ml which was sufficient to record the CD spectra. To estimate the secondary structure, the CD spectra were analyzed based on Reed J & Reed TA, 1997. The CD spectrum of SAUL1 (Figure 30, A1) shows one positive maximum at 192 nm and two negative minima at 207 nm and 222 nm indicating an overall structure of 76 % α-helical domains, 6 % β-sheet, and 8 % turns (Figure 30, A2). The CD-Spectrum of ARM 7-11ΔC (Figure 30, B1) shows one positive maximum at about 194 nm and two negative minima at 207 nm and 222 nm, indicating an overall structure of 42 % α-helical domains, 19 % β-sheet and 5 % Turns (Figure 30, B2). The pooled GST-SAUL1 fusion protein, SAUL1-full length and ARM 7-11ΔC fractions after size exclusion chromatography were concentrated to 1-2 mg/ml and

analyzed by dynamic light scattering in order to judge the homogeneity of the proteins in solution.

A2 Fractions	Ratio (%)
Helix	75
Beta	6
Turn	8
Random	11
RMS value	4

B2 Fractions	Ratio (%)
Helix	42
Beta	19
Turn	5
Random	34
RMS value	4
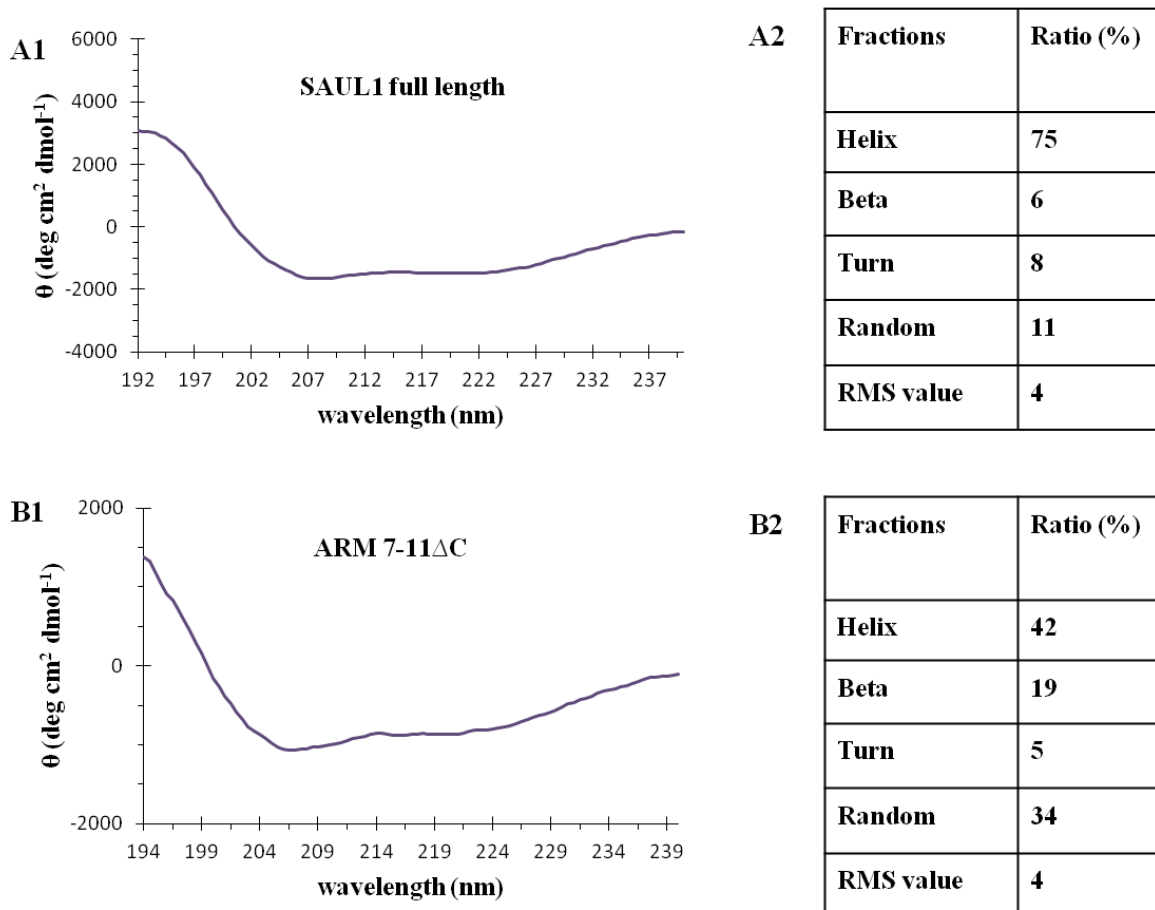
Figure 30: CD spectra and secondary structure estimation of SAUL1 and ARM 7-11ΔC.

A1: CD spectrum of the SAUL1-full length protein after SEC. B1: CD spectrum of the ARM 7-11ΔC protein after SEC. A2: Secondary structure estimation of the SAUL1-full length protein based on Reed J & Reed TA (1997). B2: Secondary structure estimation of the ARM 7-11ΔC protein based on Reed J & Reed TA (1997) using JASCO software.

The three radius distribution plots, showed a narrow peak corresponding to a particle size of 7.2 ± 0.5 nm for GST-SAUL1 fusion protein, 5.3 ± 0.3 nm for SAUL1-full length and 5.3 ± 0.2 nm for ARM 7-11ΔC respectively. As the calculated molecular weight of the GST-SAUL1, SAUL1 and ARM 7-11ΔC monomers are 115 kDa, 89 kDa and 45 kDa respectively, a particle size of about 5 nm for GST-SAUL1, 4 nm for SAUL1 and 3 nm for ARM 7-11ΔC,

was anticipated, assuming a nearly globular shape. This indicates that, GST-SAUL1 fusion protein and ARM7-11ΔC (Figure 31, A1, A2 and C1, C2 respectively) were present in solution as trimers or elongated dimers, while the SAUL1-full (Figure 31, B1 and B2) protein was present in solution as dimer or as elongated monomer. A thermal denaturation assay of SAUL1 was performed, showing that the melting already starts at about 38 °C (Figure 32), which shows, that SAUL1 protein might be relative unstable. More tests were then subsequently performed to investigate the stability of SAUL1in more detail.
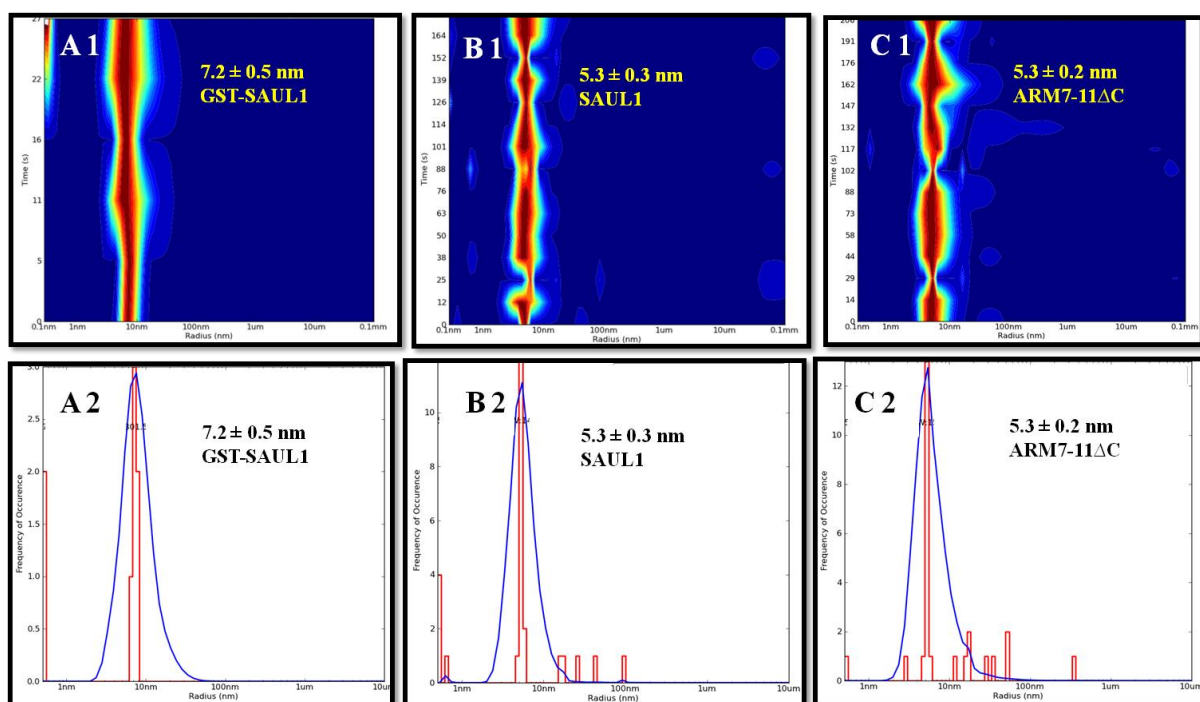
Figure 31: Radius distribution of GST-SAUL1 fusion protein, SAUL1 and ARM 7-11ΔC fractions obtained by dynamic light scattering, depicted as heat map and histogram respectively. *A: Radius distribution of SAUL1 full length with N-terminal GST-tag fusion SEC. B: Radius distribution of SAUL1 after SEC. C: Radius distribution of ARM 7-11ΔC after SEC. Proteins were concentrated to 1 mg/ml using AmiconUltra (MWCO: 30 kDa) device.*

In conclusion, DLS measurements indicate that GST-SAUL1, SAUL1 and ARM7-11ΔC are present in solution as oligomers. Subsequent DLS and SAXS measurements were needed to investigate this in more details. The CD-Spectra (Figure 31, A1 and B1) indicate that SAUL1 and ARM 7-11ΔC are well folded with overall structures of predominantly α-helical domains.

However, unlike SAUL1 (11 % random structure), the quota of random structure of the ARM 7-11ΔC was relatively high (34 %). A thermal denaturation assay of SAUL1 was performed, showing that the melting already starts at about 38 °C (Figure 32), which shows, that SAUL1 might be relative unstable. More tests were then subsequently performed to investigate the stability of SAUL1in more detail.
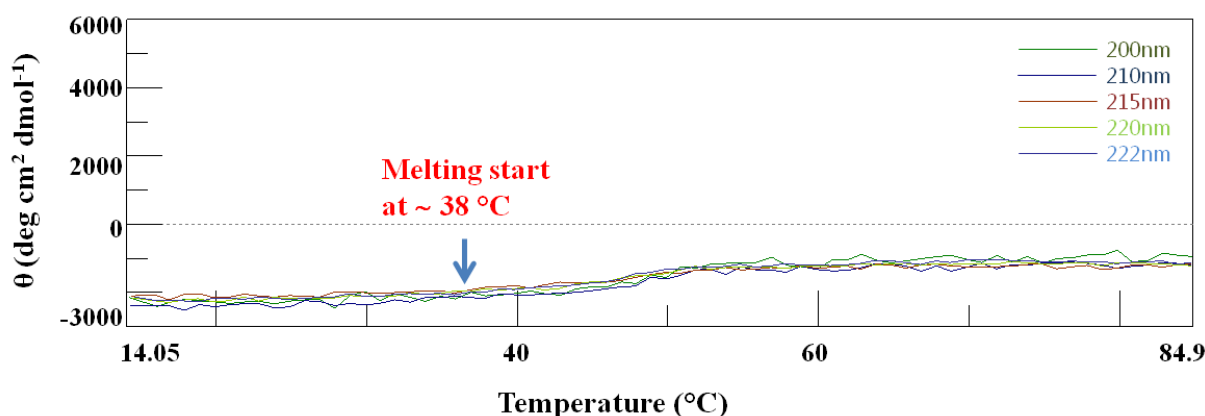

Figure 32: Thermal denaturation assay of SAUL1:

Temperature gradient 14-85 °C, the temperature was increased by 1 °C per minute, with a 5 minutes equilibration time at the initial step. A sample buffer has been used for control. Experiment has been carried out using J-815 CD spectrometer (Jasco, Germany) at 200, 210, 215, 220 and 222 nm wavelengths.

4.2.4 Microscale thermophoresis and thermal stability assay

Microscale thermophoresis experiments were performed in order to investigate the interaction of SAUL1 with different ions which may increase the stability of the protein. Binding affinities (K_d-values) were intended to be measured using a biophysical method, based on individual migration of disolved molecules within a temperature gradient, named microscale thermophoresis (MST, Duhr *et al.*, 2006; Baaske *et al.*, 2010; Wienken *et al.*, 2010). The microscale thermophoresis was followed by a thermal stability assay (Figure 33), performed with the help of Dr. Stephane Boivin, EMBL Hamburg (see method section; Chapter 3.2.7; Boivin *et al.*, 2013). Analysis of the thermophoresis traces by data fitting allowed the determination of the binding affinity of the SAUL1 for the different compounds. No binding

for any of the tested ions was detected. Furthermore, the addition of bivalent ions caused strong precipitation/aggregation of SAUL1.
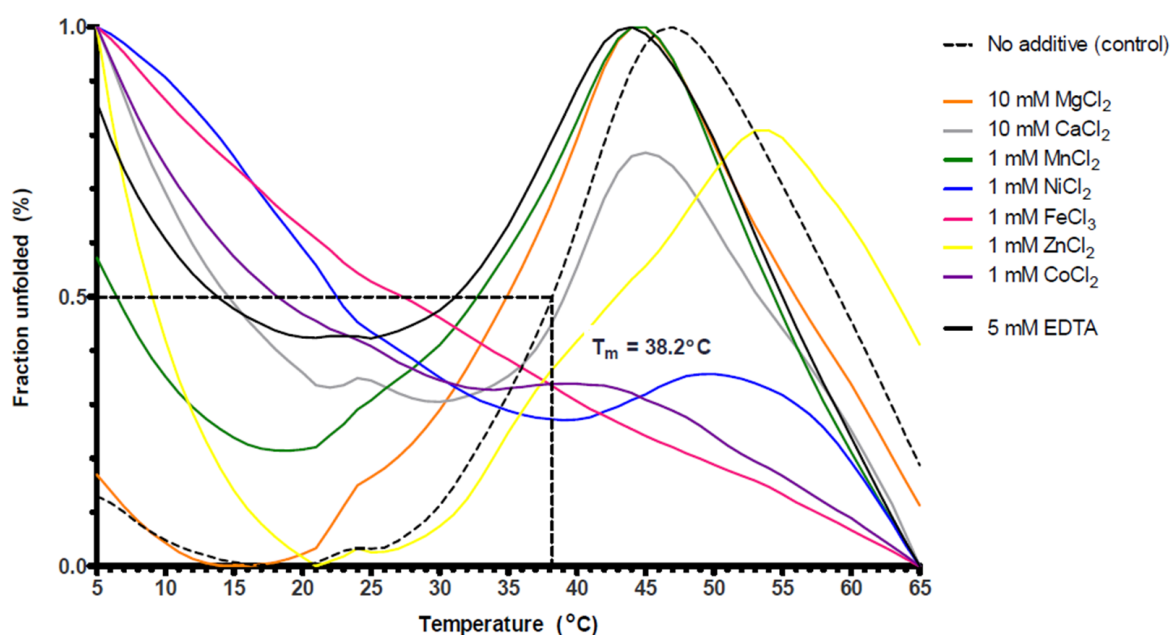
Figure 33: Thermal stability assay of SAUL1 using biltivalent metal ions:

Thermal stability assay was performed using different metal ions. Data was hard to interpret due to unstable baseline and most of the multivalent ions destabilize the protein.

Protein sample at a concentration of 3.5 mg/ml was incubated with a 2 µl Proteostat solution dye or Sypro-Orange solution (10 x) dye in a total volume of 25 µL. Protein solution was then mixed with different bivalent metal ions (Ca^{2+}, Zn^{2+}, Cu^{2+}, Fe^{2+}, Mn^{2+}, Ni^{2+}, Co^{2+}, Mg^{2+}).

4.2.5 Stability tests of SAUL1 and ARM 7-11ΔC proteins

To test the stability of the proteins dependent on the concentration, SAUL1 and ARM 7-11ΔC were further concentrated to 9 mg/ml. The stability of GST-SAUL1 fusion protein dependent on the concentration could not be tested due to aggregation of the protein already at a concentration of 2 mg/ml. The radius distribution plots of the ARM 7-11ΔC protein showed a relative stable narrow peak with particle size of about 5.3 ± 0.2 nm from 1 mg /ml until a concentration of about 4-5 mg/ml (Figure 35, E). At a concentration of 6 mg/ml, the

determined radius increases to 7.2 ± 0.8 nm (Figure 35, F). The radius distribution plots of the SAUL1-full length (Figure 35, A, B, C and D) increase (5.3 ± 0.3 nm, 6.3 ± 0.3 nm, 6.9 ± 0.4 nm and 8.8 ± 0.2 nm) by increasing the concentration of the protein (1-2 mg/ml, 3-4 mg/ml, 5-7 mg/ml and 8-9 mg/ml respectively). Thus, concentrations dependent oligomerization was observed, which is also confirmed by the native pages performed for both proteins (Figure 34). The different oligomerization states are indicated by black arrows (Figure 34). The results obtained, indicate an interaction of SAUL1 with itself.
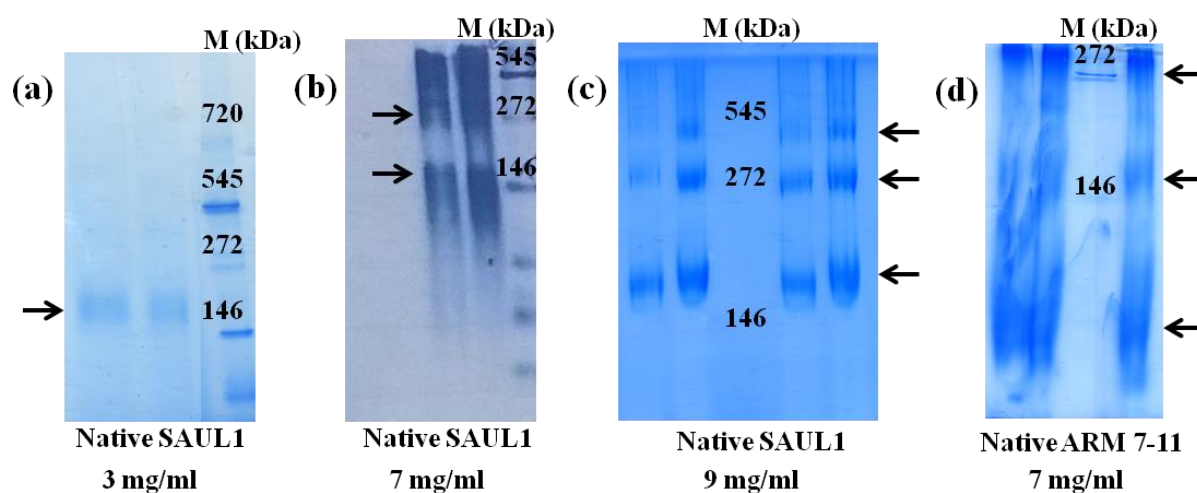
Figure 34: Native page of SAUL1 and ARM 7-11ΔC proteins: (a): Native page of SAUL1 at a protein concentration of 3 mg/ml. (b): Native page of SAUL1 at a protein concentration of 7 mg/ml. (c): Native page of SAUL1 at a protein concentration of 9 mg/ml. (b): Native PAGE of ARM 7-11ΔC at a proteins concentration of 7 mg/ml. The different oligomerization states are indicated by black arrows.

In conclusion, a concentration dependent oligomerization of SAUL1 and ARM 7-11ΔC was observed. Conversely to the results obtained by the native PAGE gels, which show the presence of different oligomeric states upon increasing the concentration, DLS measurements show, a rather monodisperse protein solutions. Thus, additional investigations were required to determine the interaction in more detail and to obtain first structural insights about SAUL1 and ARM 7-11ΔC.
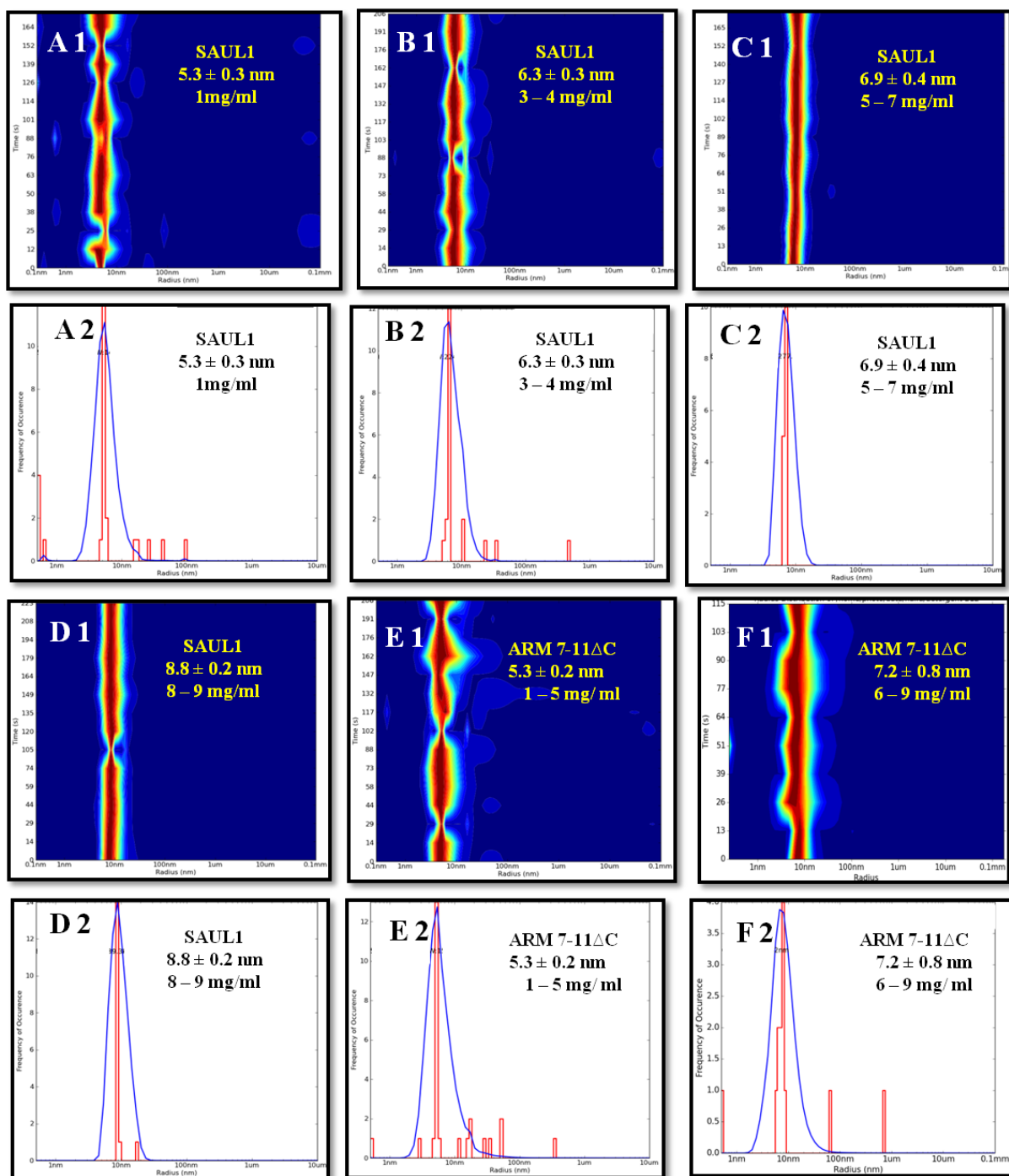
Figure 35: Concentration dependency of the hydrodynamic radius: *A, B, C, and D: Dynamic light scattering of SAUL1. E and F: Dynamic light scattering of ARM 7-11ΔC. Fifteen measurements of 15 seconds were performed at an interval of 10 seconds.*

4.2.6 Structure investigation applying small angle X-ray scattering

Small angle X-ray scattering (SAXS) was applied to analyze GST-SAUL1, SAUL1 without tag and the selected ARM-repeats (ARM 7-11ΔC). The overall parameters derived from the scattering pattern are summarized in Table 4.2.6.

Table 4.2.6: SAXS data collection and analysis parameters

Data collection parameters	GST-SAUL1 fusion protein	SAUL1-full length	ARM7-11ΔC
Instrument	EMBL beamline P12 (Blanchet *et al*. 2015)		
Wavelength (nm)	0.124		
s-range (nm^{-1})	0.03–4.8		
Exposure time (s)	0.05×20		
Concentration range (mg/ml)	0.5–1	6–7	2-5
Temperature (K)	283		
Structural parameters			
R_g (nm) (from Guinier)	7.3 ± 0.1	5.6 ± 0.0 / 6.0 ± 0.0	4.5 ± 0.5
D_{max} (nm)	24 ± 3.0	17 ± 2 / 18 ± 2	15 ± 1.0
Molecular mass determination			
MW (kDa) from Porod volume	447 ± 50	230 ± 23 and 295 ± 30	150 ± 15
MW (kDa) from DAMMIF volume	500 ± 30	250 ± 25 and 320 ± 20	165 ± 16
Calculated MM (kDa) from sequence	115	89	46
Software employed			
Primary data reduction and processing	Automated SAXS data analysis pipeline (Franke *et al*. 2012)		
Ab initio analysis	DAMMIF (Franke and Svergun 2009)		
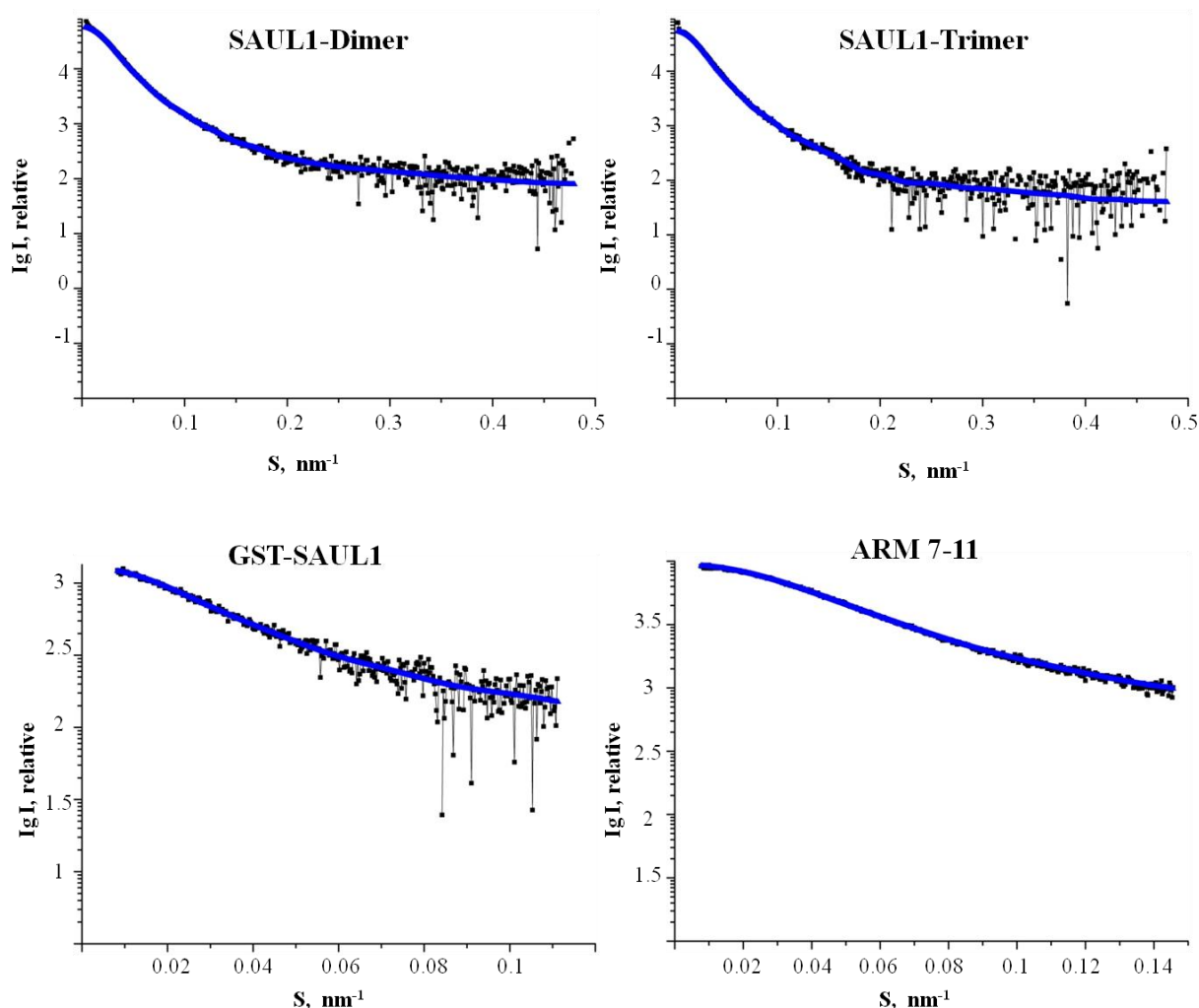
Figure 36: *Scattering curves of the best of ab initio models of GST-SAUL1, SAUL1 and ARM 7-11ΔC proteins generated using Origin as software. The best of ab initio models fitting the experimental data, was tacked out of ten calculated models operating with the rapid ab initio shape determination tool in small angle scattering DAMMIF (Franke & Svergun, 2009). X-ray synchrotron radiation scattering data were collected on the beamline P12 (Petra-III, Hamburg, Germany). See table 4.2.6 for data collection parameters.*

Due to the GST-SAUL1 protein aggregation at a concentration higher then to 1 mg/ml, only samples at a concentration of 0.5 mg/ml and 1 mg/ml could be analyzed. For SAUL1, samples at a concentration of 2, 3, 6 and 7 mg/ml were prepared. Due to the low data quality of the samples with 2 and 3 mg/ml protein, only the solutions at a concentration of 6 and 7 mg/ml

were processed and analyzed. For ARM 7-11ΔC, samples at a concentration of 2 and 5 mg/ml were prepared and processed.
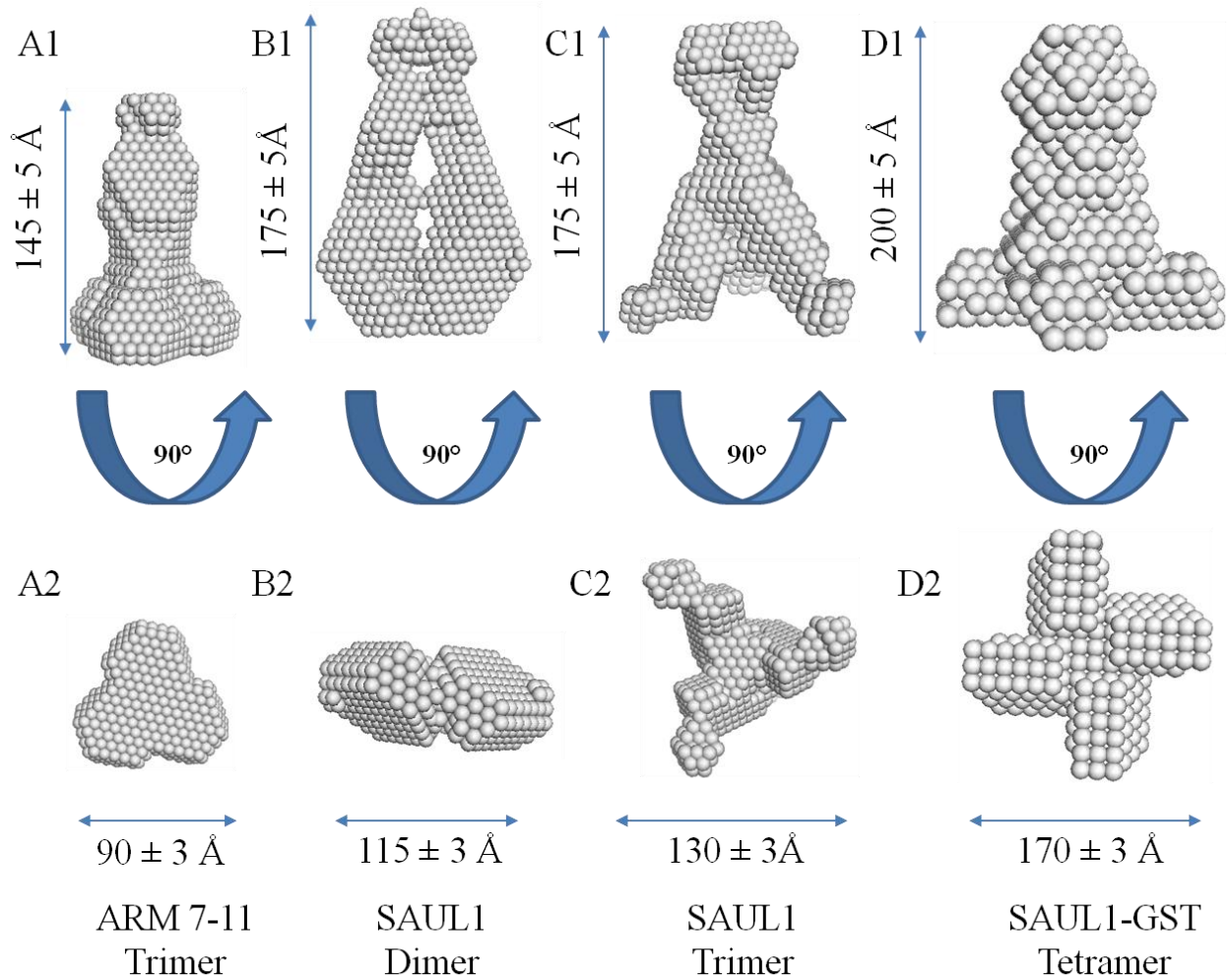
Figure 37: SAXS ab initio models:

A1 and A2: Ab initio model of ARM 7-11ΔC protein. B1and B2: Ab initio model of SAUL1-full length protein (dimeric form). C1 and C2: Ab initio model of SAUL1-full length protein (timeric form). D1 and D2: Ab initio model of GST-SAUL1 full length protein (tetrameric form).

After primary reduction and processing, the calculated data of the GST-SAUL1 protein reveals a MW of 447 ± 50 kDa estimated from the Porod volume and 500 ± 30 kDa estimated from the *ab initio* reconstruction, an R_G of 7.3 ± 0.1 nm and a D_{max} of approximately 24 nm

(Table 4.2.6) intimating a tetrameric elongated shape of the protein in solution (Figure 37, D1 and D2). Two different MWs, 230 ± 23 kDa and 295 ± 30 kDa, were estimated from the Porod volume of SAUL1 in solution. The MWs estimated from the *ab initio* reconstruction were 250 ± 25 kDa and 320 ± 20 kDa, indicating the presence of a mixture of dimer and trimer of SAUL1 in solution (Figure 37, B1, B2 and C2, C2). SAUL1 was characterized by a radius of gyrations (R_g) of 5.6 ± 0.01 nm and 6.0 ± 0.02 nm, the maximum intraparticle distance (D_{max}) were 17 ± 2 nm and 18 ± 2 nm. For ARM 7-11ΔC a concentration range of 2 - 5 mg/ml was prepared revealing a MW from the Porod volume of about 150 ± 15 kDa. The MW estimated from the *ab initio* reconstruction was 165 ± 16 kDa. ARM 7-11ΔC was characterized by a radius of gyration (R_g) of 4.5 ± 0.5 nm, D_{max} was 15 ± 1 nm, showing a trimeric form of the protein in solution (Figure 37, panel A1 and A2). The shape of the proteins in solution was reconstructed *ab initio* using the program DAMMIF: Using P4 symmetry for GST-SAUL1, P2 and P3 symmetry for SAUL1 and P3 symmetry for ARM 7-11ΔC, the resulting shape was relatively elongated (ellipsoidal). The final models were constructed resulting in a good fit (χ^2 = 0.7 for GST-SAUL1, χ^2 = 1.2 for SAUL1, and χ^2 = 0.6 for ARM 7-11ΔC, Figure 36).

Concluding, the *ab initio* shapes of the three proteins were relative compatible to each other (Figure 37). The *ab initio* shapes of the GST-SAUL1, SAUL1 and ARM 7-11ΔC proteins (Figure 37) have a perrin friction factor of p > 1 (p = (220/150) = 1.46 for GST-SAUL1, 180/120 = 1.56 for SAUL1 trimer 180/114 = 1.56 for SAUL1 dimer and 140/90 = 1.55 for ARM 7-11ΔC), confirming the elongated shapes of the SAUL1 and ARM 7- 11 proteins.

4.2.7 Structure investigation applying electron microscopy

Negative stain electron microscopy was carried out at the Max Plank Institute Berlin to get more information about the shape and size of SAUL1. Images were recorded and collected to observe the negatively stained protein sample (Figure 38, A and B). The collected data set from the negative stained grids indicated a relatively heterogeneous protein solution containing a mixture of monomer and dimer. The particles have a size of 10 - 12 nm in diameter (Figure 38, panels A and B) confirming the size obtained by SAXS analysis.

SAUL1 full length was then coupled to a C-terminal GFP-tag and injected into the plant leaves of *A. thaliana* by Catharina Briske in the Laboratory of Prof. Dr. Stefan Hoth. Stochastic optical reconstruction microscopy (STORM) was then accomplished by Prof. Dr.

Christian A. Voigt, (Figure 38, (a), (b), (c) and (d)). The *in planta* cell imaging shows the heterogeneity of the protein since different oligomeric states were observed (dimer, trimer, tetramer and hexamer, figure 38, (a), (b), (c) and (d) respectively) pointing out that SAUL1 has an intrinsic tendency to form high ordered polymers.
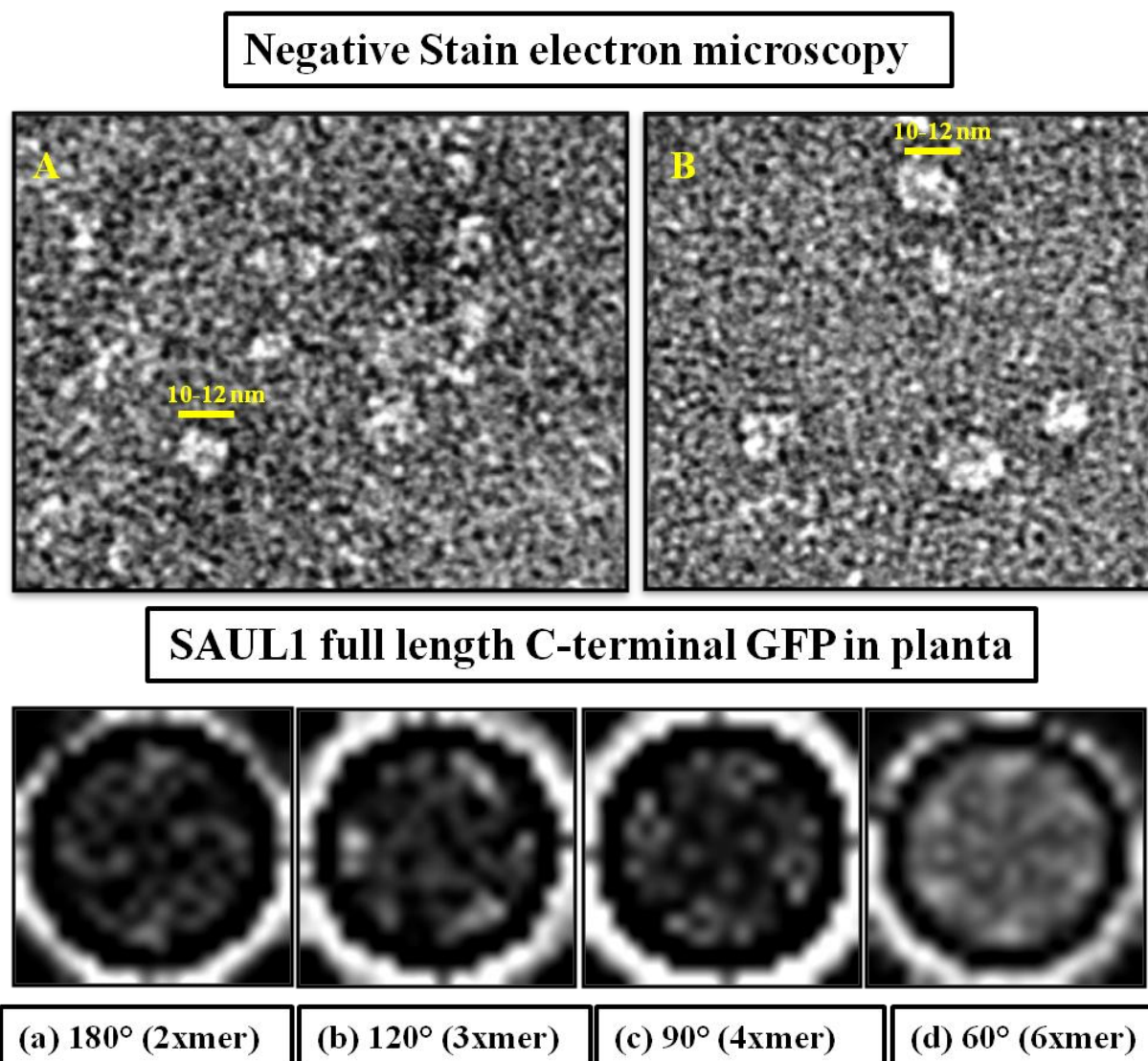
Figure 38: *A and B: Negative stain electron microscopy using uranyl acetate as stain. (a), (b), (c) and (d): In planta super-resolution-microscopy: The SAUL1 full length was coupled with a C-terminal GFP-Tag.*

Concluding, the results obtained by DLS (Figure 36) and native PAGE (Figure 35) of the SAUL1 and ARM 7-11ΔC proteins show a concentration dependent oligmerization. Moreover, The SAUL1 oligomers were also present in the negative stain electron microscopy

(Figure 38, A and B) and in the *in planta* cell imaging (Figure 38, (a), (b), (c) and (d)) at low protein concentration, pointing out that SAUL1 has an intrinsic tendency to build high ordered oligomers. The shape and the oligomeric state of GST-SAUL1, SAUL1 and ARM 7-11ΔC in solution were verified by the accomplished SAXS measurements. *Ab initio* models of the proteins were constructed. The calculated data of the GST-SAUL1 protein reveals a MW of about 447 ± 50 kDa estimated from the Porod volume and about 500 ± 30 kDa estimated from the *ab initio* reconstruction, intimating a tetrameric elongated form of the protein in solution (Figure 38, D1 and D2). Two different MWs, 230 ± 23 kDa and 295 ± 30 kDa, were estimated from the Porod volume of SAUL1 in solution. The MWs estimated from the *ab initio* reconstruction were 250 ± 25 kDa and 320 ± 20 kDa, indicating the presence of a mixture of dimer and trimer of SAUL1 in solution (Figure 38, B1, B2 and C2, C2). For ARM 7-11ΔC a MW from the Porod volume of about 150 ± 15 kDa and a MW from the *ab initio* reconstruction of about 165 ± 16 kDa were estimated, intimating a trimeric form of the protein in solution (Figure 38, A1 and A2). The ab initio models were constructed resulting in a good fit (χ^2 = 0.7 for GST-SAUL1, χ^2 = 1.2 for SAUL1, and χ^2 = 0.6 for ARM 7-11ΔC, Figure 37). The *ab initio* shapes of the GST-SAUL1, SAUL1 and ARM 7-11ΔC proteins were well compatible to each other, showing an elongated (ellipsoids) form of the protein in solution.

5 Discussion

5.1 Intracellular loop of the *A. thaliana* glucan synthase-like 5 (AtGSLO5-IL)

5.1.1 Purification of the AtGSLO5-IL

Cellulose (1,4-β glucan) and callose (1,3-β glucan) are fundamental components of the plant cell wall. These two cell wall polymers interact directly with each other´s forming a three-dimensional network as a response to a plant-pathogen attack (Eggert & Naumann, 2014). While the structure, oligomerization, and biochemical and signal pathways of the cellulose synthases could be investigated in different studies (Delmer, 1999; Williamson *et al*., 2002; Saxena and Brown, 2005; Somerville, 2006; Crowell *et al*., 2010; Lei *et al*, 2012 and Jacobs *et al*, 2003). The overexpression, solubilization and purification to homogeneity and characterization of a 1,3-beta-glucan (callose) synthase was very challenging, making its structural and biochemical investigations more difficult. In this work, the putative active domain of the callose synthase 12 of *A. thaliana* (AtGSLO5-IL protein) could be purified using Ni^{2+}-affinity chromatography followed by SEC. The identity of the AtGSLO5-IL protein was verified with MALDI-TOF MS, using peptide mass fingerprint (PMF) and applying a single coomassie-stained band excised from the SDS-PAGE gel, confirming that the purified protein is the AtGSLO5-IL protein. Mueller and Brown (1980) and Delmer (1999) report, that the cellulose synthase has an intrinsic tendency to form oligomers of six subunits arranged in hexagonal symmetry. The SEC revealed the existence of higher oligomeric states of the purified AtGSLO5-IL in solution, giving a first indication that the callose synthase might be also composed of oligomers.

5.1.2 Characterization of the β-1,3-glucan synthesis

In previous studies, in vitro binding assays for the cytosolic domain of the putative (1,3)-*β*-glucan synthase from the fungus *Cordyceps militaris* showed an affinity for this cytosolic domain to UDP-glucose (Ujita *et al*., 2011). No proof of enzymatic activity was however provided. TEM analysis shows the presence of in vitro (1,3)-*β*-glucan biopolymers only in the presence of UDP-glucose as substrate. In assays without UDP-glucose as substrate, no (1,3)-

β-glucan biosynthesis was found (negative control). The presence of in vitro (1,3)-β-glucan biopolymer (Figure 20) visible in the TEM images confirm the binding affinity of the cytosolic domain of the PMR4 protein to UDP-glucose. This can be considered as evidence for the activity of the cytosolic domain of a (1,3)-β-glucan synthases and for membrane-free, in vitro cell wall biopolymer synthesis, suggesting that the cytosolic domain of the cell wall-related (1,3)-β-glucan synthase can be sufficient for membrane-free glucan biopolymer synthesis. Moreover, the AtGSLO5-IL oligomers were also present in the negative control TEM analysis without (1,3)-β-glucan biosynthesis, but were less frequent than in assay with UDP-glucose as substrate, demonstrating that the PMR4-IL may have an intrinsic tendency to form oligomers. Thus, enzymatic activity assays, DLS and native PAGE was then needed to subsequently investigate these results in more details.

5.1.2 Enzymatic activity assays

Harada (1968) and Saito (1979) described a pH-dependent gel-forming property of callose. Felle (2004) suggested that the apoplastic pH even increased in short term response to pathogen attacks, remained acidic. Whereas Saito (1979) suggested that an apoplastic slightly alkaline pH is required for callose formation. In this work, the highest enzymatic activity of the AtGSLO5-IL protein was observed when using pH values between 7.3 and 8 (Figure 22), confirming Saito´s hypothesis. Moreover, the enzyme linked-immunosorbent assay and the DLS measurements, demonstrates that the callose synthase activity is not only pH dependent but also the ion composition and concentration has a crucial role in the (1,3)-β-glucan synthases activity. The TEM shows that in vitro (1,3)-β-glucan polymer synthesis by the cytosolic domain of a (1,3)-β-glucan synthase was associated with AtGSLO5-IL oligomerization at the ends of microfibers (Figure 20). The AtGSLO5-IL oligomerization was also confirmed by DLS measurements without the UDP-glucose substrate, suggesting that AtGSLO5-IL has an intrinsic tendency to form oligomers. The lowest radius value (Figure 22, C) and the highest enzymatic activity of the cytosolic domain of a (1,3)-β-glucan synthase (Figure 21) were observed when using buffer C (pH 7.3 + 3 mM NaCl), which strongly suggest that the AtGSLO5-IL activity is dispersity dependent. TEM, quantification of enzymatic activity and the dynamic light scattering tests confirm that (1,3)-β-glucan deposition is not only buffer dependent but that the oligomerization state of the AtGSLO5-IL also plays a crucial role for the activity of the plant (1,3)-β-glucan synthases protein. Thus, more buffer optimization was needed to get a monodisperse protein solution.

5.1.3 Circular dichroism and dynamic light scattering

The CD-spectrum indicates a well folded AtGSL05-IL protein with more then 50 % α-helical structure. DLS analysis shows a hydrodynamic particle radius of 12 ± 0.2 nm. As the calculated molecular weight of the protein is approximately 79 kDa, a particle size of around 4 nm is anticipated. However, the particle size in the radius distribution plot indicates that the protein is present in solution as a large oligomer and not as a monomer, which was also confirmed by the performed native PAGE (Figure 23).

5.1.4 Structure investigation

The shape and the oligomeric state of AtGSLO5-IL in solution were verified by the SAXS measurements. An *ab initio* model of the AtGGSLO5-IL was constructed with imposed P8 symmetry (χ^2 = 1.2, Figure 24) confirming the results obtained by DLS and native page, indicating that the protein is present in solution as a large oligomer and not as monomer. The molecular weight (MW) estimated from the Porod volume of the particle in solution (634 ± 63 kDa), and the MW estimated from the *ab initio* reconstruction is 655 ± 66 kDa suggest the presence of the AtGSLO5-IL protein as an octamer in solution. The *ab initio* model shows an oblate form of the protein with extended 8-arm starfish-like sprouts on the periphery suggesting certain flexibility. The CORAL model was well compatible with the *ab initio* shape (Figure 24) showing also an oblate form of the protein with extended C- terminals 8-arm starfish-like sprouts on the periphery (including the predicted unfolded C-terminal strep-tag). The flexible extended sprouts on the periphery of the CORAL and *ab initio* SAXS models and the presence of in vitro (1,3)-*β*-glucan biopolymer in the presence of UDP-glucose as substrate, showed by the TEM analysis, confirm the Østergaard hypothesis, that the N and C-terminal domains might be involved in channel formation and membrane anchorage at the plasma membrane, to facilitate delivery of (1,3)-*β*-glucan to the cell wall, whereas the central cytosolic loop (AtGSLO5-IL) might be the conserved catalytic domain and sufficient for enzymatic activity (Østergaard *et al.*, 2002). The presence of the AtGSLO5-IL oligomers in the SAXS measurement, TEM analysis (Figure 20), negative stain electron microscopy and the *in planta* super-resolution-microscopy (Figure 25) confirm that AtGSLO5 has an intrinsic tendency to form oligomers. Moreover, AtGSLO5-IL oligomers were present in the negative control of the TEM analysis without (1,3)-*β*-glucan biosynthesis, but were less abundant than in assay with UDP-glucose as substrate (Figure 20), indicating that the intrinsic

5 Discussion

tendency of the AtGSLO5-IL to form oligomer might be strongly promoted by (1,3)-β-glucan biosynthesis.

Based on these SAXS measurement, EM, SEC, DLS and the native page result, a self-protein interaction was hypothesized. Computing various physico-chemical properties using the tool Protparam (Gasteiger *et al*., 2005), a high amount of hydrophobic amino acids (Hydrophobic: 42.8 %; Hydrophilic: 22.5 % and positive charged amino acids (K: 5.9 %, R: 7.0 %, H: 2.2 %) was deduced from the AtGSLO5-IL protein sequence, without considering the N- and C-terminal tags. To obtain an insight into its surface properties, a predicted 3D structure of the AtGSLO5-IL, fitting the secondary structure estimated by CD spectroscopy (Chapter 4.1.5), was generated using the prediction web portal IntFOLD (McGuffin *et al*., 2015; Figure 39 A, the same 3D predicted structure was used for rigid body modelling). The electrostatic surface potential of the AtGSLO5-IL protein plays an important role for protein-protein interaction. Positive potential values are drawn in blue, negative values in red (Figure 39, D and E). The electrostatic surface shows a predominant negative charge distribution, indicating a potential favorable surface protein interaction. The high amount of Lysine, Arginine and Histidine amino acids on the surface of the protein, (colored orange, blue and pink respectively; figure 39, B and C) also indicates a possible interaction between oppositely charged residues favoring a protein-protein interaction or a self-protein interaction of AtGSLO5-IL, confirming the results obtained using SAXS measurement and the native PAGE.

No crystal structure of the plants cellulose or callose synthases were solved till today. Hu (2010) reports an octamer crystal structure of the bacterial cellulose synthase *Acetobacter xylinum* subunit D (*Ax*CeSD). Comparing the *Ax*CeSD structure with the AtGSLO5-IL *ab initio* and the coral rigid body models (Figure 40), I conclude that both *Ax*CeSD and AtGSLO5-IL proteins show an octameric assembly with different arrangement but with a common central pore, which might have direct implications for the glucan chain extrusion into the extracellular medium (Hu *et al*., 2010). The *Ax*CeSD crystal structure and the AtGSLO5-IL coral rigid body model shows a C-terminal flexible extended sprouts, suggesting that the C-terminal domain might be involved in the plasma membrane anchoring, to facilitate delivery of (1,3)-β-glucan to the cell wall. Whereas, the N termini are positioned inside both proteins, confirming that the N-termini of the proteins might influence the central pore assembly (Hu *et al*., 2010) inducing a channel formation facilitating the extracellular extrusion of cellulose and callose.
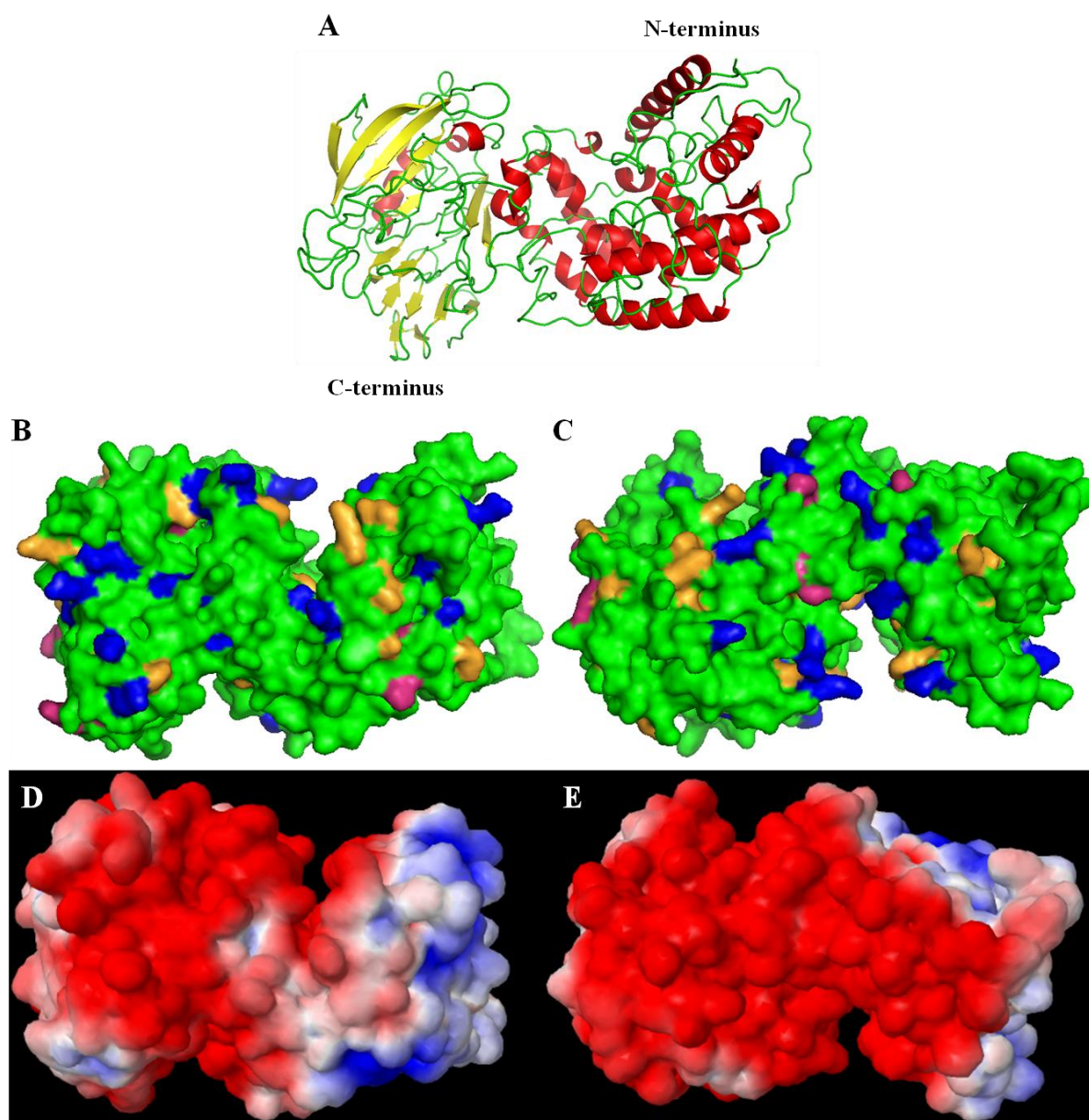
Figure 39: *A: 3D structure of AtGSLO5-IL was modeled using the web server for protein modelling, prediction and analysis, (McGuffin et al., 2015). B and C: Surface distribution of the amino acids K, R and H colored orange, blue and pink respectively. The electrostatic potentials were calculated using the Adaptive Poisson-Boltzmann Solver (APBS) and PDB2PQR Server (a molecular solvation software package). Figures were made using PyMol (PyMOL Molecular Graphics System, Version 1.3, Schrödinger, LLC.).*
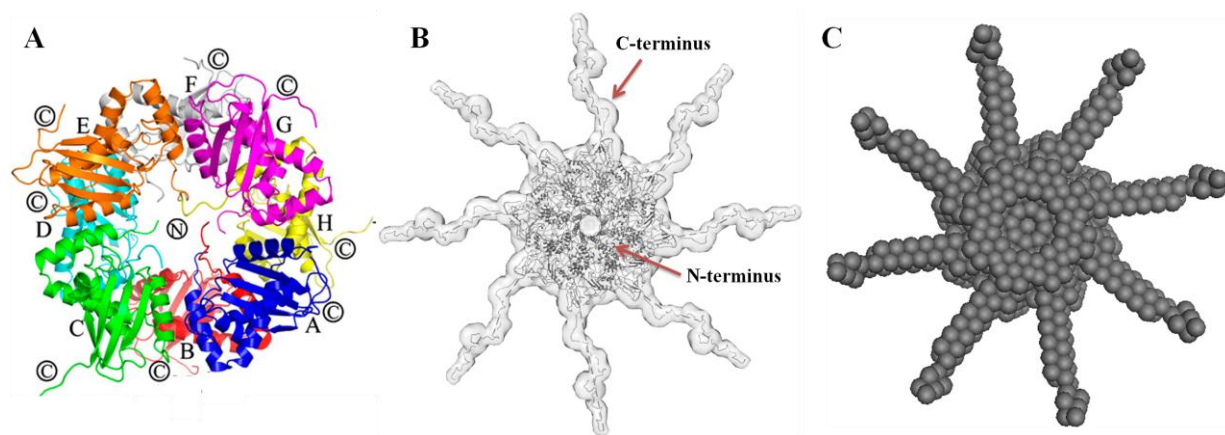
Figure 40: Structure comparison of the **AxCeSD** *cellulose synthase and the SAXS ab initio and rigid body model of the AtGSLO5-IL.* A: AxCeSD *cellulose synthase*, B: *Multi-domain rigid body model obtained using CORAL, C: Ab initio model of AtGSLO5-IL. Figure of the* AxCeSD *cellulose synthase was adapted from Hu et al., 2010, PDB codes: 3AJ1 and 3AJ2.*

5.2 Senescence associated ubiquitin ligase1 (SAUL1) and armadillo (ARM) 7-11 repeats

5.2.1 Purification and circular dichroism of SAUL1 and ARM 7-11ΔC proteins

E3 ligases of the plant *Arabidopsis thaliana* are divided into four types, based on their different functions and protein domains: HECT, RING, cullin-RING and U-box ligases (Drechsel *et al*., 2011). SAUL1 belong to the plant U-box (PUB) protein family, which is characterized by a highly conserved U-box, essential for activity of these ligases, and multiple tandem armadillo (ARM) repeats, forming interfaces for protein–protein interactions. Because of its crucial role as a suppressor of premature senescence and cell death for plants (Raab *et al*, 2009; Drechsel *et al*, 2011) structural and biochemical investigations were highly needed to get more insights about the protein. In this work, a protocol for gene overexpression, solubilization and purification of *A. thaliana* SAUL1 protein was established using GST-affinity chromatography followed by SEC. The identity of the protein was verified with MALDI-TOF MS, using peptide mass fingerprint (PMF) and applying a single coomassie-stained band excised from the SDS-PAGE gel, confirming that the purified protein is SAUL1.

Size exclusion chromatography revealed the existence of a monomeric state for the purified GST-SAUL1, SAUL1 and ARM 7-11ΔC in solution. Whereas DLS measurements show concentration dependent oligmerization, which was confirmed by the native PAGE, performed for SAUL1 and ARM7-11ΔC (Figure 34). Thus, additional investigations were required to determine the interaction in more detail and to obtain first structural insights about SAUL1, which was subsequently provided by the *ab initio* shapes of the GST-SAUL1, SAUL1 and ARM 7-11ΔC. CD-spectra (Figure 30) indicate that SAUL1 and ARM 7-11ΔC are well folded with overall structures of predominantly α-helical domains. However, unlike SAUL1 (11 % random structure), the quota of random structure of the ARM 7-11ΔC was relatively high (34 %), which may be explained by the presence of some disordered segments in the ARM 7-11ΔC protein. Thus, in contrast to the putative arrangement of SAUL1 domains (Drechsel *et al*., 2011) a new arrangment of the ARM repeats could be hypothesized. A thermal denaturation assay of SAUL1 was performed, showing that the melting already starts at about 38 °C (Figure 32), which shows, that SAUL1 might be relative unstable.

5.2.2 Structure investigation of SAUL1 and ARM 7-11ΔC proteins

The shape and the oligomeric state of GST-SAUL1, SAUL1 and ARM 7-11ΔC in solution were verified by the accomplished SAXS measurements. The GST-SAUL1 MW estimated from the Porod volume and from the *ab initio* reconstruction, reveals a tetrameric elongated form of the protein in solution (Figure 37). Two different MWs, were estimated from the Porod volume and from the *ab initio* reconstruction of SAUL1, indicating the presence of a mixture of dimer and trimer of SAUL1 in solution (Figure 37). ARM 7-11ΔC, intimate a trimeric form in solution (Figure 37). The ab initio models were constructed resulting in a good fit (χ^2 = 0.7 for GST-SAUL1, χ^2 = 1.2 for SAUL1, and χ^2 = 0.6 for ARM 7-11ΔC, Figure 37). The *ab initio* shapes of the GST-SAUL1, SAUL1 and ARM 7-11ΔC proteins were well compatible to each other, showing an elongated (ellipsoids) form of the protein in solution. The *ab initio* shapes of the three proteins were relative compatible to each other (Figure 37). The calculated shape factors, characterized by the radius of gyration against the hydrodynamic radius ($\rho = R_g/R_h$), of GST-SAUL1 (R_g/R_h ~1), SAUL1 (R_g/R_h ~0.85) and ARM 7-11ΔC (R_g/R_h ~0.85) proteins suggest that the proteins intimate an elongated (coil) form (Figure 35; Bruce & Weiner, 2010).

A concentrations dependent oligmerization of SAUL1 and ARM 7-11ΔC was observed. Despite the concentrations dependent oligmerization of SAUL1 and ARM 7-11ΔC, DLS measurements shows, rather monodisperse protein solutions. From the *ab initio* models, GST-SAUL1 tetramer (M_W= 460 kDa), SAUL1 trimer (267) kDa, SAUL1 dimer (178 kDa) and ARM 7-11ΔC trimer (135 kDa) can be described as 220 x 150 Å, 180 x 120 Å, 180 x 114 Å and 140 x 90 Å ellipsoids respectively. Taken the Perrin friction factor into consideration (Cantor & Schimmel, 1980), which is characterized by the axial ratio p = a/b where (a) is the axial semiaxis and (b) is the equatorial semiaxis. Assuming a nearly globular shape, p = 1. If p > 1 since the axial semiaxis is longer than the equatorial semiaxes, then the protein has a prolate ellipsoid shape. To get more information about the protein shape the Perrin factor (F) can be calculated in relation with the mass equivalent spherical radius (R_M) and the measured hydrodynamic radius (R_H). The calculation of R_M can be performed using the equation below

$$R_M = [3V/4\pi r]^{1/3} = 0.066 \times (M_W)^{1/3}$$

5 Discussion

The R_M of the GST-SAUL1 tetramer (5.09 nm), SAUL1 trimer (4.25 nm), SAUL1 dimer (3.71 nm) and ARM 7-11ΔC trimer (3.39 nm) are more than 30% smaller than the measured R_H of 7.2 nm, 6.9 nm, 6.3 nm and 5.3 nm respectively, suggesting an elongated form of the proteins. The Perrin factor (F) can be calculated in relation with R_M and R_H using the expression shown below

$$F = \frac{f_H}{f_M}(4\pi N_A/3M_W\bar{V})^{\frac{1}{3}} = (R_H - SL)/R_M$$

Where:

SL: is per default equal to 0.25 nm and is the thickness of a single layer of solvent

f_H: The frictional coefficient for the mass equivalent hard sphere

f_M: The frictional coefficient for the hydrodynamic sphere

$\bar{V}$: The partial specific volume

N_A: The Avogadros number

Perrin factors of 1.36 (GST-SAUL1 tetramer), 1.56 (SAUL1 trimer), 1.6 (SAUL1 dimer) and 1.5 (ARM 7-11ΔC trimer) are consistent with a prolate ellipsoid, which correspond to the axial ratios of 1.46 (GST-SAUL1 tetramer), 1.5 (SAUL1 trimer), 1.58 (SAUL1 dimer) and 1.55 (ARM 7-11ΔC trimer), calculated using *ab initio* structural dimensions, confirming the SAXS results.

Comparing the shape and the diameter size of the *ab initio* model of ARM 7-11ΔC, which is a 140 ± 5 Å diameter long trimer, to the *ab initio* models of SAUL1 (trimer) and the GST-SAUL (tetramer), we can clearly see that the ARM 7- 11 model fits to the upper part of SAUL1 and GST-SAUL1 models (Figure 41), suggesting that the lower wide part of the *ab initio* models might be the N-terminal region of the protein.

To obtain an insight into the surface properties of SAUL1 and ARM 7-11ΔC, a predicted 3D structure of SAUL1 full length was generated using different web servers (ModWeb, M4T, Swiss-Model, I-Tasser, HHpred, Phyre2, InFOLD2, Raptorx). Most models were similar to each other (Figure 42). The predicted 3D structures of the SAUL1 protein correspond to the secondary structure estimated by CD spectroscopy (76 % α-helical domains, 6 % β-sheet, and 8 % Turns). While, for ARM 7-11ΔC protein unlike the structure estimated by CD

spectroscopy (42 % α-helical domains, 19 % β-sheet and 5 % Turns), the predicted 3D structures indicates an overall structure of more than 85 % α-helical domains and no presence of β-sheets. Thus confirm the presence of some disordered segments in the purified ARM 7-11ΔC protein.
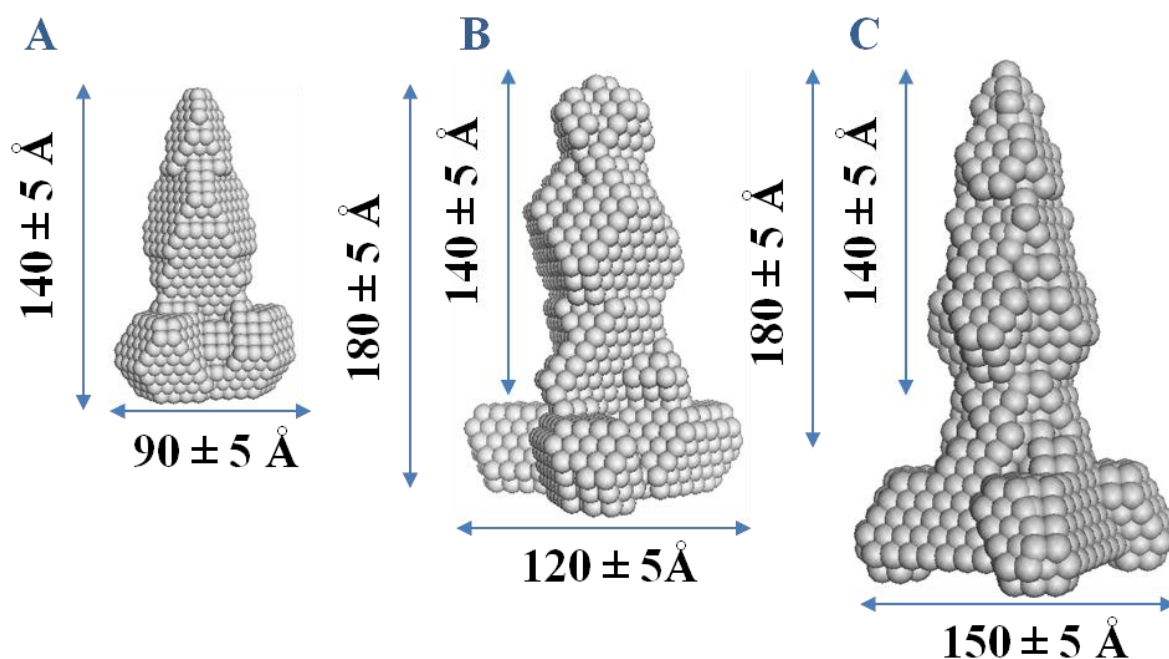
Figure 41: Comparison of SAXS ab initio models:

A: Ab initio model of ARM 7-11ΔC protein (trimer). B: Ab initio model of SAUL1- protein (trimer). C: Ab initio model of GST-SAUL1 protein (tetramer). ARM 7- 11 corresponds to the upper part of the SAUL1 full length.

According to Huber *et al* (1997), ARM repeats are a repeated long tandem sequence motifs characterized by the triangular arrangement of three right-handed helices, consisting of about 40 amino acids. Drechsel *et al* (2011) report a putative arrangement of ARM repeats which was taking in consideration for the cloning of ARM 7-11ΔC. However, the CD spectroscopy shows a high quota of random structure of the ARM 7-11ΔC (34 %). Thus, in contrast to Huber *et al* and Drechsel *et al* theories, low conservation of ARM repeats and new arrangement of the SAUL1 domains could be hypothesized. The best of model, 97 % of residues was modeled at more than 90 % confidence, was taken from the prediction web portal *Phyre2*. Overlaying the *ab initio* model with the predicted 3D structure of SAUL1 protein (Figure 43) confirms the suggestion that the lower wide part of the *ab initio* model

might be the N-terminal region of the protein and the upper part might be the C-terminus of SAUL1.
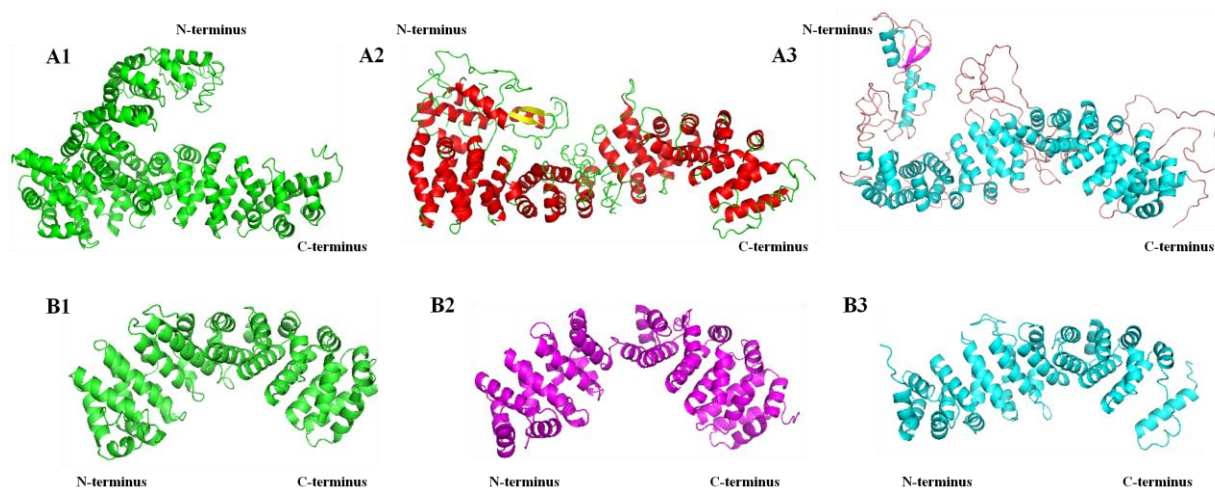
Figure 42: *A1, A2 and A3: 3D structures of SAUL1 modeled using web portals for protein modeling, prediction and analysis, I-Tasser (Yang et al., 2015), Phyre2 (Kelley et al., 2015) and Raptorex (Källberg et al, 2012), respectively. B1, B2 and B3: 3D structures of ARM 7-11ΔC protein modeled using web portals I-Tasser, Phyre2 and Raptorex, respectively. Most models were similar to each other. Figures were prepared using PyMol (PyMOL Molecular Graphics System, Version 1.3, Schrödinger, LLC.).*

Computing various physico-chemical properties using the tool Protparam (Gasteiger *et al.*, 2005), a high amount of hydrophobic amino acids (hydrophobic: 43.8 %; hydrophilic: 21.6 %) and positive charged amino acids (K: 5.2 %, R: 6.1 %, H: 2.2 %) was calculated from the SAUL1 protein sequence. The electrostatic surface potential of SAUL1 plays an important role for protein-protein interaction. Positive potential values are drawn in blue, negative values in red (Figure 44, B and C). The electrostatic surface shows a predominant negative charge distribution, supporting the assumption of a potential favorable surface for protein interaction. The high amount of Lysine, Arginine and Histidine amino acids, which are mainly distributed on the surface of the protein, (colored orange, blue and pink respectively, figure 44, D and E) also indicates a possible interaction between oppositely charged residues

favoring a protein-protein interaction or a self-protein interaction of SAUL1, confirming the results obtained by SAXS measurements and the native PAGE.
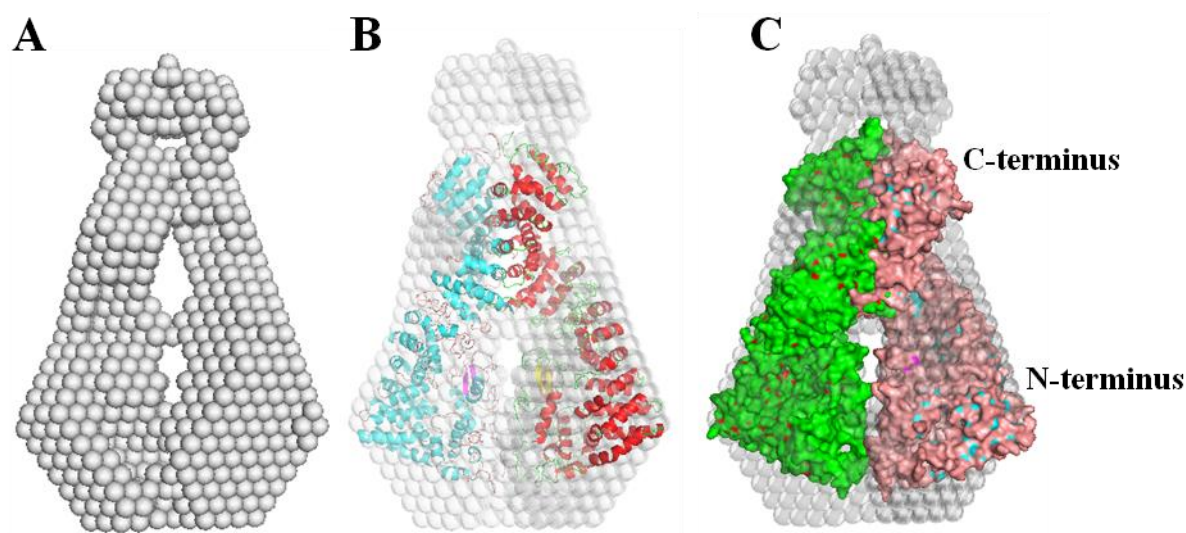
Figure 43: Comparison of the SAXS ab initio model with the predicted 3D structure of SAUL1: *A: Ab initio model of SAUL1- protein (dimer). C: Overlaying of the ab initio model with the predicted 3D structure, shown as ribbon. B: Overlaying of the ab initio model with the predicted 3D structure, shown as surface. Models were manually overlayed and figures were prepared using PyMol (PyMOL Molecular Graphics System, Version 1.3, Schrödinger, LLC.).*

The results obtained by DLS (Figure 35) and native PAGE (Figure 34) of the SAUL1 and ARM 7-11ΔC show a concentrations dependent oligmerization. Moreover, SAUL1 oligomers were also present in the negative stain electron microscopy (Figure 38) and in the *in planta* cell imaging (Figure 38) at low protein concentration, pointing out that SAUL1 has an intrinsic tendency to from high ordered oligomers, which might explain the unsuccessful attempts to crystallize SAUL1. Moreover, the reason to pick ARM 7-11 as construct was to avoid any protein-protein interaction, since reported by Drechsel *et al* (2011), that ARM 1-6 repeats are responsible for protein-protein interaction and ARM 7-11 are responsible for plasma membrane association. However, the results obtained by DSL measurements, native PAGE and SAXS experiments suggest that ARM 7-11 repeats might also interfere in protein-protein interactions.
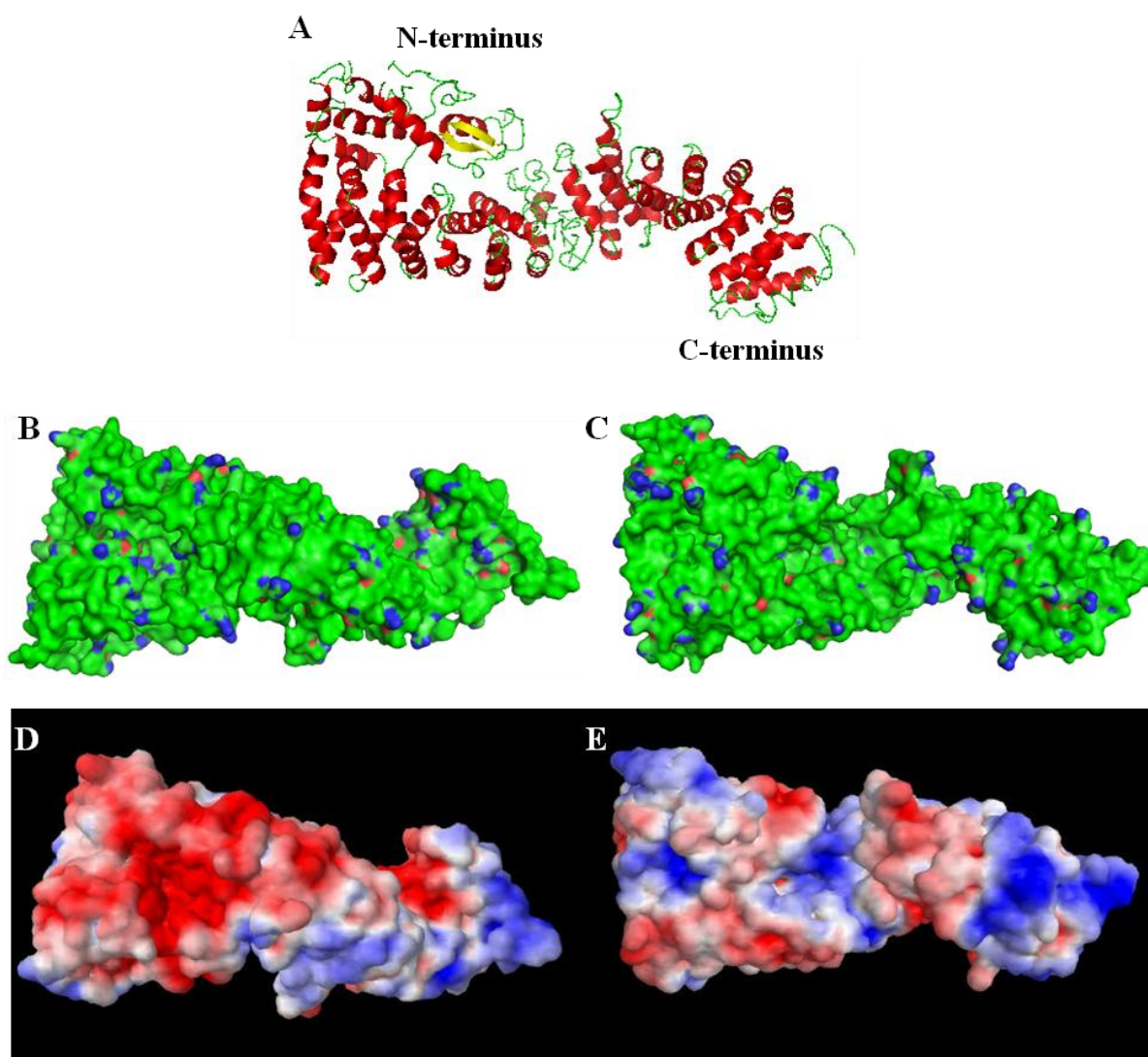
Figure 44: *A: 3D structure of SAUL1 modelled using the web portal for protein modeling, prediction and analysis, Phyre2 (Kelley et al. 2015). B and C: Surface distribution of the amino acids K, R and H colored orange, blue and pink respectively. The electrostatic potentials were calculated using the Adaptive Poisson-Boltzmann Solver (APBS) and PDB2PQR Server (a molecular solvation software package). Figures were prepered using PyMol (PyMOL Molecular Graphics System, Version 1.3, Schrödinger, LLC.).*

6 Summary

As sessile organisms, plants are exposed to changing environmental conditions. Different abiotic and biotic stresses such as drought and pathogen infestation affect plant growth. Understanding molecular events regulating plant responses to abiotic and biotic stresses is highly important to improve plant resistance to different stress scenarios and thus productivity of plants. Since the perception of the different stress signals occurs at cellular interaction modules, and in order to elucidate the molecular principles of selected stress-related plant proteins, two proteins of the components of the interaction modules "plasma membrane of the cell" and "plant cell wall" of *Arabidopsis thaliana* were selected: Senescence associated ubiquitin ligase1 (SAUL1) protein, which is a plasma membrane-associated protein that serves as a suppressor of premature senescence and cell death under unfavorable environmental conditions, such as low light or salt stress (Raab *et al*, 2009; Drechsel *et al*., 2011) and the cytosolic loop, carrying the catalytic domain for the formation of (1,3)-*ß*-glucan, of the Arabidopsis thaliana glucan synthase-like 5 (ATGSLO5-IL) protein, which is one of the main structural components in the cell wall of fungi as well as in plants (Pitson, 1993; Stone & Clark, 1992). Insights into the structure and function of these two proteins will help to develop new strategies in order to improve plant resistance towards complex abiotic and biotic stress scenarios.

The work performed during the period of this PhD project included methods to analyze the structures of AtGSLO5-IL, SAUL1 and selected ARM repeats with particular emphasis on the generation of soluble proteins within prokaryotic cells. Due to the fact that structural information of homologous proteins does not exist, my aim was to overexpress the respective genes, purify those proteins and determine their structures. Protocols for the expression and purification of the AtGSLO5-IL, SAUL1 and ARM 7-11 repeats proteins were successfully established. Hexahistidine and GST fusion tags allowed the successful purification of AtGSLO5-IL, SAUL1 and the ARM repeat protein in large quantities, supporting the solubility of the proteins. Mass spectrometry was used to identify AtGSLO5-IL, SAUL1 and ARM repeats. Dynamic light scattering (DLS) and circular dichroism (CD) data were also used to confirm and analyze the monodispersity, stability and the folding of the proteins respectively. Small angle X-ray scattering (SAXS) measurements for the AtGSLO5-IL, GST-SAUL1 fusion protein, SAUL1 and ARM 7-11 proteins were successfully performed, at the synchrotron source PETRA III, and analyzed enabling the elucidation of more structural

details. Moreover, electron microscopy (EM) data were collected for the AtGSLO5-IL and SAUL1 proteins, which allow obtaining complementary insights into the dimensions of the proteins.

The results obtained by DLS and native gel electrophoresis indicate that SAUL1 shows a concentration dependent oligomerization, pointing out that SAUL1 has an intrinsic tendency to build different oligomeric states, which was also confirmed by the negative stain electron microscopy and the *in planta* cell imaging, which might explain the unsuccessful attempts to crystallize SAUL1 protein. The shape and the oligomeric state of GST-SAUL1, SAUL1 and ARM 7-11 in solution were verified by the accomplished SAXS measurements. The MWs estimated from the Porod volume of the particle in solution and from the *ab initio* reconstruction, reveals an elongated tetrameric form of the GST-SAUL1 protein, a trimeric form of the ARM 7-11 protein and the presence of a mixture of dimer and trimer of SAUL1 protein in solution. The *ab initio* shapes of the GST-SAUL1, SAUL1 and ARM 7-11 proteins were well compatible to each other, showing a relative elongated (ellipsoids) form of the protein in solution.

The shape and the oligomeric state of AtGSLO5-IL in solution were verified by the accomplished SAXS measurements. An *ab initio* model of the AtGGSLO5-IL was constructed with imposed P8 symmetry, confirming the results obtained by DLS and native PAGE, indicating that the protein is present in solution as a large oligomer and not as monomer. The MWs estimated from the Porod volume of the particle in solution and from the *ab initio* reconstruction confirm the presence of the AtGSLO5-IL protein as an octamer in solution. The *ab initio* model shows an oblate form of the protein with extended sprouts on the periphery suggesting certain flexibility. The CORAL model was well compatible with the *ab initio* shape, showing also an oblate form of the protein with an extended C- terminus on the periphery. The negative stain electron microscopy and the *in planta* super-resolution-microscopy confirm the AtGSLO5 intrinsic tendency to form octamers.

7 Zusammenfassung

Als sessile Organismen sind Pflanzen veränderten Umweltbedingungen ausgesetzt. Verschiedene abiotische und biotische Stressfaktoren wie Trockenheit und Krankheitserregerbefall beeinflussen das Pflanzenwachstum. Die molekularen Ereignisse, die für die Regulation der Reaktionen der Pflanzen auf abiotischen und biotischen Stress verantwortlich sind, zu verstehen, ist sehr wichtig, um die Resistenz von Pflanzen auf verschiedene Stressszenarien und damit die Produktivität der Pflanzen zu verbessern. Da die Wahrnehmung der verschiedenen Stresssignale innerhalb von zellulären Interaktionsmodulen auftritt, und um die molekularen Grundlagen ausgewählterstressabhängiger Pflanzenproteine zu vestehen, wurden zwei Proteine unter den Komponenten der Wechselwirkungsmodule "Plasmamembran" und "Pflanzenzellwand" von *Arabidopsis thaliana* wurden ausgewählt: Die senescence associated ubiquitin ligase 1 (SAUL1) ist ein Plasmamembran-assoziiertes Protein, das unter ungünstigen Umgebungsbedingungen, wie wenig Licht oder Salzstress, als Suppressor zum vorzeitiger Seneszenz und Zelltod dient (Raab *et al*, 2009;. Drechsel *et al*, 2011). Als weiteres Protein wurde der putative cytosolische Loop der *Arabidopsis thaliana* glucan synthase-like 5 (ATGSLO5-IL), der die katalytische Domäne für die Bildung von (1,3) -β-Glucan enthält, gewählt. Callose ist eine der Hauptstrukturkomponenten in der Zellwand von Pflanzen und Pilzen (Pitson, 1993; Stone & Clark, 1992). Einblicke in die Struktur und Funktion dieser Proteine wird dazu beitragen neue Strategien zu entwickeln, um die Resistenz von Pflanzen gegenüber komplexen abiotischen und biotischen Stressszenarien zu verbessern.

Im Rahmen der Promotionsarbeit, wurden komplementäre biophysikalische Methoden eingesetzt, um die Strukturen von AtGSLO5-IL, SAUL1 und ausgewählten ARM Repeats zu analysieren, mit besonderem Schwerpunkt auf die Produktion von löslichen Proteinen in prokaryotischen Zellen. Aufgrund der Tatsache, dass bislang kein homologe Proteine Strukturen existieren, war mein Ziel, die entsprechenden Gene zu überexprimieren, zu reinigen und ihre Strukturen zu bestimmen. Protokolle für die Expression und Reinigung von AtGSLO5-IL, SAUL1 und ARM7-11 von SAUL1 wurden erfolgreich etabliert. Die Verwendung von Hexa-Histidin und GST-getaggten Proteinen erlaubte die erfolgreiche Reinigung von AtGSLO5-IL, SAUL1 und ARM7-11 in genügend großen Mengen. Durch Massenspektrometrie wurde die Identität von AtGSLO5-IL, SAUL1 und eines ARM Repeat-Proteins bestätigt. Dynamische Lichtstreuung (DLS) und Cirkulardichroismus-Spektroskopie (CD) wurden auch verwendet, um die Monodispersität, die Stabilität und die Faltung der

7 Zusammenfassung

Proteine zu bestätigen und zu analysieren. Röntgenkleinwinkelbeugungsmessungen (SAXS) für AtGSLO5-IL, GST-SAUL1, SAUL1 und das ARM 7- 11 Protein wurden an der Sychrotronsstrahlungsquelle PETRA III erfolgreich durchgeführt und analysiert, was die nähere Aufklärung von strukturellen Eigenschaften ermöglicht hat. Darüber hinaus konnten gesammelte Elektronenmikroskopie (EM)-Daten von AtGSLO5-IL und SAUL1 ergänzende Einblicke in die 2/ 3D-Struktur ermöglichen.

Die erhaltenen Ergebnisse der DLS Messungen und nativen Gelelektrophoresen belegen, dass das SAUL1 Protein eine konzentrationsabhängige Oligomerisierung zeigt, was darauf hinweist, dass SAUL1 eine intrinsische Tendenz aufweist, verschiedene Oligomere zu bilden. Die auch durch die Negativfärbung-Elektronenmikroskopie und die *in planta* Super-Resolution-Mikroskopie bestätigte Oligomerisierung, könnte die erfolglosen Versuche SAUL1 zu kristallisieren erklären. Die Form und der Oligomerisierungszustand von GST-SAUL1, SAUL1 und ARM 7-11 in Lösung wurden durch die durchgeführten SAXS-Messungen verifiziert. Die angenäherten Molekulargewichte basierend auf dem Porod Volumen und den *ab initio* Rekonstruktionen der Partikel in Lösung offenbaren eine längliche tetramere Form des GST-SAUL1 Proteins, eine trimere Form der ARM 7-11 Protein und die Anwesenheit einer Mischung aus Dimer und Trimer des SAUL1 Proteins in Lösung. Die *ab initio*-Formen von GST-SAUL1, SAUL1 und ARM 7-11 waren gut miteinander kompatibel. Eine relativ längliche (ellipsoide) Form des Proteins in Lösung wurde gezeigt.

Die Form und der Oigomerisierungszustand des AtGSLO5-IL in Lösung wurden über die durchgeführten SAXS-Messungen verifiziert. Das *ab-initio*-Modell des AtGGSLO5-IL wurde mit P8 Symmetrie konstruiert, was die Ergebnisse, die durch DLS Messungen und native Gele gemacht wurden, bestätigt. Dies alles weist darauf hin, dass dass das Protein in Lösung als ein großes Oligomer liegt und nicht als Monomer. Die geschätzten MWs des Porod Volumens und von der *ab initio* Rekonstruktion der Teilchen in Lösung sprechen für das Vorhandensein des AtGSLO5-IL-Protein als Oktamer in Lösung. Das *abinitio* Modell zeigt ein sehr flaches Protein mit einer verlängerten Sprosse an der Peripherie, was auf eine gewisse Flexibilität hindeutet. Das CORAL Modell ist dem *abinitio*Modell sehr ähnlich, und zeigt auch eine sehr flache Form des Proteins mit einem erweiterten C-Terminus an der Peripherie. Die Negativfärbung-Elektronenmikroskopie und die *In planta* Super-Resolution-Mikroskopie bestätigen die Tendenz, dass AtGSLO5 Oktamere bildet.

8 References

➢ Almén, M., Nordström, K.J., Fredriksson, R. and Schiöth, H.B. (2009). "Mapping the human membrane proteome: A majority of the human membrane proteins can be classified according to function and evolutionary origin". BMC Biology. 7: 50.

➢ Altschul, S.F., Gish, W., Miller, W., Myers, E.W. and Lipman, D.J. (1990). Basic local alignment search tool. Journal of molecular biology. 215(3): 403-410.

➢ Amador V., Monte E., Garcia-Martinez J.L. and Prat S. (2001). Gibberellins signal nuclear import of PHOR1, a photoperiod responsive protein with homology to Drosophila armadillo. Cell 106: 343–354.

➢ Applied Photophysics (2015). Ltd. Registered No. 1006739; VAT No GB 564 2354 43.

➢ Arabidopsis Genome Initiative (2000). Analysis of the genome sequence of the flowering plant Arabidopsis thaliana. Nature. 408: 796-815.

➢ Aravind L. and Koonin E.V. (2000). The U box is a modified RING finger - a common domain in ubiquitination. Curr Biol. 10(4): R132-4.

➢ Azevedo C., Santos-Rosa M.J. and Shirasu K. (2001). The U-box protein family in plants. Trends in Plant Science. 6: 354–358.

➢ Baaske P., Wienken C.J., Reineck P., Duhr, S. and Braun, D. (2010). Optical thermophoresis for quantifying the buffer dependence of aptamer binding. Angew. Chem. 49: 2238-2241.

➢ Berne B.J. and Pecora R. (1990). Dynamic light scattering with applications to chemistry, biology and physics. Krieger, R. E. Pub., Florida.

➢ Blanchet C.E., Spilotros A., Schwemmer F., Graewert M.A., Kikhney A.G., Jeffries C.M., Franke D., Mark D., Zengerle R., Cipriani F., Fiedler S., Roessle M. and Svergun D.I. (2015). Versatile sample environments and automation for biological solution X-ray scattering experiments at the P12 beamline (PETRA III, DESY) J. Appl. Cryst. 48 (2).

➢ Boivin S., Kozak S. and Meijers R. (2013). Optimization of protein purification and characterization using Thermofluor screens. Protein Expr Purif. 91 (2): 192-206

➢ Bruce B. and Weiner Ph.D. (2010). What Is Particle Size?. Brookhaven Instruments.

➢ Cantor C. and Schimmel P. (1980) Biophysical Chemistry. Part II. Techniques for the study of biological structure and function. p. 561-562.

8 References

➤ Carpenter E.P., Beis K., Cameron A.D. and Iwata S. (2008). Overcoming the challenges of membrane protein crystallography. Curr Opin Struct Biol. 18 (5): 581–586.

➤ Chen X.Y. and Kim J.Y. (2009). Callose synthesis in higher plants. Plant Signaling and Behavior. 4:6, 489-492.

➤ Cheng Y. and Walz T. (2009). The advent of near-atomic resolution in single-particle electron microscopy. Annu. Rev. Biochem. 78: 723-742.

➤ Cooper GM. (2000). The Cell: A Molecular Approach. 2nd edition.

➤ Crowell E.F., Gonneau M., Stierhof Y.D., Hofte H. and Vernhettes S. (2010). Regulated trafficking of cellulose synthases. Curr. Opin. Plant Biol. 13: 700–70510

➤ Cui X., Shin H., Song C., Laosinchai W., Amano Y. and Brown R.M. Jr. (2001). A putative plant homolog of the yeast ß-1,3-glucan synthase subunit FKS1 from cotton (Gossy hirsutum L) fibers. Planta. 213: 223–230.

➤ Cutler A. and Krochko J. (1999). Formation and breakdown of ABA. Trends in Plant Science. 4: 472-478

➤ Davey J. (2004). G-protein-coupled receptors: new approaches to maximise the impact of GPCRS in drug discovery. Expert Opin. Ther. Targets 8: 165–170.

➤ Delmer D.P. (1999). Cellulose biosynthesis: exciting times for a difficult field of study. Annu. Rev. Plant Physiol. Plant Mol. Biol. 50: 245–27610.

➤ Doblin M.S., Melis L.De, Newbigin E.., Bacic A. and Read S.M. (2001). Pollen Tubes of Nicotiana alata Express Two Genes from Different β-Glucan Synthase Families. Plant Physiol. 125: 2040–2052.

➤ Dong X. (2005). Functional investigation of Arabidopsis callose synthase and the signal transduction pathway. The PhD thesis, Ohio State University.

➤ Dong X., Hong Z., Sivaramakrishnan M., Mahfouz M. and Verma DPS. (2005). Callose synthase (CalS5) is required for exine formation during microgametogenesis and for pollen viability in Arabidopsis. Plant J. 42: 315-28.

➤ Drechsel G., Bergler J., Wippel K., Sauer N., Vogelmann K. and Hoth S. (2011). C-terminal armadillo repeats are essential and sufficient for association of the plant U-box armadillo E3 ubiquitin ligase SAUL1 with the plasma membrane. Journal of Experimental Botany. 62: 775–785.

➤ Drenth J., Principles of protein X-Ray crystallography. Bosten, USA, 1999.

8 References

➢ Duhr S. and Braun D. (2006). Why molecules move along a temperature gradient. Prot. Nat. Acad. Sci. USA. 103: 19678-19682.

➢ Eggert D., Naumann M., Reimer R. and Voigt, C.A. (2014). Nanoscale glucan polymer network causes pathogen resistance. Sci Rep. 4: 4159.

➢ Ellinger D., Naumann M., Falter C., Zwikowics C., Jamrow T., Manisseri C., Somerville S.C. and Voigt, C.A. (2013). Elevated early callose deposition results in complete penetration resistance to powdery mildew in Arabidopsis. Plant Physiol. 161: 1433–1444.

➢ Enns L.C., Kanaoka M.M., Torii K.U., Comai L., Okada K. and Cleland R.E. (2005). Two callose synthases, GSL1 and GSL5, play an essential and redundant role in plant and pollen development and in fertility. Plant Mol Biol. 58:333-49.

➢ Felle H.H., Herrmann A., Hanstein S., Hückelhoven R. and Kogel, K.H.(2004). Apoplastic pH signaling in barley leaves attacked by the powdery mildew fungus Blumeriagraminisf.sp.hordei. Mol.PlantMicrobe.Interact. 17: 118–123.

➢ Field C.B., Behrenfeld M.J., Randerson J.T. and Falkowski P. (1998). "Primary production of the biosphere: Integrating terrestrial and oceanic components". Science. 281 (5374): 237–240.

➢ Flors V., Ton J., Jakab G. and Mauch-Mani. B.J. (2005). Abscisic Acid and Callose: Team Players in Defence Against Pathogens?. Phytopathology. 153: 377–383.

➢ Franke D. and Svergun D.I. (2009). DAMMIF, a program for rapid ab-initio shape determination in small-angle scattering. J Appl Cryst. 42: 342-346.

➢ Franke D., Kikhney A.G. and Svergun D.I. (2012). Automated acquisition and analysis of small angle X-ray scattering data. Nuclear Instruments and Methods in Physics Research A. 689: 52–59.

➢ Gasteiger E., Hoogland C., Gattiker A., Duvaud S., Wilkins M.R., Appel R.D., Bairoch A. (ed) Walker J.M.: (2005) The Proteomics Protocols Handbook. Protein Identification and Analysis Tools on the ExPASy Server, Humana Press pp. 571-607.

➢ Glatter O. and Kratky O. (1982). Small Angle X-ray Scattering. Academic Press; ISBN 0-12: 286280-5.

➢ Gomez-Gomez L. and Boller T. (2000). "FLS2: an LRR receptor-like kinase involved in the perception of the bacterial elicitor flagellin in Arabidopsis". Mol Cell. 5 (6): 1003–11.

8 References

➢ Gomez-Gomez L., Felix G. and Boller T. (1999). "A single locus determines sensitivity to bacterial flagellin in Arabidopsis thaliana". Plant J. 3 (3): 277–84.

➢ Goujon M., McWilliam H., Li W., Valentin F., Squizzato S., Paern J., and Lopez R. (2010). A new bioinformatics analysis tools framework at EMBL–EBI. Nucleic acids research. 38 (2): 695-699.

➢ Guinier A. (1939). La Diffraction des rayons X aux très pétits angles - application à l'etude de phénomènes ultramicroscopiques…

➢ Harada T., Misaki A., and Saito H. (1968). Curdlan: a bacterial gel-forming β-1,3-glucan. Arch. Biochem. Biophys. 124: 292–298.

➢ Hofmann K. (2009). Ubiquitin-binding domains and their role in the DNA damage response. Scienc Direct. 8: 544–556.

➢ Hong Z., Delauney A.J., and Verma D.P.S. (2001). A cell-platespecific callose synthase and its interaction with pragmoplastin. Plant Cell. 13: 755–768.

➢ Hu S.Q., Gaoa Y.G., Tajimab K., Sunagawab N., Zhoua Y., Kawanob S., Fujiwara T., Yod T., Shimura D., Satoh Y., Munekata M., Tanaka I., and Yao M. (2010). Structure of bacterial cellulose synthase subunit D octamer with four inner passageways. Proc Natl Acad Sci. 107 (42): 17957–17961.

➢ Huber A., Nelson W. and Weis W. (1997). Three-dimensional structure of the armadillo repeat region of beta-catenin. Cell. 90 (5): 871-82.

➢ Jacobs A.K., Lipka V., Burton R.A., Panstruga R., Strizhov N., Schulze-Lefert P. and Fincher G.B. (2003). An arabidopsis callose synthase, GSL5, is required for wound and papillary callose formation. Plant Cell. 15 (11): 2503-13.

➢ Jensen G. (2010). Methods in Enzymology: Cryo-EM, Part A, Sample Preparation and Data Collection; Academic Press, Elsevier: San Diego, CA; Vol. 481.

➢ Källberg M., Wang H., Wang S., Peng J., Wang Z. and Lu H., Xu J., (2012). Template-based protein structure modeling using the RaptorX web server. Nature Protocols. 7: 1511-1522.

➢ Kang Z. J. (2002). Salt and Drought Stress Signal Transduction in Plants. Annual Review of Plant Biology. 53: 247–73.

➢ Kelley L.A., Mezulis S., Yates C.M, Wass M.N. and Sternberg M. J.E. (2015). The Phyre2 web portal for protein modeling, prediction and analysis. Nature Protocols. 10: 845–858.

8 References

➢ Knepper C. and Day B. (2010). "From Perception to Activation: The Molecular-Genetic and Biochemical Landscape of Disease Resistance Signaling in Plants". The Arabidopsis Book. 8: 1–17.

➢ Koch M., Vachette P. and Svergun D. I. (2003). Small-angle scattering: a view on the properties, structures and structural changes of biological macromolecules in solution. Quart. Rev. Biophys. 36: 147-227.

➢ Koegl M., Hoppe T., Schlenker S., Ulrich H.D., Mayer T.U. and Jentsch S. (1999). A novel ubiquitination factor, E4, is involved in multiubiquitin chain assembly. Cell. 96 (5): 635-44.

➢ Konarev P.V. and Svergun D.I. (2012). New developments in the ATSAS program package for small-angle scattering data analysis. J. Appl. Cryst. 45: 342-350.

➢ Kurtz M. and Douglas C. (1997). Lipopeptide inhibitors of fungal glucan synthase. J Med Vet Mycol. 35 (2): 79-86.

➢ Lacombe S., Rougon-Cardoso A., Sherwood E., Peeters N., Dahlbeck D., van Esse H.P., Smoker M., Rallapalli G., Thomma B.P., Staskawicz B., Jones J.D. and Zipfel C. (2010). "Interfamily transfer of a plant pattern-recognition receptor confers broad-spectrum bacterial resistance". Nat Biotechnol. 4 (4): 365–9.

➢ Lei L., Li S., and Gu Y. (2012). Cellulose Synthase Complexes: Composition and Regulation. Front Plant Sci. 3: 75

➢ McCormick S. (1993) Male gametophyte development. Plant Cell; 5: 1265-75.

➢ McGuffin L.J., Atkins, J., Salehe B.R., Shuid A.N. and Roche D.B. (2015). IntFOLD: an integrated server for modelling protein structures and functions from amino acid sequences. Nucleic Acids Research. 43: 169-73.

➢ McWilliam H., Li W., Uludag M., Squizzato S., Park Y.M., Buso N., and Lopez R. (2013). Analysis tool web services from the EMBL-EBI. Nucleic acids research. 41 (1): 597-600.

➢ Moraes I., Evans G., Sanchez-Weatherby J., Newstead S. and Stewart P.D. (2014). Membrane protein structure determination - the next generation. Biochim Biophys Acta. 1838: 78-87.

➢ Mudgil Y., Shiu S.H., Stone S.L., Salt J.N. and Goring D.R. (2004). A Large Complement of the Predicted Arabidopsis ARM Repeat Proteins Are Members of the U-Box E3 Ubiquitin Ligase Family. Plant Physiology. 134: 59–66.

8 References

- ➢ Mueller S.C. and Brown Jr R.M. (1980) Evidence for an intramembrane component associated with a cellulose microfibril synthesizing complex in higher plants. J. Cell Biol. 84: 315-326.

- ➢ Niedermeyer T.H.J. and Strohalm M. (2012). mMass as a Software Tool for the Annotation of Cyclic Peptide Tandem Mass Spectra. PLoS ONE 7 (9): e44913

- ➢ Nishimura M.T., Stein M., Hou B.H., Vogel J.P., Edwards H. and Somerville S.C. (2003). Loss of a callose synthase results in salicylic acid-dependent disease resistance. Science. 301 (5635): 969-72.

- ➢ Ohi M., Li Y., Cheng Y., and Walz T. (2004). Negative Staining and Image Classification - Powerful Tools in Modern Electron Microscopy. Biol. Proced. 6: 23-34.

- ➢ Østergaard L., Petersen M., Mattsson O., and Mundy J. (2002). An Arabidopsis callose synthase. Plant Mol. Biol. 49: 559–566.

- ➢ Patty P.J. and Frisken B.J. (2006). Direct determination of the number-weighted mean radius and polydispersity from dynamic light scattering data. Appl. Opt. 45: 2209-2216.

- ➢ Perrimon N. and Mahowald A.P. (1987). Multiple functions of segment polarity genes in Drosophila. Dev. Biol. 119: 587-605.

- ➢ Petoukhov M.V. and Svergun D.I. (2005). Global rigid body modelling of macromolecular complexes against small-angle scattering data. Biophys. J. 89: 1237-1250.

- ➢ Petoukhov M.V., Franke D., Shkumatov A.V., Tria G., Kikhney A.G., Gajda M., Gorba C., Mertens H.D., Konarev P.V. and Svergun D.I. (2012). New developments in the ATSAS program package for small-angle scattering data analysis. J Appl Crystallogr. 45: 342-350.

- ➢ Pettersen E.F., Goddard T.D., Huang C.C., Couch G.S., Greenblatt D.M., Meng E.C. and Ferrin T.E. (2004). UCSF Chimera—a visualization system for exploratory research and analysis. Journal of computational chemistry. 25 (13): 1605-1612.

- ➢ Pickart C.M. (2001). Mechanisms underlying ubiquitination. Annu Rev Biochem. 70: 503-33.

- ➢ Pitson S.M., Seviour R.J. and McDougall B.M. (1993) Non cellulolytic fungal β-glucanases: their physiology and regulation. Enz Microb Technol. 15: 178–190.

8 References

- Prilusky J., Felder C.E., Zeev-Ben-Mordehai T., Rydberg E.H., Man O., Beckmann J.S., Silman I. and Sussman J.L. (2005). FoldIndex©: a simple tool to predict whether a given protein sequence is intrinsically unfolded. Bioinformatics. 21 (16): 3435-3438.

- Privé G.G. (2007). Detergents for the solubilization and crystallization of membrane proteins. ScienceDirect. 41: 388-397.

- Putnam D., Hammel M., Hura G.L. and Tainer J.A. (2007). X-ray solution scattering (SAXS) combined with crystallography and computation: defining accurate macromolecular structures, conformations and assemblies in solution. Quart. Rev. Biophys. 40: 191-285.

- Raab S., Drechsel G., Zarepour M., Hartung W., Koshiba T., Bittner F. and Hoth S. (2009). Identification of a novel E3 ubiquitin ligase that is required for suppression of premature senescence in Arabidopsis. Plant Journal. 59: 39–51.

- Rabl J. (2008). Mechanism of gate opening in the 20S proteasome by the proteasomal ATPases. Mol. Cell. 30 (3): 360-368.

- Radermacher M., Wagenknecht T., Verschoor A., and Frank J. (1987). Three-dimensional reconstruction from a single-exposure, random conical tilt series applied to the 50S ribosomal subunit of Escherichia coli. J. Microsc. 146 (2): 113-136.

- Reed J. and Reed T.A. (1997). A set of constructed type spectra for the practical estimation of peptide secondary structure from circular dichroism. Analytical Biochemistry. 254: 36–40.

- Renart J., Reiser, J. and Stark G.R. (1979). Transfer of proteins from gels to diazobenzyloxymethyl-paper and detection with antisera: a method for studying antibody specificity and antigen structure. Proceedings of the National Academy of Sciences. 76 (7): 3116-3120.

- Richmond T.A and Somerville C.R. (2000). The cellulose synthase superfamily. Plant Physiol. 124: 495-8.

- Saito H., Ohki T., and Sasaki T. (1979). A13C-nuclear magnetic resonance study of polysaccharidegels.Molecular architecture in the gels consisting of fungal, branched (1→3)-β-D-glucans (lentinan and schizophyllan) as manifested by conformational changes induced by sodiumhydroxide. CarbohydrateRes. 74: 227–240.

- Saxena I.M. and Brown R.M.J. (2005). Cellulose biosynthesis: current views and evolving concepts. Ann. Bot. 96: 9–2110.

8 References

➢ Schmid M., Kindsmüller K., Wimmer P., Groitl P., Gonzalez R.A. and Dobner T. (2011). The E3 Ubiquitin Ligase Activity Associated with the Adenoviral E1B-55K–E4orf6 Complex Does Not Require CRM1-Dependent Export. J Virol. 85 (14): 7081–7094.

➢ Seo M. and Koshiba T. (2002). Complex regulation of ABA biosynthesis in plants. Trends in Plant Science. 7 (1): 41–8.

➢ Shi X., Sun X., Zhang Z., Feng D., Zhang Q., Han L., Wu J. and Lu T. (2015). GLUCAN SYNTHASE-LIKE 5 (GSL5) Plays an Essential Role in Male Fertility by Regulating Callose Metabolism During Microsporogenesis in Rice. Plant Cell Physiol. 56 (3): 497–509.

➢ Sievers F., Wilm A., Dineen D., Gibson T.J., Karplus K., Li W. and Higgins D.G. (2011). Fast, scalable generation of high quality protein multiple sequence alignments using Clustal Omega. Molecular systems biology. 7(1): 539.

➢ Somerville C. (2006). Cellulose synthesis in higher plants. Annu. Rev. Cell Dev. Biol. 22: 53–7810.

➢ Stepanek P. (1993): Data analysis in dynamic light scattering, in Brown, W. (ed.): Dynamic light scattering. The method and some applications. Oxford Uni. Press, Oxford, pp. 177-241.

➢ Stieren E.S., El Ayadi A., Xiao Y., Siller E., Landsverk M.L., Oberhauser A.F., Barral J.M. and Boehning D. (2011). Ubiquilin-1 is a molecular chaperone for the amyloid precursor protein. J Biol Chem. 286 (41): 35689-98.

➢ Stone B.A. and Clarke A.E.. 1992. The chemistry and biology of $(1–3)$-β-glucans Melbourne, Australia. La Trobe University Press. 565-742

➢ Stone S.L., Anderson E.M., Mullen R.T. and Goring D.R. (2003). ARC1 is an E3 ubiquitin ligase and promotes the ubiquitination of proteins during the rejection of self-incompatible Brassica pollen. The Plant Cell. 15: 885–898.

➢ Strohalm M., Hassman M., Košata B. and Kodíček M. (2008). mMass Data Miner: an Open Source Alternative for Mass Spectrometric Data Analysis. Rapid Commun Mass Spec 22 (6): 905-908.

➢ Strohalm M., Kavan D., Novák P., Volný M. and Havlíček V. (2010). mMass 3: A Cross-Platform Software Environment for Precise Analysis of Mass Spectrometric Data. Anal Chem. 82 (11): 4648-4651.

8 References

➢ Svergun D. I. (1999). Restoring low resolution structure of biological macromolecules from solution scattering using simulated annealing. Biophys J. 2879-2886.

➢ Svergun D.I. (1992). Determination of the regularization parameter in indirect-transform methods using perceptual criteria. J. Appl. Crystallogr. 25: 495-503.

➢ Svergun D.I. and Koch M. (2003). Small-angle scattering studies of biological macromolecules in solution. Rep. Prog. Phys. 66: 1735-1782.

➢ Svergun D.I., Barberato C. and Koch M.H.J. (1995). CRYSOL - a Program to Evaluate X-ray Solution Scattering of Biological Macromolecules from Atomic Coordinates J. Appl. Cryst. 28: 768-773.

➢ TAIR - About Arabidopsis. www.arabidopsis.org. Retrieved 2015-11-15.

➢ Terstappen G.C. and Reggiani A. (2001). *In silico* research in drug discovery. Trends Pharmacol. Sci. 22: 23–26.

➢ Thiele K., Wanner G., Kindzierski V., Jürgens G., Mayer U., Pachl F. and Assaad F.F. (2009). The timely deposition of callose is essential for cytokinesis in Arabidopsis. Plant J. 58 (1): 13-26.

➢ Töller A., Brownfield L., Neu C., Twell D. and Schulze-Lefert P. (2008). Dual function of Arabidopsis glucan synthase-like genes GSL8 and GSL10 in male gametophyte development and plant growth. Plant J. 54: 911-23.

➢ Ujita M., Inoue R., Makino Y., Katsuno Y. and Okumura H. (2011). Binding specificity of the recombinant cytoplasmic domain of Cordyceps militaris β-1,3-glucan synthase catalytic subunit. Biosci Biotechnol Biochem. 75: 171-4.

➢ Valentini E., Kikhney A.G., Previtali G., Jeffries C.M. and Svergun D.I. (2015). SASBDB, a repository for biological small-angle scattering data. Nucleic Acids Res. 43: 357-63.

➢ van Wijk S.J. and Timmers H.T. (2010). The family of ubiquitin-conjugating enzymes (E2s): deciding between life and death of proteins. FASEB J. 24 (4): 981-93.

➢ Verma D.P.S. and Hong Z. (2001). Plant callose synthase complexes. Plant Mol Biol. 47: 693-701.

➢ Wallin E. and von Heijne G. (1998). Genome-wide analysis of integral membrane proteins from eubacterial, archaean, and eukaryotic organisms. Protein Sci. 7 (4): 1029-38.

➢ Wawrzynska A., Rodibaugh N.L. and Innes R.W. (2010). Synergistic Activation of Defense Responses in Arabidopsis by Simultaneous Loss of the GSL5 Callose

8 References

Synthase and the EDR1 Protein Kinase. Molecular Plant-Microbe Interactions. 23 (5): 578-84

➤ Wienken C.J., Baaske P., Rothbauer U., Braun D. and Duhr S. (2010). Protein binding assays in biological liquids using microscale thermophoresis. Nature Com. 1: 10.

➤ Wieschaus E. and R. Riggleman (1987). Autonomous requirements for the segment polarity gene armadillo during Drosophila embryogenesis. Cell 49: 177-184.

➤ Williamson R.E., Burn J.E. and Hocart C.H. (2002). Towards the mechanism of cellulose synthesis. Trends Plant Sci. 7: 461–46710

➤ Yang J., Yan R., Roy A., Xu D., Poisson J. and Zhang Y. (2015). The I-TASSER Suite: protein structure and function prediction. Nature methods. 12 (1): 7-8.

➤ Yang J.T., Wu C.S. and Martinez H.M. (1986). Calculation of protein conformation from circular dichroism H.M. Methods Enzymol. 130: 208-69.

➤ Yue J., Hu X., Sun H., Yang Y. and Huang J. (2012). Widespread impact of horizontal gene transfer on plant colonization of land. Nature Communications 3: 1152

➤ Zhang J. and Zhou J.M. (2010). "Plant immunity triggered by microbial molecular signatures". Mol Plant 3 (5): 783–93.

➤ Zhao J., Wu G., Bu F., Lu B., Liang A. and Cao, L. (2010). Epigenetic silence of ankyrin repeat- containing and proline-rich region-containing protein1 (ASPP1) and ASPP2 genes promote tumor growth in hepatitis B viruspositive hepatocellular carcinoma. Hepatology. 51: 142-153.

➤ Zipfel C., Kunze G., Chinchilla D., Caniard A., Jones J.D., Boller T. and Felix G. (19 May 2006). "Perception of the bacterial PAMP EF-Tu by the receptor EFR restricts Agrobacterium-mediated transformation". Cell 4 (4): 749–60.

9 Risk and safety statements

9.1 Chemicals (GHS classification)

Chemicals	GHS hazard	Hazard statements	Precautionary statements	Supplier
APS	GHS03 GHS07 GHS08	H272, H302, H315, H317, H319, H334; H335	P280, P305+351+338, P302+352, P304+341, P342+311	Merck
Acetic acid	GHS02 GHS05	H226, H314	P280, P305+351+338, P310	Chemsolute
AMP-PCP	GHS06	H301, H311, H315, H319, H331, H335	P261, P280, P301+P310, P305+P351+P338	Sigma
Acrylamide	GHS06 GHS08	H301, H312, H316, H317, H319, H332, H340, H350, H361f, H372	P201, P280, P301+310, P305+351+338, P308+313	Carl Roth
ATP	-	-	-	Carl Roth
Agarose	-	-	-	Serva
(NH4)2SO4	-	-	-	Carl Roth
NH4NO3	GHS03	H272	P210	Applichem
Bromphenolblue	GHS03 GHS07 GHS08	H272, H302, H315, H317, H319, H334; H335	P280, P305+351+338, P302+352, P304+341, P342+311	Bio-RAD
CaCl$_2$	GHS07	H319	P305+351+338	Merck
Ca(H$_3$CCOO)$_2$	-	H315, H319, H335	P261, P305+P351+P338	Sigma
Citric acid	GHS05	H318	P305+351+338, P311	Sigma
Coomassie Brilliant Blue	-	-	-	Applichem

CHES	-	H319	P305+P351+P338	Sigma
DTT	GHS07	H302, H315, H319, H335	P302+352, P305+351+338	Applichem
EDTA	GHS07	H319	P305+351+338	Sigma
Ethanol	GHS02	H225	P210	Carl Roth
Ethidiumbromide	GHS06, GHS08	H302, H330, H341	P260, P281, P284, P310	Sigma
Glycerol	-	-	-	Carl Roth
Guanidinhydro chlorid	GHS07	H302, H315, H319	P305+P351+P388, P302+P352	Applichem
HEPES (4-(2-hydroxyethyl)-1 piperazineethanesulfonic acid)	-	-	-	Applichem
Hydrochloric acid >25 %	GHS05, GHS07	H314, H335	P261, P280, P310, P305+351+338	Merck
Isopropanol	GHS02, GHS07	H225, H319, H336	P210, P233, P305+351+338	VWR
Imidazole	GHS05, GHS06, GHS08	H301; H314; H361	P260, P281, P303+P361+P353, P301+P330+P331, P305+P351+P338, P308+P313	Applichem
KCl	-	-	-	Carl Roth
LiCl	GHS07	H302; H315, H319, H33	P302+352, P305+351+338	Merck
Li2SO4	GHS07	H302	-	Merck
Mg(HCOO)2	-	-	-	Fluka

MgCl2	-	-	-	Carl Roth
MgOAc	-	-	-	Merck
MgSO4	-	-	-	Merck
Methanol	GHS02, GHS06, GHS08	H225, H301, H311, H331, H370	P210, P280, P233, P302+P352, P309, P310	Carl Roth
MPD	GHS07	H315, H319	-	Carl Roth
2-Mercaptoethanol	GHS06, GHS09	H302, H411, H315, H335, H311, H319	P280, P312, P302+P350, P261, P273, P301+P312, P305+P351+P338	Fisher Scientific
NaOAc	-	-	-	Applichem
NaBr	-	-	-	Merck
(CH3)2AsO2Na)	GHS09, GHS06	H301, H331, H410	P261, P273, P301+P310, P311, P501	Sigma
NaCl	-	-	-	Carl Roth
NaH2PO4	-	-	-	Applichem
NaOH	GHS05	H314	P280, P310, P305+351+338	Merck
Na3 citrate	-	-	-	Sigma
Ni(II)SO4	GHS08, GHS09, GHS07	H332, H315, H334, H317, H341, H350i, H360D, H372 H410	P280, P273, P201, P342+P311, P308+P313, P302+P352	Applichem
Paraffin	-	-	-	-
Polyethylenglycol 200 (PEG 200)	-	-	-	Applichem

PEG 10000	-	-	-	Merck
PEG 1500	-	-	-	Fluka
PEG 2000 MME	-	-	-	Fluka
PEG 300	-	-	-	Applichem
PEG 3350	-	-	-	Sigma
PEG 400	-	-	-	Sigma
PEG 4000	-	-	-	Merck
PEG 6000	-	-	-	Merck
PEG 8000	-	-	-	Sigma
PMSF	GHS06, GHS05	H301, H314	P280, P305+P351+P338, P310	Applichem
SDS	GHS02 GHS06	H228, H302, H311, H315, H319, H335	P210, P261, P280, P312, P305+351+338	Sigma
Sodium citrate	-	-	-	Sigma
Sodium tartrate		-	-	Applichem
Tetramethylethyldiamin (TEMED)	GHS02 GHS05 GHS07	H225, H302, H314, H332	P261, P280, P305+351+338	Merck
tert-Butanol	GHS02 GHS07	H225, H319, H332, H335	P210, P305+351+338, P403+233	AppliChem
Tris (2-amino-2-(hydroxymethyl)-propane-1,3-diol)	GHS07	H315, H319, H335	P261, P305+351+338	Carl Roth
Tween 20	-	-	-	Carl Roth
Yeast Extract	-	-	-	Serva

9.2 Commercial protein screens and kits

Name	Supplier	Risk label	Risk phrases	Safety phrases
PCT	Hampton	T, N	R41, R42, R36/37/38	S20, S26, S45, S53, S61, S36/37/39 -
Floppy Choppy	Jena Bio Science	C, Xn, Xi	R35, R41, R42, R36/37/38	S22, S26, S45, S24/25, S36/37/39:
Macrosol	Molecular Dimensions	T, N	R10, R45, R46, R60, R61, R25, R36/37/38, R48/20/22, R51/53	S20, S26, S45, S53, S61, S36/37/39
Morpheus	Molecular Dimensions	T, N	R10, R45, R46, R60, R61, R63, R23/25, R36/37/38, R48/20/22, R51/53	S20, S26, S45, S53, S61, S36/37/39
PACT premier	Molecular Dimensions	T	R23/25, R52/53	S20, S36, S45, S61
Stura /Footprint	Molecular Dimensions	T, N	R10, R45, R46, R60, R61, R25, R36/37/38, R48/20/22, R51/53	S20, S26, S45, S53, S61, S36/37/39
AmSO4 Suite	Qiagen	T+, N	R10, R25, R26, R45, R46, R60, R61, R48/23/25, R51/53	S45, S53, S61, S36/37.
Classic Suite	Qiagen	T, N	R10, R45, R46, R60, R61, R23/25, R36/37/38, R48/20/22, R51/53	S20, S26, S45, S53, S36/37/39.
ComPAS Suite	Qiagen	T	R10, R45, R23/24/25, R36/38, R39/23/24/25, R51/53	S13, S26, S45, S53, S61, S36/37/39.
Cryos Suite	Qiagen	T, N	R10, R45, R46, R60, R61, R23/25, R36/37/38, R48/20/22,	S20, S26, S45, S53, S61, S36/37/39.

			R51/53	
JCSG+ Suite	Qiagen	T, N	R10, R21, R41, R45, R23/25, R37/38, R51/53	S13, S20, S26, S45, S53, S36/37/39
ComPAS Suite	Qiagen	T	R10, R45, R23/24/25, R36/38, R39/23/24/25, R51/53	S13, S26, S45, S53, S61, S36/37/39.
Pure Link PCR Purification Kit	Invitrogen	Xn	R22, R36/38	S28, S24/25
peqGOLD Plasmid Mini Kit	peqlab	-	-	-

9.3 GHS and risk symbols

Figure 47: GHS pictograms according to (http://www.evansvanodine.com) Evans Vanodine International plc/ global Hygiene Solutions / UK).

Figure 48: Hazard symbols according to http://www.sigmaaldrich.com for formulations and respective risk labels.

9.4 Hazard, risk, safety- and precaution statements

Risk statements	
R8	Contact with combustible material
R10	May cause fire
R20	Flammable
R21	Harmful by inhalation
R22	Harmful in contact with skin
R25	Harmful if swallowed
R35	Toxic if swallowed
R36	Causes severe burns
R38	Irritating to eyes / Irritating to skin
R41	Risk of serious damage to eyes
R42	May cause sensitization by inhalation
R43	May cause sensitization by skin contact
R45	May cause cancer

R46	May cause heritable genetic damage
R60	May impair fertility
R61	May cause harm to the unborn child
R39/23/24/25	Toxic: danger of very serious irreversible effects through inhalation, in contact with skin and if swallowed
R36/37/38	Irritating to eyes, respiratory system and skin
R23/24/25	Toxic by inhalation, in contact with skin and if swallowed
R20/21/22	Harmful by inhalation, in contact with skin and if swallowed
R48/20/22	Harmful: danger of serious damage to health by prolonged exposure through inhalation and if swallowed
R23/25	Toxic by inhalation and if swallowed
R36/38	Irritating to eyes and skin
R51/53	Toxic to aquatic organisms, may cause long-term adverse effects in the aquatic environment
R37/38	Irritating to respiratory system and skin

GHS precautionary statements	
P201	Obtain special instructions before use
P210	Keep away from heat/sparks/open flames/hot surfaces – No smoking
P233	Keep container tightly closed
P260	Do not breathe dust/fume/gas/mist/vapors/spray
P261	Avoid breathing dust/fume/gas/mist/vapors/spray
P264	Wash thoroughly after handling

P273	Avoid release to the environment
P281	Use personal protective equipment as required
P280	Wear protective gloves / protective clothing/ eye protection / face protection
P284	Wear respiratory protection
P309	IF exposed or you feel unwell
P310	Immediately call a POISON CENTER or doctor/physician
P311	Call a POISON CENTER or doctor/physician
P312	Call a POISON CENTER or doctor/physician if you feel unwell
P321	Specific treatment (see respective MSDS)
P362	Take off contaminated clothing and wash before reuse
P501	Dispose of contents/container to
P301+310	If swallowed: Immediately call a poison center or doctor/physician
P301+P312	If swallowed: call a poison center or doctor/physician if you feel unwell
P301+P330+P331	If swallowed: Rinse mouth. Do not induce vomiting
P302+P352	If on skin: Wash with soap and water
P303+P361+P353	If on skin (or hair): Remove/Take off immediately all contaminated clothing. Rinse skin with water/shower
P304+341	If in halted: If breathing is difficult, remove victim to fresh air and keep at rest in a position comfortable for breathing
P305+351+338	If in eyes: Rinse cautiously with water for

	several minutes. Remove contact lenses if present and easy to do – continue rinsing
P308+313	If exposed or concerned: Get medical advice/attention
P332+313	If skin irritation occurs: Get medical advice/attention
P342+311	Call a poison center or doctor/physician
P403+233	Store in a well-ventilated place. Keep container tightly closed

Safety statements	
S20	When using do not eat or drink. Do not breathe dust
S22	In case of contact with eyes, rinse immediately with plenty of water and seek medical advice
S26	In case of accident or if you feel unwell seek medical advice immediately (show the label where possible).
S28	After contact with skin, wash immediately with plenty of water (to be specified by the manufacturer)
S45	If swallowed, seek medical advice immediately and show this container or label
S46	Avoid exposure - obtain special instructions before use
S53	Avoid release to the environment
S61	Refer to special instructions/safety data sheet
S24/25	Avoid contact with skin and eyes
S36/37	Wear suitable protective clothing and gloves

S36/37/39	Wear suitable protective clothing, gloves and eye/face protection

GHS hazard statements	
H 225	Highly flammable liquid and vapor
H 226	Flammable liquid and vapour
H 228	Flammable solid
H 272	May intensify fire; oxidizer
H 301	Toxic if swallowed
H 302	Harmful if swallowed
H 311	Toxic in contact with skin
H 312	Harmful in contact with skin
H 314	Causes severe skin burns and eye damage
H 315	Causes skin irritation
H 316	Causes mild skin irritation
H 317	May cause an allergic skin reaction
H 318	Causes serious eye damage
H 319	Causes serious eye irritation
H 330	Fatal if inhaled
H 331	Toxic if inhaled
H 332	Harmful if inhaled
H 334	May cause allergy or asthma symptoms or breathing difficulties if inhaled
H 335	May cause respiratory irritation
H 336	May cause drowsiness or dizziness
H 340	May cause genetic defects
H 360	May damage fertility or the unborn child
H 341	Suspected of causing genetic defects
H 350	May cause cancer
H 350i	May cause cancer by inhalation
H 360D	May damage the unborn child

H 361	Suspected of damaging fertility or the unborn child
H361f	Suspected of damaging fertility
H 370	Causes damage to organs
H 372	Causes damage to organs through prolonged or repeated exposure
H 410	Very toxic to aquatic life with long lasting effects
H 411	Toxic to aquatic life with long lasting effects

10 Acknowledgement

11 Curriculum Vitae

Personal data

Name: Haifa El Kilani

Date of Birth: 12/09/1979

Place of Birth: Sousse/Tunisia

Graduation:

Since 12.12: PhD Student, University of Hamburg, Institute for Biochemistry and Molecular Biology and Laboratory for Structural Biology of Infection and Inflammation, c/o DESY, Build. 22a, Notkestr. 85 22607, Hamburg, Germany.

10.10-11.12: Study of Molecular Life Science (Master of Science), University of Lübeck, Germany

Thesis title: Crystal structure analysis of the S135A mutant of the NS2B/NS3 protease from dengue virus serotype 2

10.08-09.10: Study of Molecular Life Science (Bachelor of Science), University of Lübeck, Germany

09.01-06.04: Study of Molecular Life Science of the Public Health (Bachelor of Science), Major subject "Cyto-morphology" at the Superior School of Health Science and Technology of Tunis, Tunisia.

Thesis title: Laryngeal papillomatosis, Identification of HPV using in situ hybridization

06.00: High school graduation, "Cité Erriadh" High School, Sousse, Tunisia.

Work experience

12.05-04.06: Staff Scientist at the Department of Anatomy and Pathological Cytology, Farhat Hached University Hospital, Sousse, Tunisia.

05.06-09.07: Staff Scientist at the Department of Human and Experimental Anatomy Pathology, Pasteur Institute of Tunis, Tunisia.

12 Eidesstattliche Erklärung

Hiermit erkläre ich an Eides statt, die vorliegende Dissertation selbst verfasst und keine anderen als die angegebenen Hilfsmittel benutzt zu haben.

Ferner versichere ich, dass ich noch keine Promotionsversuche an anderen Universitäten unternommen habe.

Hamburg, 15. Juni 2016

Haifa El Kilani